SLAC--414

DE93 009617

# WORKSHOP ON SCIENTIFIC APPLICATIONS OF SHORT WAVELENGTH COHERENT LIGHT SOURCES

W. Spicer - Chair
J. Arthur, H. Winick - Co-Chairs

*Stanford Linear Accelerator Center*
*Stanford Synchrotron Radiation Laboratory*
*Stanford University, Stanford, California 94309*

October 21, 1992

Prepared for the Department of Energy under contract number DE-AC03-76SF00515

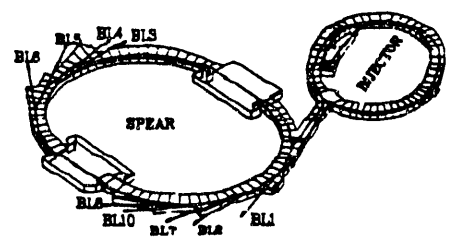


Printed in the United States of America. Available from the National Technical Information Service, U.S. Department of Commerce, 5285 Port Royal Road, Springfield, Virginia 22161

# TABLE OF CONTENTS

# I. EXECUTIVE SUMMARY

# WORKSHOP ON SCIENTIFIC APPLICATIONS OF SHORT WAVELENGTH COHERENT LIGHT SOURCES

## EXECUTIVE SUMMARY

by
H. Winick, J. Arthur and W. Spicer

This workshop was motivated by two recent developments which have opened the possibility that the SLAC linac could be used to drive an x-ray laser at very short wavelengths. The workshop was called to explore possible scientific applications of the extremely high power, brightness, and coherence of such a source.

The first development is the success at Los Alamos and elsewhere with high brightness, rf photocathode electron guns which can now deliver low emittance (3-4 mm-mrad normalized emittance), high charge (>1 nC) electron beams, meeting the requirements of linac-driven short wavelength x-ray lasers. The second is the development at SLAC, as part of the SLC project, of the equipment, tools, and understanding associated with the transport, acceleration, and compression of such high brightness electron bunches without dilution of phase space density.

The design of a short wavelength linac-based x-ray laser, which we call a Linac Coherent Light Source (LCLS), has been studied in detail by a SLAC, UCLA, LBL, LLNL group since it was proposed at the Workshop on Fourth Generation Light Sources (1) held at SLAC in February 1992.

The Charge to the present workshop is given below. The design and performance of a 4 nm LCLS were described in opening talks and are summarized in a paper (included in this report) presented at the 13th International FEL Conference held in Kobe, Japan in August 1992. The characteristics of the light produced by the LCLS at 4 nm are projected to be:

| | |
|---|---|
| Peak Coherent Power (GW) | ~10 |
| Pulse Repetition Rate (Hz) | 120 |
| Pulse Width (1 sigma - fs) | <160 |
| Energy/pulse (mJ) | 5 |
| Photons/pulse | $\sim 10^{14}$ |
| Peak Brightness * | $\sim 10^{31}$ |
| Average Brightness * | $\sim 10^{21}$ |
| Bandwidth (1 sigma) | 0.1-.2% |

* photons/(s,mm$^2$,mrad$^2$) within 0.1% bandwidth

The average values of brightness and coherent power are about 3 orders of magnitude greater than projected for 3rd generation synchrotron light sources such as the ALS and the peak values are about 9 orders of magnitude higher. Even higher brightness may be expected at shorter

This workshop has built on previous workshops (2-7) on the design and applications of short wavelength coherent radiation sources. Most of these have emphasized applications in the UV and VUV part of the spectrum. This workshop dealt with a broad spectral range down to 0.1

nm, with emphasis on the 2-4 nm range. Talks by invited speakers covered applications of such a source in atomic physics, biological imaging, time resolved spectroscopy, surface science, materials science and chemical physics as described in this report. In addition to the discussions during and after each talk, there was a long open discussion period in the afternoon at which more than 20 speakers made comments. A summary of this session is included in this report.

In his remarks at the opening of the workshop, Dr. Marianelli said that DOE was receiving an increasing number of ideas for producing and using short wavelength lasers from several DOE laboratories. However, funding was scarce and there was some danger that funding for such advanced sources could come at the expense of budgets for existing facilities.

During and after the workshop, the perspective on this project changed. Before the workshop, it was thought that the SLAC linac should be used as the basis of a full User facility. Based on reactions at the workshop, reinforced by recommendations from a Technical Review Committee that examined the project in November 1992, it is now thought that, as a first step, an r&d facility should be built to explore both the feasibility of such a source and the new and innovative science which could be done with it.

As has been pointed out by many, using the SLAC linac to construct relatively inexpensive short wavelength lasers as test beds for the development and utilization of such a new source is analogous to the parasitic use of SPEAR by the Stanford Synchrotron Radiation Project (SSRP) in the early 1970's. SSRP was able to explore inexpensively the potential of multi-GeV storage rings as synchrotron radiation sources, including the development of new beam line instrumentation and techniques for beam steering and stability as well as the first use of wiggler and undulator insertion devices as high brightness and high intensity sources for experiments.

The availability of intense x-ray beams stable over many hours led to the development of a whole range of scientific studies in x-ray spectroscopy, angle-resolved photoelectron spectroscopy, small angle x-ray diffraction and protein crystallography. These demonstrated the power of these new sources.

The success of SSRP and SSRL led to the construction of much larger synchrotron radiation research facilities, including the third generation facilities now coming on line throughout the world. We should not fail to exploit a similar opportunity for testing short wavelength linac-based lasers.

Many at the workshop felt that the large increase in power, brightness and coherence (particularly the peak values of these quantitities during the short pulse) would require new experimental approaches as well as opening new possibilities. A major concern, especially among biologists, is the rate at which a sample would be destroyed by such a beam. The large number of photons delivered in a single sub-picosecond pulse ($\sim 10^{14}$) opens the possibility of acquiring information on a time scale short compared to the time for damage to manifest itself. For example, it is possible that a hologram of a live biological sample could be acquired in a single shot, before the damage to the sample changes the structure.

Of course, before single shot holograms could be realized, it would be necessary to develop suitable detectors or recoding media to capture the image during the brief pulse and then read it out in a useful way.

Several speakers pointed out that this source would provide enough coherent photons to permit techniques currently employed in the visible part of the spectrum, such as non-linear optics, to be extended to the x-ray region. Also, the extremely short pulse allows time resolved studies of fast chemical reactions and phase transitions.

References:

1. See contributions by C. Pellegrini, by K.-J. Kim, and by W. Barletta, A. Sessler, and L. Yu in "Workshop on Fourth Generation Light Sources", M. Cornacchia and H. Winick (editors); SSRL report 92/02, Feb 24-27, 1992

2. R. London, D. Matthews, S. Suckewer (editors); Applications of X-ray Lasers, January 12-14, 1992. Conf. 9206170; Available from Office of Scientific and Technical Information, P.O. Box 62, Oak Ridge, TN 37831.

3. J. Gallardo (editor); Proceedings of the Workshop Prospects for a 1 Angstrom Free Electron Laser. Sag Harbor, New York. April 22-27, 1990 BNL Report 52273

4. David Attwood, Bob Barton (editors); X-ray Microimaging for the Life Sciences, LBL Report 27660, May 24-26, 1989.

5. D. Deacon, R. Haglund, B. Newnam, H. Schlossberg (editors); Physics of Free-Electron-Laser Applications, Jour. Opt. Soc. of Amer. B. 6, (1989) 969-1089.

6. Free-Electron Laser Applications in the Ultraviolet, Meeting in Cloudcroft, New Mexico, March 2-5, 1988. Optical Society of America, 1988 Technical Digest Series Volume 4

7. Brian Newnam (editor); Applications of Coherent, Extreme-Ultraviolet Radiation. Feb. 7, 1986 (Los Alamos)

WORKSHOP ON SCIENTIFIC APPLICATIONS OF SHORT WAVELENGTH COHERENT LIGHT SOURCES

CHARGE TO THE WORKSHOP

1. Examine possible applications for an x-ray laser operating in the 2-4 nm range and also at other wavelengths down to 0.1 nm.

2. Review unique performance characteristics of the proposed FEL based on the SLAC linac; suggest new scientific applications which these open up as well as possible changes that would add capability.

3. Identify critical issues and possible fundamental limits on the applications of such a device.

4. Consider the need for a pilot, single user program to gain experience with operating and using an x-ray laser as a first step towards a full user facility.

# II. PRESENTATIONS BY INVITED SPEAKERS

SLAC-PUB-594:
LBL-32970
September 1992
(A)

# A 2 to 4nm HIGH POWER FEL ON THE SLAC LINAC* ^

C. Pellegrini, J. Rosenzweig
UCLA Department of Physics, Los Angeles, California 90024
H.-D. Nuhn, P. Pianetta, R. Tatchyn, H. Winick
Stanford Synchrotron Radiation Laboratory, Stanford, California
K. Bane, P. Morton, T. Raubenheimer, J. Seeman
Stanford Linear Accelerator Center, Stanford, California
K. Halbach, K.-J. Kim
Lawrence Berkeley Laboratory, Berkeley California
J. Kirz
State University of New York at Stony Brook, Stony Brook, NY

## ABSTRACT

We report the results of preliminary studies of a 2 to 4nm SASE FEL, using a photoinjector to produce the electron beam, and the SLAC linac to accelerate it to an energy up to 10 GeV. Longitudinal bunch compression is used to increase ten fold the peak current to 2.5 kA, while reducing the bunch length to the subpicosecond range. The saturated output power is in the multi-gigawatt range, producing about $10^{14}$ coherent photons within a bandwidth of about 0.2% rms, in a pulse of several miilijoules. At 120 Hz repetition rate the average power is about 1 W. The system is optimized for x-ray microscopy in the water window around 2 to 4nm, and will permit imaging a biological sample in a single subpicosecond pulse.

## 1. INTRODUCTION

The Self Amplified Spontaneous Emission mode of an FEL has been proposed [1] and analyzed [2] as a source of tunable, coherent, high peak power soft X-rays, capable of

* Work supported by the US Department of Energy, Offices of Basic Energy Sciences, and High Energy Physics.

^ Presented at the 13th Intern. FEL Conference, Kobe, Japan, August 1992.

producing a radiation beam with a brightness eight orders of magnitude larger than synchrotron light sources, and pulse duration shorter than one picosecond. Such a large increase in radiation flux, and the short pulse duration, will open new exciting and unique research possibilities in physics, biology and other sciences.

The SASE approach produces lasing in a single pass of a high peak current electron beam through a long undulator, eliminating the need for optical cavities, difficult to build at these short wavelengths. The requirements on the electron beam peak current, emittance, and energy spread are very stringent [2], and until recently difficult to satisfy. The recent development of high-brightness photocathode electron guns [3], and the expected availability of the SLAC linac, open the possibility to make this major extension of FEL operation, from the shortest wavelength yet achieved (240 nm) to 2-4 nm, the wavelength range suitable for biological imaging and other applications.

The recognition of this possibility was one of the main conclusions of the Workshop on Fourth Generation Light Sources held at SSRL/SLAC on February 24-27, 1992. The workshop report [4] contains many contributions relevant to linac-driven short wavelength FELs. In particular, the use of the SLAC linac for this purpose is discussed by C. Pellegrini [5], K.-J. Kim [6], and by W. Barletta, A. Sessler and L. Yu [7]. The advantage of using the SLAC linac is that its properties are extensively characterized, because of its use as a linear collider [8-12].

The wavelength range 2 to 4 nm, corresponding to the "water window", is most suitable for imaging biological materials and other applications in which the short pulse and high coherent power are important. In particular we consider the use of this system for x-ray microscopy and holography of biological samples, with images obtained in a single pulse [13]. This requires an energy in a single photon pulse of the order of 300 $mJ/cm^2$, and a

subpicosecond pulse duration. Under this condition an image is obtained for a sample "in vivo" before it has time to change, or be affected by the radiation.

The system for the 2-4 nm FEL consists of : a 10 MeV, S-band photoinjector; part of the SLAC linac to accelerate the beam up to 10 GeV; two longitudinal bunch compressors, to increase the peak current to 2500 A, and reduce the rms bunch length to 0.16 ps; the undulator; optical beam transport lines and experimental areas. These components will be discussed in the next sections.

It is interesting to notice that, with an improvement of present photocathode gun technology, it appears possible to reduce in the near future the normalized emittance by a factor of about 3 below that used for the 4 nm FEL. This would open the possibility to construct a 0.1 nm FEL using the entire SLAC linac, permitting acceleration up to 55 GeV.

## 2. THE PHOTOINJECTOR

The electron source is a critical component, since it defines the electron beam properties. The requirements for the 2-4 nm FEL are given in Table 1. A preliminary study indicates that an electron beam of characteristics approaching the design goal can be obtained from an RF photocathode gun. This source consists of a three and a half cell $\pi$-mode standing wave accelerating structure, excited to 100MV/m peak field on axis, with a metal photocathode illuminated by a two picosecond laser pulse.

Using a simple analytical model [14], we estimate that for a bunch with radial size $\sigma_r$=3 mm, and longitudinal size $\sigma_z$= 0.54 mm, the emittance growth due to the space charge force, is

2.5 mm-mrad. Additional emittance growth due to the time dependent RF field is small, 0.7 mm-mrad, because of the size of the electron beam.

The beam envelope is controlled without additional solenoidal or quadrupole focusing using alternating gradient (ponderomotive) focusing effects [15] of the high gradient RF field.

The normalized, rms, according to Parmela simulation is 6 mm-mrad for a bunch charge of 1 nC. This is larger than the actual emittance obtainable from the source, as numerical noise in the space charge calculation done by Parmela typically inflates the emittance by a factor of two when compared to experimental results and to calculations using particle-in-cell codes. On this basis we assume that the gun will produce the required design value of 3 mm-mrad. Calculations using a particle-in-cell model for our gun are in progress.

The longitudinal phase space has an rms pulse length of $\sigma_l$= 0.5 mm, peak current of 250 A, rms momentum spread $1.8 \times 10^{-3}$. The uncorrelated momentum spread which appears towards the rear of the bunch is due to the longitudinal space charge field of the bunch and its image near the cathode.

## 3. BEAM TRANSPORT, ACCELERATION AND COMPRESSION

We consider the acceleration and compression of the bunch produced by the photoinjector. We initially consider the case of acceleration to 7 GeV, with a longitudinal compression by a factor of 10. At the end of the linac, we require a peak current of 2.5kA and a peak-to-peak energy spread $\Delta_E$ <0.2%.

In deciding at what energy to compress we need to consider the longitudinal and transverse wakefields and RF deflections in the linac[8-12] . The first will increase the beam's

energy spread and is harder to compensate for short bunches; the last will increase the transverse emittance and are more severe for long bunches. In addition we have to consider the characteristics of the bunch compressors, which limit the compression factor we can expect to achieve in a single stage of compression.

We compress in two stages, once at 70 MeV to achieve the shortest bunch length, 200μm, consistent with correcting the correlated energy spread to the level of 0.2%, and again at 7 GeV to 30 μm, to achieve the desired high peak current. To study the development of longitudinal phase space we use a computer program that considers the effects of both the longitudinal wakefields and the curvature of the RF wave. After the initial compression the beam shape is still very similar to a gaussian. After the second compression, the beam distribution is more sharply spiked and has long tails, as shown in Fig. 1. We note that the peak current and the final energy spread satisfy our requirements.

Next, we calculate the transverse emittance dilution due to the transverse wakefields, rf deflections, and dispersive errors. To model the SLAC linac, we assume 150μm rms random misalignments of the quadrupoles and BPMs, 300μm rms random misalignments of the accelerator structures, and a random transverse-longitudinal coupling $g_{rms}=2\times10^{-4}$ for the RF deflections. Finally, we assume a transverse beam jitter equal to the rms beam size. The results, averaged from ten sets of random errors, are plotted in Fig. 2, along with the final peak-to-peak energy spread, as a function of the bunch length in the linac.

The apparent knee in the energy spread occurs because one cannot use the curvature of the RF to fully cancel the longitudinal wakefield for bunches shorter than roughly 200μm. At a bunch length of 200μm, we find 25% emittance growth along the linac.

## 4. FEL PERFORMANCE

The FEL design goal is to produce $10^{14}$ photons in a subpicosecond pulse for biological imaging. To reach this goal we optimize the FEL for maximum laser power. There are two possible design strategies: a.) large electron energy, in the range of 5 to 10 GeV, and a long undulator to obtain the required FEL power directly at saturation; b.) a lower electron energy, 2 to 3 GeV, with the option of using a tapered wiggler after the SASE saturation, to increase the FEL power further when necessary.

We will investigate both options to optimize the system design. To obtain an initial estimate of the FEL performance and explore the parameter space we have been using the analytical form of the FEL gain obtained by Chin, Kim, and Xie [16]. We have also used a program developed by I. Ben-Zvi and L.-H. Yu [17], and the simulation code TDA [18]. These theories and codes include energy spread, three dimensional effects, and a general betatron focusing. The results are shown in Table 1.

We have considered one case with a high energy beam, option a. This is optimized using the largest undulator parameter, K=6, and minimum beam energy, 7 GeV, compatible with a simple undulator design, and an output power larger than 10 GW. The FEL characteristics for this case are given in Table 1, column 2. In the same Table, in column 3, we show the case for a reduced beam energy, and a smaller undulator parameter K=3.7. When comparing to the 7 GeV case one should also notice that the betatron wavelength has been reduced as the energy ratio, so that the beam transverse radius is the same in the two cases. Note that at smaller energy the uncorrelated energy spread is larger, affecting the FEL gain, while the correlated component

remains the same. The gain length is shorter at 3.5 GeV than at 7 GeV. The saturated power is lower than in option a, but is still acceptable.

Another possibility is the use of low field, long period undulator, to obtain a large value of the undulator period in a simple electromagnetic structure [19,20,21].

## 5. UNDULATOR

Our initial discussion of the undulator is done for the parameters given in Table 1, column 2. A simple undulator design can be based on an iron free permanent magnet undulator. For a period of 8.3 cm and a peak magnetic field of 0.78 Tesla, we can select a gap of 1.5 cm. This is a conveniently large gap, that would allow us to install instrumentation for beam diagnostic all along the undulator.

The natural betatron wavelength for a planar undulator with these characteristics is $\lambda_\beta = 2^{1/2}\lambda_w\gamma/K = 273$ m. We add additional focusing, to obtain the required betatron wavelength of 62 m, using a FODO type quadrupole system. To obtain the 62m betatron wavelength at 7 GeV we can use 40 cm long quadrupoles separated by 40 cm of drift, with a gradient of 14 T/m. The phase shift per cell is 9°, and the modulation of the betatron wavelength is quite small, with a ratio of maximum to minimum values of only 1.1.

Because of the choice of an iron free undulator the quadrupoles can be placed around the undulator. Their radius is 12 cm, corresponding to a pole tip field of 0.84 Tesla. Having the quadrupoles around the undulator has the advantage that no interruption is required in the undulator itself, avoiding phase matching problems. For the same reason it is possible to position beam steering magnets and other correctors around the undulator in between quadrupoles.

If the selected site at SLAC could contain a 220 m insertion device, one could consider using the weak-field structure discussed in [19-21].

## 6. X-RAY BEAM LINES AND OPTICS

Extracting and processing the FEL output radiation presents challenging optical engineering problems, because of the unprecedented peak power and brevity of the anticipated radiation pulses. The main tasks will be to: 1) deflect the output radiation out of the bremsstrahlung cone produced by the electrons on the residual gas in the FEL and the upstream collimators; 2) to further monochromatize the radiation, if needed. At the power densities expected at normal incidence, of the order of $10^{16}$ W/cm$^2$, it is easy to assess that energy in excess of 1 eV/atom will be deposited in the irradiated volume and that ablation of the irradiated surface will become probable due to the comparatively long time constants of alternative energy-removal channels. This precludes the use of solid state optics, such as multilayers, that work at large angles of incidence, leaving multi-faceted optics operating at extreme grazing incidence as perhaps the only viable choice.

An alternative approach that could mitigate the damage problem would be to configure a series of gas jets with density gradients.

## REFERENCES


1. C Pellegrini, Jour. Opt. Soc. of Amer. B2, 259 (1985).
2. K.-J. Kim et al., Nucl. Instr. and Meth. A239, 54 (1985); K.-J. Kim, Phys. Rev. Letters 57, 1871 (1986); C. Pellegrini, Nucl. Instr. and Meth. A272, 364 (1988); L.-H. Yu and S. Krinsky, Nucl. Instr. and Meth. A285, 119 (1989).

3. R. L. Sheffield, Photocathode RF Guns, in Physics of Particle Accelerators, AIP vol.184, p. 1500, M. Month and M. Dienes eds., (1989).
4. Workshop on Fourth Generation Light Sources, SSRL Report 92/02, M. Cornacchia and H. Winick, editors.
5. C. Pellegrini, ibid, p.364.
6. K.-J. Kim, ibid. p. 315.
7. W. Barletta, A. Sessler and L. Yu, ibid, p. 376-84
8. K. Bane, "Wakefield Effects in a Linear Collider", AIP Conf. Proc., vol. 153, p. 971 (1987).
9. J. Seeman et al, "Summary of Emittance Control in the SLC Linac", US Particle Accelerator Conference, IEEE Conf. Proc. 91CH3038-7, p. 2064 (1991).
10. M. Ross et al, "Wire Scanners for Beam Size and Emittance Measurements at the SLC", US Particle Accelerator Conference, IEEE Conf. Proc. 91CH3038-7, p. 1201 (1991).
11. J. Seeman et al, "Multibunch Energy and Spectrum Control in the SLC High Energy Linac", US Particle Accelerator Conference, IEEE Conf. Proc. 91CH3038-7, p. 3210 (1991).
12. T. Raubenheimer, "The Generation and Acceleration of Low Emittance Flat Beams for Future Linear Colliders", SLAC-Report 387 (1991).
13. J. C. Solem and G. C. Baldwin, Science 218, 229 (1982 ); M. Howells and J. Kirz, in Free Electron Generation of Extreme UV Coherent Radiation, J. M. J. Madey and C. Pellegrini eds., AIP Vol. 118, p. 85 (1984).
14 K.-J. Kim, Nucl. Instr. and Meth. A275, 201 (1989).
15. C. Hartman and J.B. Rosenzweig, "Ponderomotice Focusing in Axisymmetric RF Linacs", submitted to Phys. Rev. A (1992).
16. Y. H. Chin, K.-J. Kim, and M. Xie, Three Dimensional Free Electron Laser Theory Including Betatron Oscillations, LBL Rep. 32329 (1992), submitted to Phys. Rev. A.
17. I. Ben Zvi and L.-H. Yu, private communication.
18, T.M. Tran and J. S. Wurtele, Comp. Phys. Commun. 54, 263 (1989).
19. R. Tatchyn, "Optimal Insertion Device Parameters for SASE FEL Operation," Workshop on Fourth Generation Light Sources, SSRL Report 92/02, M. Cornacchia and H. Winick. eds., 605(1992).
20. R. Tatchyn, T. Cremer, and P. Csonka, "Design considerations for a new weak-field soft X-ray undulator/FEL driver for PEP," Nucl. Instrum Meth. A308, 152(1991).
21. R. Tatchyn, "Fourth Generation Insertion Devices: New Conceptual Directions, Applications, and Technoiogies," Workshop on Fourth Generation Light Sources, SSRL Report 92/02, M. Cornacchia and H. Winick. eds., 417(1992).

## FIGURE CAPTION

1. Current distribution after the final compression (solid line) and a gaussian fit to the core (dots); the head of the bunch is to the left. The energy variation correlated with longitudinal position is shown on the right axis; the uncorrelated energy spread is 0.04%.
2. Transverse emittance dilution (solid line) and peak-to-peak energy spread (dashed line) as a function of the bunch length. The points are the values calculated and the lines are for guidance.

## TABLE 1

## FEL CHARACTERISTICS

| ELECTRON BEAM PROPERTIES: GUN EXIT | Option A | Option B |
|---|---|---|
| Energy, MeV | 10 | 10 |
| Emittance, normalized, rms, mm-mrad | 3 | 3 |
| Pulse duration, rms, ps | 1.6 | 1.6 |
| Relative energy spread, rms, % | 0.15 | 0.15 |
| Peak current, A | 250 | 250 |
| ELECTRON BEAM PROPERTIES: HIGH ENERGY | | |
| Energy, GeV | 7 | 3.5 |
| Emittance, normalized, rms, mm-mrad | 3 | 3 |
| Peak current, A | 2,500 | 2,500 |
| Uncorrelated energy spread, rms, % | 0.04 | 0.07 |
| Correlated energy spread, rms, % | 0.1 | 0.1 |
| UNDULATOR PROPERTIES | | |
| Period, cm | 8.3 | 5 |
| Magnetic field, T | 0.78 | 0.8 |
| Undulator parameter | 6 | 3.7 |
| Betatron wavelength, m | 62.8 | 31.4 |
| FEL PROPERTIES | | |
| Wavelength, nm | 4 | 4 |
| Field gain length, m | 6.9 | 5.3 |
| Undulator saturation Length, m | 60 | 48 |
| Peak power at saturation, GW | 28 | 10 |
| Pulse duration, rms, ps | 0.16 | 0.16 |
| Line width, rms, including chirping, % | 0.2 | 0.2 |
| Photons per pulse | $2.7\times10^{14}$ | $1\times10^{14}$ |
| Energy per pulse, mJ | 11 | 4 |
| Peak brightness, Ph/mm$^2$/mrad$^2$ /s/0.1% ($\Delta\omega/\omega$) | $5.3\times10^{31}$ | $2.0\times10^{31}$ |
| Repetition rate, Hz | 120 | 120 |
| Average power, W | 1.2 | 0.5 |
| Average brightness, Ph/mm$^2$/mrad$^2$ /s/0.1% ($\Delta\omega/\omega$) | $1.0\times10^{21}$ | $3.7\times10^{20}$ |

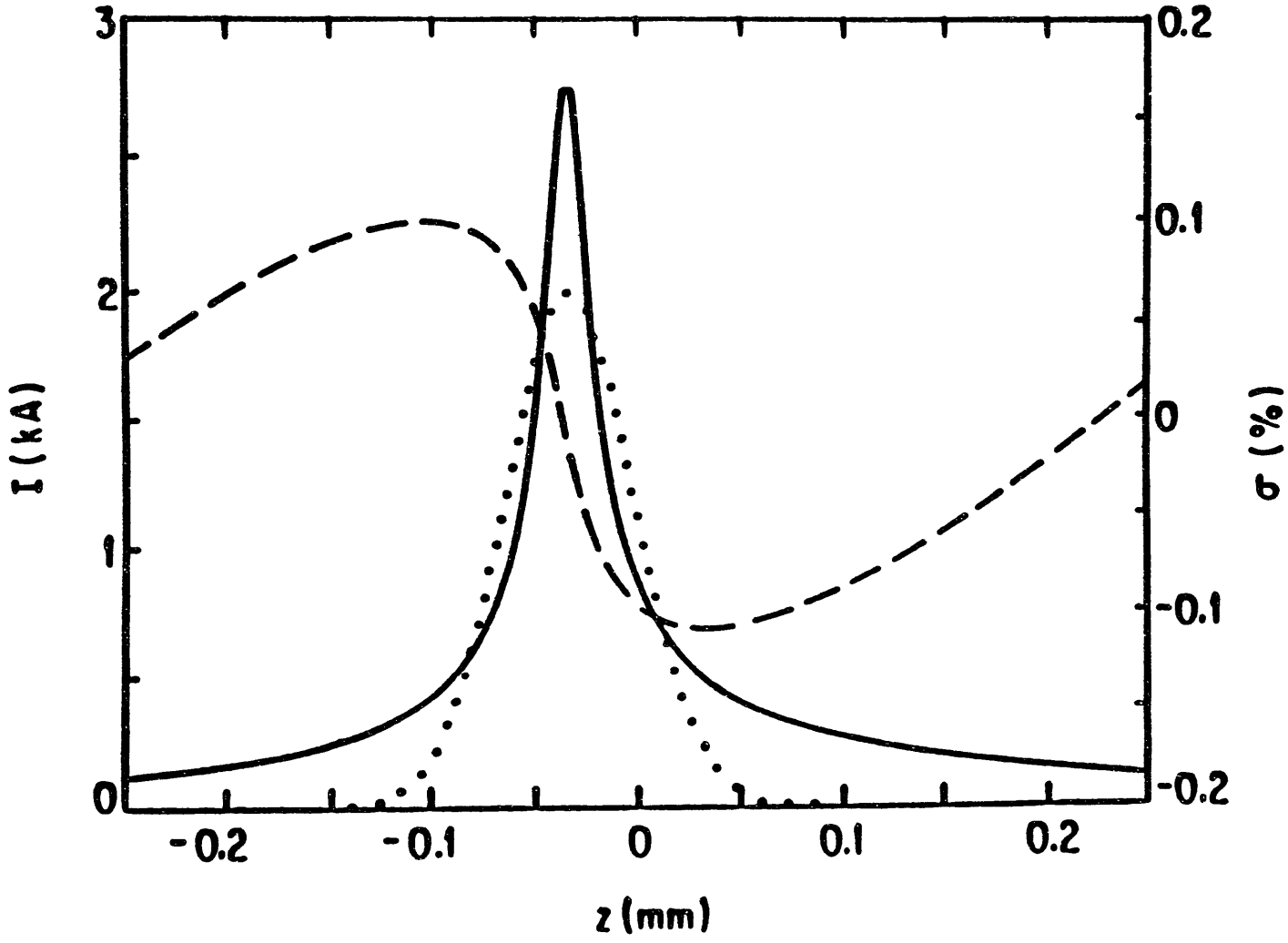
3
2
1
0
0.2
0.1
0
-0.1
-0.2
I (kA)
σ (%)
-0.2
-0.1
0
0.1
0.2
z (mm)

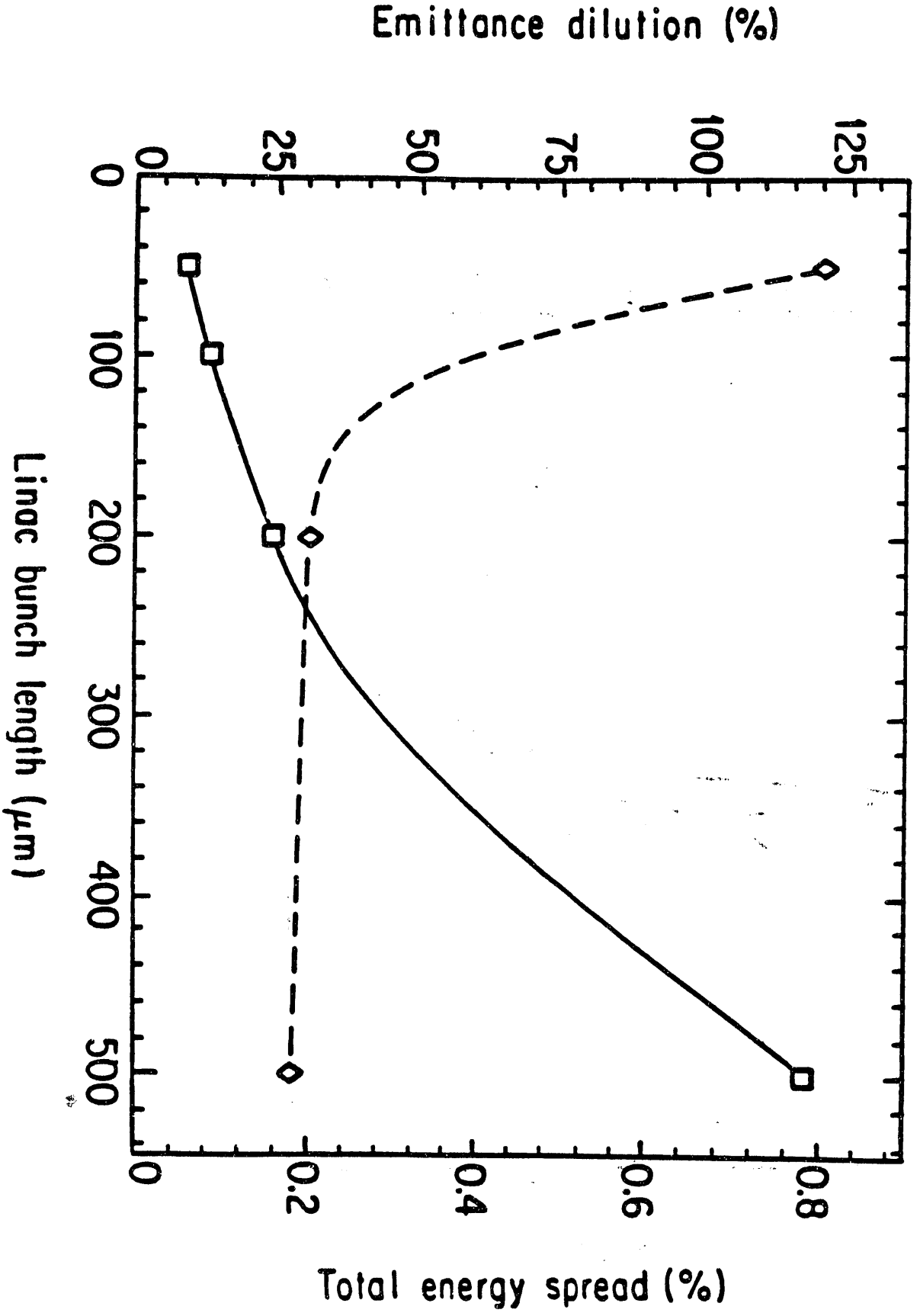
Emittance dilution (%)
0
25
50
75
100
125
Linac bunch length (μm)
0
100
200
300
400
500
0
0.2
0.4
0.6
0.8
Total energy spread (%)

PITT-444
December 1992

# Atomic Physics Research with an X-ray Laser*

R. H. Pratt

*Department of Physics and Astronomy, University of Pittsburgh, Pittsburgh, Pennsylvania 15260*

Bernd Crasemann

*Department of Physics, University of Oregon, Eugene Oregon 97403*

The monochromaticity, brightness, coherence and time structure of x-ray lasers will provide striking new opportunities for the study of inner-shell atomic structures and processes, including relativistic and quantum electrodynamical features. Here we describe some of the anticipated applications to the investigation of structure and dynamics, utilizing the monochromaticity and brightness of the sources. We focus on non-dipolar effects in x-ray photoionization and on scattering of x-rays from atoms and ions.

## I. INTRODUCTION

X-ray lasers will provide a source of energetic photons with the monochromaticity, brightness, coherence and time structure now familiar to us from optical sources [1]. With such photons we can probe inner-shell atomic structures and processes, including threshold and resonance phenomena. We can begin to examine the relativistic, retardation, and higher multipole features of interactions that are difficult to access at lower energies, and we can begin to trace out more of the consequences of the fundamental quantum-electrodynamic interaction. In these respects, x-ray laser sources are likely to complement synchrotron radiation sources and extend their potential in some important investigations.

In the following sections we discuss two promising subjects of investigation, inner-shell photoionization and photon-atom scattering (both elastic and inelastic). We outline what is thusfar known about the use of more energetic photons, both from experiment and from existing theory, and what one may hope to learn. Our discussion focuses on the relativistic, retardation and higher multipole features which begin to come into play at x-ray energies, already by 100 Å. Research on this subject will benefit further from lasers producing radiation with wave lengths closer to 1 Å; clearly the attainment of such sources would require some drastic improvement over the present state of the art, yet may not be out of the question. With presently envisioned devices producing light of wavelengths below 100 Å, perhaps down to the "water window" in the 30-40 Å regime, there should also be very interesting many-electron and many-photon features to be seen near inner shell thresholds. These include direct and indirect ejection of more than one electron in photoionization, direct photon scattering, and resonance phenomena associated with the transition from one-step to two-step processes and with the structure of the target. Some of the possible uses of x-ray lasers in such investigations have been discussed previously [2].

## II. NONDIPOLAR EFFECTS IN X-RAY PHOTOIONIZATION

With increasing energy it is no longer appropriate in the description of photoionization to approximate the electromagnetic field $\boldsymbol{\varepsilon}\exp(i\mathbf{k}\cdot\mathbf{r})$ of the photon, where $\boldsymbol{\varepsilon}$ is the polarization vector and $\mathbf{k}$ the momentum, by $\boldsymbol{\varepsilon}$, as in the usual nonretarded dipole approximation. Instead, one should consider the full retarded multipole expansion of the field. (By neglecting retardation we understand taking the long-wave-length small-k limit for the magnitude of $\mathbf{k}$, while by dipole approximation we understand neglecting higher multipoles in dependence on the direction of $\mathbf{k}$.) Higher multipole transitions contribute significantly to the photoionization cross section and can be measured, providing further information about the process. In addition to the five parameters of the dipole "complete" experiment, there is now a set of quadrupole parameters. Below and into the soft x-ray regime, dipole and quadrupole terms generally suffice for an adequate description. At the same time, smaller distances $|\mathbf{r}|$ play an increasingly important role. While it is no longer correct to assume that $\mathbf{k}\cdot\mathbf{r}$ is small within the atom, it is also true that regions for which $\Delta\cdot\mathbf{r}>>1$ will not contribute to the transition matrix elements, where $\Delta = \mathbf{k} - \mathbf{p}$ is the momentum transfer to the atom, with $\mathbf{p}$ the ejected electron momentum. With increasing photon energy, regions increasingly closer to the nucleus are probed, saturating eventually at electron Compton wave length distances in the determination of the total photoionization cross section. One may picture a transition from a low-energy region, characterized by a residual ionic 1/r potential at larger distances and wave functions reflecting more interior behavior through quantum defects, strongly affected by electron-electron correlations in the

outer part of the atom, to a high-energy region, characterized by a (point-) nuclear Coulomb potential at smaller distances and wave functions reflecting more exterior behavior through their normalization (and phases), relativistic and including higher angular momentum.

When we consider higher multipole matrix elements we must generally, at the same time, consider retardation corrections to the dominant dipole matrix elements, which will affect cross sections in the same order. In total cross sections relativistic effects will also enter in the same order, while in angular distributions retardation and higher multipoles enter in a lower order (integrating to zero in total cross sections). Contrary to the usual expectations, higher multipole effects can be *big* at low energy, even at threshold - in angular distributions. Contrary to the usual expectations, higher multipole, retardation and relativistic effects can be *small* at quite high energy - in *total* cross sections.

Under the assumption that (at most) initial photon momentum $\mathbf{k}$ and polarization $\boldsymbol{\epsilon}$, ejected electron momentum $\mathbf{p}$ and spin $\mathbf{s}$, are determined in an observation of photoionization, the most general form for the differential cross section is

$$\frac{d\sigma}{d\Omega} = \left.\frac{d\sigma}{d\Omega}\right|_{unpol} \frac{1}{2} \sum_{ij} [\, 1 + \xi_i \zeta_j C_{ij} (\hat{\mathbf{p}} \cdot \hat{\mathbf{k}})],$$

where the cross section from unpolarized photons, not observing final electron spin, is

$$\left.\frac{d\sigma}{d\Omega}\right|_{unpol} = \frac{\sigma}{4\pi} \sum_{n} B_n P_n(\cos \hat{\mathbf{p}} \cdot \hat{\mathbf{k}}),$$

with the polarization correlations $C_{ij}$ functions of incident photon energy and emitted electron angle $\theta$ with respect to the photon, the $B_n$ functions of energy, with $B_0 = 1$, $\sigma$ the total cross section. Here the $\xi_i$ are the Stokes parameters which specify the polarization of the incident photon (or the average polarization of the incident beam) and the $\zeta_j$ specify the spin direction of the observed ejected electron in its rest system. Systematic studies of cross sections, angular distributions and polarizational correlations for x-ray energies have been reported [2].

Considering the unpolarized differential cross section for photoionization, in dipole approximation the only other non-zero $B_n$ is $B_2$, related to the angular asymmetry factor $\beta = -2B_2$, and the angular distribution is symmetric about 90°.When quadrupole transitions are included, $B_1$ and $B_3$ are non-zero, breaking the symmetry. Early studies of these effects in the x-ray regime were reported by Krause [4] and by Wuilleumier and Krause [5]. Typically, higher B's become large above 10 keV, as increasing numbers of multipoles contribute. For high energies angular distributions become increasingly forward peaked, roughly as $(1 - \beta \cos\theta)^{-4}$as in Coulomb Born approximation, with $\beta = v/c$, as is seen in $\gamma$-ray experiments. At 6756 keV, the highest energy for which atomic photoeffect has been measured, Blakeway et al. [6] found that the cross section dropped a factor of 400 from 5° to 40°. With decreasing energy the peak diminishes and moves out to larger angles, in some cases beyond 90°, in some cases with repeated oscillations between more forward and more backward angles. For example, in the 5s subshell of tin, these oscillations result from five sign changes in $B_1$ and $B_3$ between 1 eV and 10 keV, caused by sign changes with energy in the dipole and quadrupole matrix elements and in the cosine of the phase shift difference $\Delta$ of continuum p and d waves [7]. $B_1$ and $B_3$ may be enhanced near

zeroes of the dominant matrix element, but also in other circumstances. The effects are greater than 5% in several x-ray regimes, but also at lower energies.

It is often supposed that quadrupole contributions will vanish at threshold, as seen in the nonrelativistic analytic point Coulomb cross section for the K shell, where higher multipole contributions vanish at threshold as v/c. This is contrary to the estimate of the magnitude of the retardation correction, and indeed one finds [8] that one obtains v/c only when cos $\Delta$ vanishes near threshold as v/c, as in the point Coulomb potential. In a screened potential $\Delta$ is finite at threshold and the correction is of order $Z\alpha$, oscillating in sign with Z. In this simple model one sees a 5% effect at threshold for Z=18, a 20% effect for Z=36. In light elements at higher energies, where cross sections become more Coulombic, $\beta$ can provide an estimate of the magnitude of multipole effects. Similar results [9] have been obtained for the L shell, including a discussion of the consequences of using polarized photons. An alternative formalism has been given by Cooper [10].

With increasing energy more multipole matrix elements will contribute. However this does not mean that the independent non-Coulombic information obtainable from these matrix elements will similarly continue to grow. At high energies it is a good approximation to describe the cross section as the point Coulomb potential cross section multiplied by the square of the ratio of the small-distance normalization of the bound state wave function to its point Coulomb value [11]. If the ratio of the screened cross section to the normalization screened Coulomb cross section is expanded in $P_n(\cos\theta)$,

$$\left.\frac{d\sigma}{d\Omega}\right|_{\text{screened}} = (N_s/N_c)^2 \left.\frac{d\sigma}{d\Omega}\right|_{\text{Coulomb}} \sum_n C_n P_n(\cos \hat{\mathbf{p}}\cdot\hat{\mathbf{k}}),$$

all the coefficients become small at high energy and only the first few coefficients are important at lower energies; it is these few coefficients which characterize the nonCoulombic information in the cross section. One may anticipate that energies through the x-ray range will suffice for this purpose.

At the same time that we see multipole matrix element contributions persisting to low energies in photoelectron angular distributions, there is a tendency for nonrelativistic dipole total cross sections to remain valid throughout the x-ray regime, particularly for photoionization of s subshells [12]. A Coulombic estimate would suggest multipole effects in total cross sections of magnitude $\beta^2$, smaller than in angular distributions, similar in magnitude to relativistic effects, and this is generally observed. But for s states the cancellation among relativistic, retardation, and higher multipole effects persists above 100 keV; a nonrelativistic retarded full multipole calculation does far worse than nonrelativistic nonretarded dipole approximation. In partial explanation of this behavior, it has recently been noticed [13] that the singularity structure in complex energy for nonrelativistic dipole approximation (non-relativistic kinematics, no retarded multipole structure) and the full calculation (relativistic kinematics, retarded multipole structure) are the same, while nonrelativistic kinematics with a retarded multipole structure introduces additional singularities near $mc^2$. Studies in the x-ray regime should be able to probe these features and address the angular momentum dependence of the phenomena.

## III. NEW DEVELOPMENTS IN X-RAY SCATTERING

In recent years it has become possible to perform systematic calculations of elastic [14] and inelastic [15] scattering of x-rays from atoms at the same (relativistic independent particle) level of approximation which has been available for some time in x-ray photoionization. Elastic x-ray scattering has long been a tool in crystallography. Now, with the advent of more intense sources and a better understanding of the anomalous scattering region, it is being exploited in the determination of the structure of complex biological macromolecules. Similarly inelastic (Compton) scattering is used to study electron momentum density in materials and now, exploiting magnetic scattering, to study magnetic properties at surfaces.

An early consequence of the elastic (Rayleigh) scattering calculation was to permit an experimental identification of the 1.33 MeV elastic Delbruck scattering component coherent with it [16]; a calculation of Delbruck scattering beyond Born approximation is still needed. More recent work has focussed on x-ray scattering in the anomalous scattering regimes near photoionization thresholds. The real and imaginary anomalous scattering factors are related through a dispersion relation. Using this relation requires knowledge of photoeffect at all energies; relativistic consequences are seen in experimental measurements of anomalous factors near threshold [17]. The best simple description of Rayleigh scattering is in terms of a modified form factor (which recognizes relativistic effects at high energy) and angle -independent anomalous scattering factors obtained via dispersion relations from photoeffect. Numerical calculations suggest that as one leaves the x-ray regime anomalous scattering factors do have some angular dependence.

The new calculations of Compton scattering from bound electrons exhibit three distinct structural features in the spectrum of scattered electrons. At high energies is the Compton peak, related to the scattering from free electrons and used to determine the momentum distribution of electrons in the atom. (The wings of the peak are related to scattering from inner shell electrons, the main peak to scattering from outer shells.) At low final photon energies there is an infrared rise and (exploiting the low energy theorem) the cross section is proportional to the photoeffect cross section. Inbetween (except for scattering from the K shell) there are resonance features (the so-called resonant-Raman-Compton cross section) associated with downward transition energies. Inner shells dominate the latter two structures, outer shells dominate the peak. The infrared rise region has not yet been successfully observed. When Compton scattering dominates absorption cross sections the Compton peak region dominates and is well described by impulse approximation and the incoherent scattering factor. Further information can be available observing final electron and photon in coincidence, or the angular correlations of transition radiation filling the vacancies produced in the scattering. The transition from two step processes (photoeffect followed by transition radiation) to one step processes (Compton) merits further attention.

* Lecture given at the *Workshop on Scientific Applications of Short Wavelength Coherent Light Sources*, SSRL/SLAC, October 21, 1992.


[1] R. C. Elton, *X-Ray Lasers* (Academic, Boston, 1990); B. J. MacGowan et al., Phys. Fluids. B **4**, 2326 (1992).

[2] B. Craseman, in *Applications of X-Ray Lasers*, edited by R. London, D. Matthews, and S. Suckewer, Lawrence Livermore National Laboratory Report No. CONF-9206170 (National Technical Information Service, Springfield, Virginia, 1992), p. 67.

[3] R. H. Pratt, Akiva Ron and H. K. Tseng, Rev. Mod. Phys. **45**, 273 (1973), Y. S. Kim, R. H. Pratt, A. Ron and H. K. Tseng, Phys. Rev. A **22**, 567 (1980), Young Soon Kim, I. B. Goldberg and R. H. Pratt, Phys. Rev. A **45**, 4542 (1992) and (to be published).

[4] M. O. Krause, Phys. Rev. **177**, 151 (1969).

[5] F. Wuilleumier and M. O. Krause, Phys. Rev. A **10**, 242 (1974).

[6] S. J. Blakeway, W. Gelletly, H. R. Faust and K Schreckenbach, J. Phys. B **16**, 3751 (1983).

[7] M. S. Wang, Young Soon Kim, R. H. Pratt and Akiva Ron, Phys. Rev. A **25**, 857 (1982).

[8] A. Bechler and R. H. Pratt, Phys. Rev. A **39**, 1774 (1989).

[9] A. Bechler and R. H. Pratt, Phys. Rev. A **42**, 6400 (1990).

[10] J. W. Cooper, (to be published); see also Phys. Rev. A **42**, 6942 (1990), but note erratum Phys. Rev. A **45**, 3362 (1992).

[11] R. Y. Yin, O. V. Gabriel and R. H. Pratt, Phys. Rev. A **36**, 1207 (1987).

[12] S. D. Oh, J. McEnnan and R. H. Pratt, Phys. Rev. A **14**, 1428 (1976). A recent more systematic survey as been given by A. Ron, I. Goldberg, J. Stein, S. Manson, R. H. Pratt and R. Yin (to be published).

[13] A. Costescu, P. Bergstrom Jr., C. Dinu and R. H. Pratt (to be published).

[14] L. Kissel, R. H. Pratt and S. C. Roy, Phys Rev. A **22**, 1970 (1980), P. P. Kane, Lynn Kissel, R. H. Pratt and S. C. Roy, Phys. Repts. **140**, 75 (1986), B. Zhou, S. Roy, L. Kissel and R. H. Pratt, (to be published).

[15] T. Suric, P. M. Bergstrom, Jr., K. Pisk and R. H. Pratt, Phys. Rev. Lett. **67**, 189 (1991), T. Suric, Nucl. Instr. & Methods **A314**, 240 (1992), P. M. Bergstrom, Jr., T. Suric, K. Pisk and R. H. Pratt, Nucl. Instr. & Methods **B71**,1 (1992) and (to be published).

[16] G. Basavaraju, P. P. Kane, and K. M. Varier, Pramana **12**, 665 (1979), W. Muckenheim and M. Schumacher, J. Phys. G **6**, 1237 (1980).

[17] Lynn Kissel and R. H. Pratt, Acta Cryst. **A46**, 170 (1990).

# High Resolution, Three Dimensional Soft X-ray Imaging

by

J. Trebes, J. Brase, R. Levesque, H. Szoke, and T. Yorkey
Lawrence Livermore National Laboratory

E. Anderson
Lawrence Berkeley National Laboratory

C. Jacobsen
State University of New York at Stony Brook

D. Kern
IBM T. J. Watson Research Laboratory

I. McNulty
Argonne National Laboratory

A long term goal of soft x-ray imaging has been to make ultrahigh resolution images of unstained, unprepared, wet, live biological microstructures in physiological normal environments. This is now being accomplished with features as small as 300Å being observed in two dimensional x-ray images. While this achievement is remarkable, most complex biological structures are three dimensional in nature and will require three dimensional images on the few hundred Angstrom scale for the structure-function studies required by modern biology. We have been endeavoring to achieve this three dimensional capability with soft x-ray techniques.

The conventional, and very successful, method of producing three dimensional images of the interiors of complex objects is x-ray tomography. This technique utilizes numerous x-ray projections of the object to produce a composite image which is truly three dimensional. Each projection is produced by illuminating the object with a parallel beam of x-rays and the resulting x-ray transmission map is recorded on a detector. The three dimensional characteristics of the image are achieved by illuminating the object from a wide range of angles to fully sample the three dimensional Fourier space of the object. These images are then combined numerically to produce the final three dimensional image.

X-ray tomography may not be appropriate for microstructures in biological objects for several reasons. First the x-ray energies used are chosen for contrast, penetrability, and to minimize diffraction. This results in x-rays whose energy is too high to utilize the "water window" x-ray contrast that exists in the 44-23Å range. Secondly a large number of views (~ 100 ) is required to achieve three dimensional images. This will result in a large x-ray dose which will destroy the biological object before the image can be obtained. Finally conventional tomography is limited in its ability to achieve high resolution by the detector pixel size although crystals can be used to magnify the x-ray beam. A

possible method of overcoming these obstacles to high resolution is to use multiview imaging techniques based on diffraction tomography. In this technique, two dimensional images are produced along different lines of sight through the object using existing high resolution soft x-ray imaging methods. For example, multiple high resolution, two dimensional images can be produced using an x-ray zone plate lens based microscope. These images can be added numerically to produce a three dimensional x-ray image with the three dimensional resolution approaching that obtained in the two dimensional images. This allows sub-1000Å resolution to be achieved. The major drawback is the process of combining images is computational intensive since diffraction must now be included explicitly. This approach is similar to that being successfully used in electron tomography. Here electron optics are used to produce high resolution electron microscope images which are then combined to give three dimensional images.

We have recently begun experiments to demonstrate these ideas using both a soft x-ray zone plate microscope and a soft x-ray Fourier transform holography system. These experiments are being conducted at the National Synchrotron Light Source. In the initial holography experiments, multiple x-ray holograms were produced along different lines of sight through a simple microfabricated object consisting of a gold wire 900Å thick, 1300Å wide and 250 microns long. A Fourier transform geometry was used with an effective numerical aperture of 0.025. With the wavelength used ( 32Å), this should result in a depth resolution of 5 microns for individual holographic images. An x-ray image of a 1 micron long portion of the wire obtained by numerically combining holograms obtained along three different lines of sight is shown in Figure 1. Six different rotational views are shown indicating the good three dimensional localization of the image and that the depth resolution is comparable to the transverse resolution of ~1000Å. Experiments using more complicated objects and with alternative imaging modalities are underway.

These preliminary results indicate that by exploiting existing high resolution soft x-ray optics and by including diffraction in the image reconstruction process we can obtain high resolution three dimensional x-ray images of biological microstructures. This will be accomplished by producing several two dimensional x-ray images along different lines of sight through the object. If these are produced simultaneously and on sub-nanosecond timescales, the image blurring effects of the natural biological motion and x-ray driven hydrodynamical motion will not have time to manifest itself and high resolution, three dimensional, x-ray images of biological objects can be produced. This will require a ultra high brightness x-ray source such as a conventional x-ray laser or an x-ray free electron laser. Once demonstrated, the short duration output pulses (< psec), the high output (~ mJ) , and the tunability of the x-ray FEL make it an extremely attractive source for high resolution, three dimensional imaging of biological microstructures.

*This work was performed under the auspices of the U.S. Department of Energy by Lawrence Livermore National Laboratory under contract No. W-7405-ENG-48.

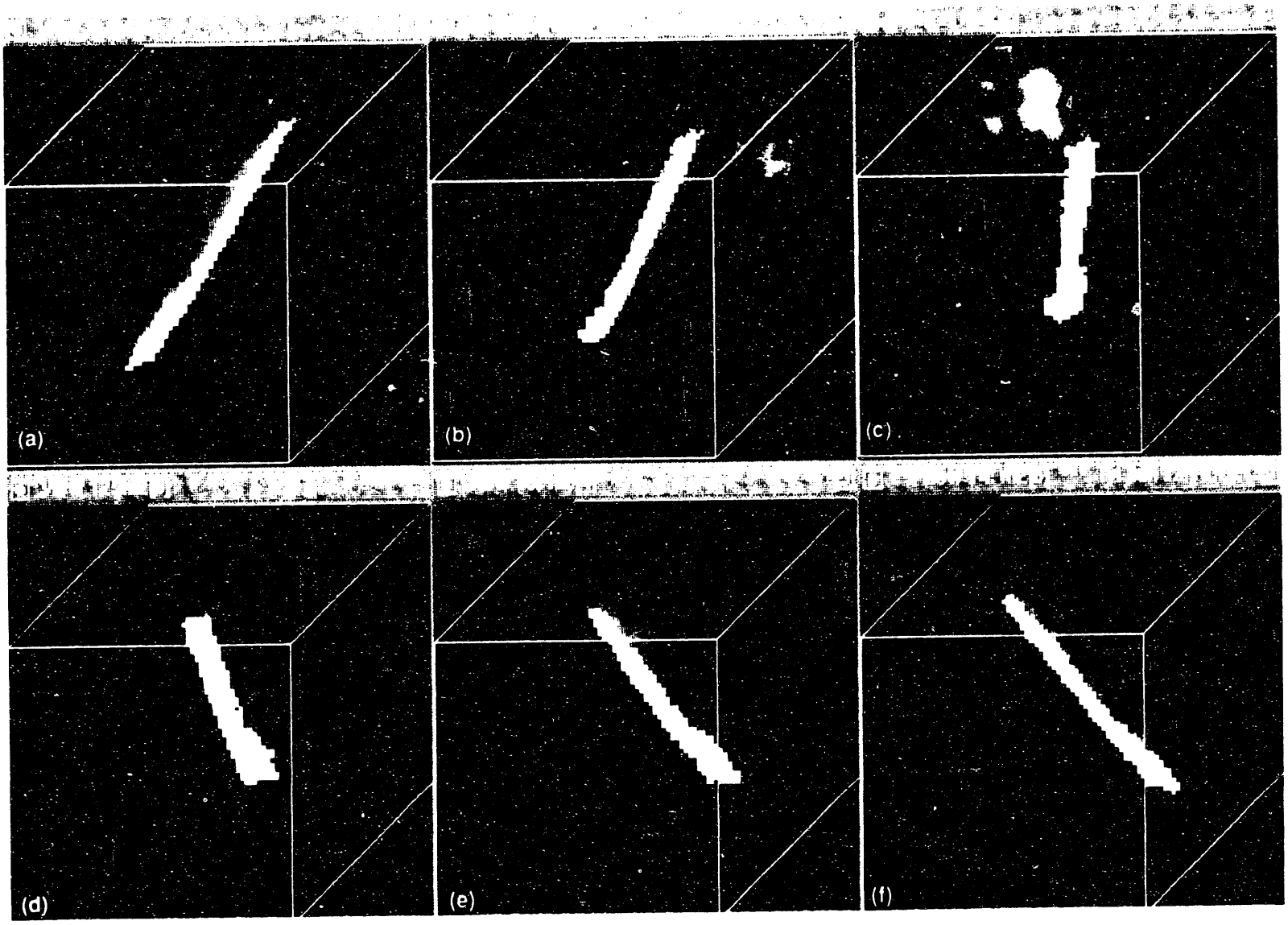


**Figure 1a-1f. Shown is a 1 micron long segment of an x-ray holographic image of a 1000Å wide bar. Each panel shows a different rotation demonstrating the true three dimensionality of the image.**

# The role of x-ray induced damage in biological micro-imaging*

Richard A. London[a], James E. Trebes[a] and Chris J. Jacobsen[b]

[a] Lawrence Livermore National Laboratory
Livermore, California 94550

[b]Department of Physics, SUNY
Stony Brook, New York 11794

## ABSTRACT

Interactions of x rays with a sample are studied to determine the optimal wavelength, source energy and exposure time for microscopy and holography. The optimal wavelength is influenced by two criteria: minimizing the required source energy and minimizing the absorbed dose and subsequent damage to the sample. The use of heavy element labels, such as colloidal gold can significantly reduce the energy and dose. Limits to the exposure time due to natural motions, x-ray induced chemical damage, heat build-up, and hydrodynamic expansion are discussed.

## 1. X-RAY INTERACTIONS

We consider two types of x-ray interactions, scattering and absorption. Scattering is essential for holography and darkfield microscopy, while absorption provides the contrast mechanism for the standard brightfield microscopy. Absorption also has the adverse effects of causing sample damage and limiting the thickness of the sample which can be imaged. In addition to these interactions phase shifts are important for phase-contrast microscopy, but are not covered in this paper

The source energy and absorbed dose are determined for three imaging modes: scanning brightfield microscopy, imaging brightfield microscopy, and holography. Figure 1 shows a schematic imaging set-up in which the basic components and system efficiencies are indicated. The energy and dose depend on the nature of the condenser optic, the windows of the sample holder, the nature and thickness of the background material, the imaging optic, and the detector. We define two efficiencies, a total efficiency $\varepsilon_t$ which includes all of the elements of the system, and an imaging efficiency, $\varepsilon_i$, including only the elements after the sample. The imaging efficiency is important in setting the dose. The noise in the image is assumed to be solely due to photon counting statistics (i.e. shot noise). In Table 1 we give formulae for the required number of detected photons per resolution element to achieve a given signal-to-noise ratio in the image, the fluence illuminating the sample, the energy required from the source, and the dose absorbed by the sample.

To calculate the area and depth of the resolution element and the scattering cross-section, we assume that the smallest resolvable features of a sample can be approximated as spheres in a background material[1]. The interaction properties are functions of the complex indices of refraction of the sample and background materials, which have been calculated from complex atomic scattering factors[2]. For holography, we use the Rayleigh-Gans scattering cross section[3]. The cross-section is proportional to the square absolute value of the difference in index between the two materials, and to the fourth power of the diameter of the spherical resolution element.

---

* This manuscript was prepared for the proceedings of the SPIE conference on *Soft X-Ray Microscopy*, held July 1992, San Diego, eds. J. E. Trebes and C. J. Jacobsen.

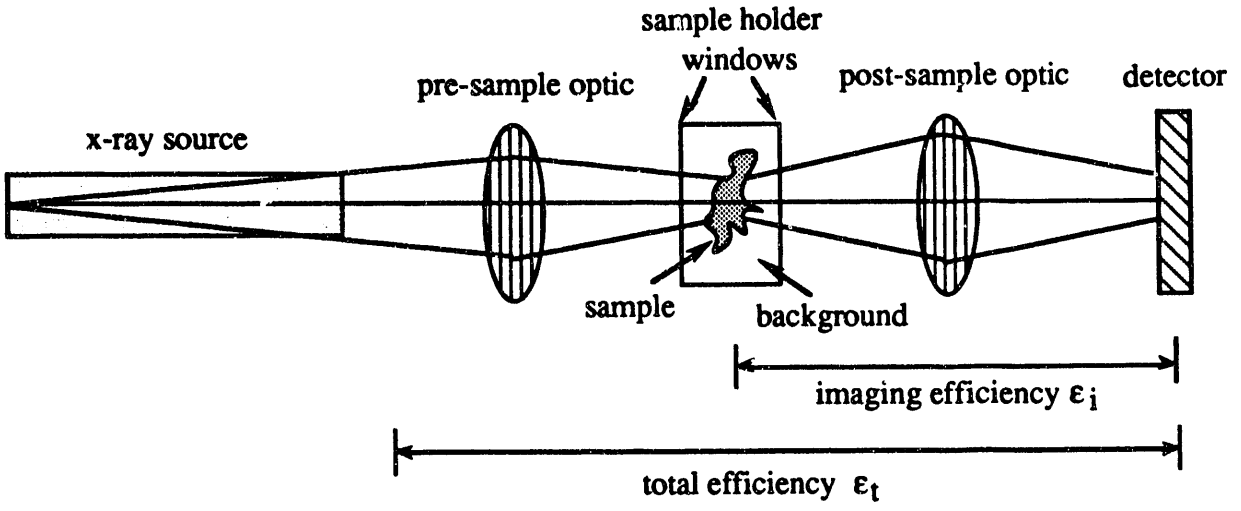


Figure 1. Schematic of systems for imaging and scanning microscopy and for holography.

Table 1 Formulae for x-ray imaging source energy and sample dose

| quantity | microscopy | holography |
|---|---|---|
| number of detected photons per res. elem. | $N = R^2 \frac{T_{obj} + T_{back}}{(T_{obj} - T_{back})^2}$ | $N = R^2$ |
| fluence | $F = N h\nu / (\varepsilon_t A_{re})$ | $F = N h\nu / (\varepsilon_t \sigma_s)$ |
| required energy | ——— $E = F A$ ——— | |
| absorbed dose | ——— $D = F\kappa_a \varepsilon_t/\varepsilon_i$ ——— | |

| | |
|---|---|
| R | signal-to-noise in the image |
| $T_{obj}$ and $T_{back}$ | transmission of object and background |
| $\varepsilon_t$ and $\varepsilon_i$ | total and imaging efficiencies |
| $A_{re}$ | resolution element area |
| $\sigma_s$ | scattering cross section of the res. elem. |
| A | area of sample |
| $\kappa_a$ | absorption opacity per unit mass |

## 2. SOURCE ENERGY AND SAMPLE DOSE FOR THREE EXAMPLES

We illustrate the parameters for imaging using three examples, one for each mode. The efficiencies are listed in Table 2. These numbers are meant only to be illustrative, and not specific to any present operating imaging system. In some cases they represent higher efficiencies than currently available; values which may be strived for in the near future, while in other cases further improvement may be expected.

Table 2. Assumed efficiencies for three imaging modes

| mode | pre-sample optic | post-sample optic | detector |
|---|---|---|---|
| holography | .05 | (1) | .2 |
| scanning | .1 | (1) | .5 |
| imaging | .1 | .1 | .2 |

For each case we assume that the sample holder windows are 60% transmissive and that the background is 2 μm thick. The loss in the background which is wavelength and material dependent is included in the calculation. The resolution element is taken to be a 300Å diameter sphere and a signal-noise ratio of 5 per resolution element is imposed. Two sample/background materials are considered: protein in water and gold in a 50-50 water-protein mixture.

In Figure 2a we show the required source energy plotted versus wavelength in the soft x-ray region near the water window (23.2 Å - 43.6Å) for the three imaging modes. The x rays must be spatially coherent for holography and scanning microscopy, but not for imaging microscopy. For all three modes the energy is minimized within the water window. With holography, the optimal region also extends just outside the long wavelength limit of the water window, due to the scattering by carbon near its K-edge (see ref. 1). For the assumed efficiencies, scanning microscopy requires a lower source energy (~10 μJ) than the other imaging modes. This is because an imaging optic is not needed and because a low space resolution and thus high efficiency detector, such as a proportional counter, can be used (see Table 2).

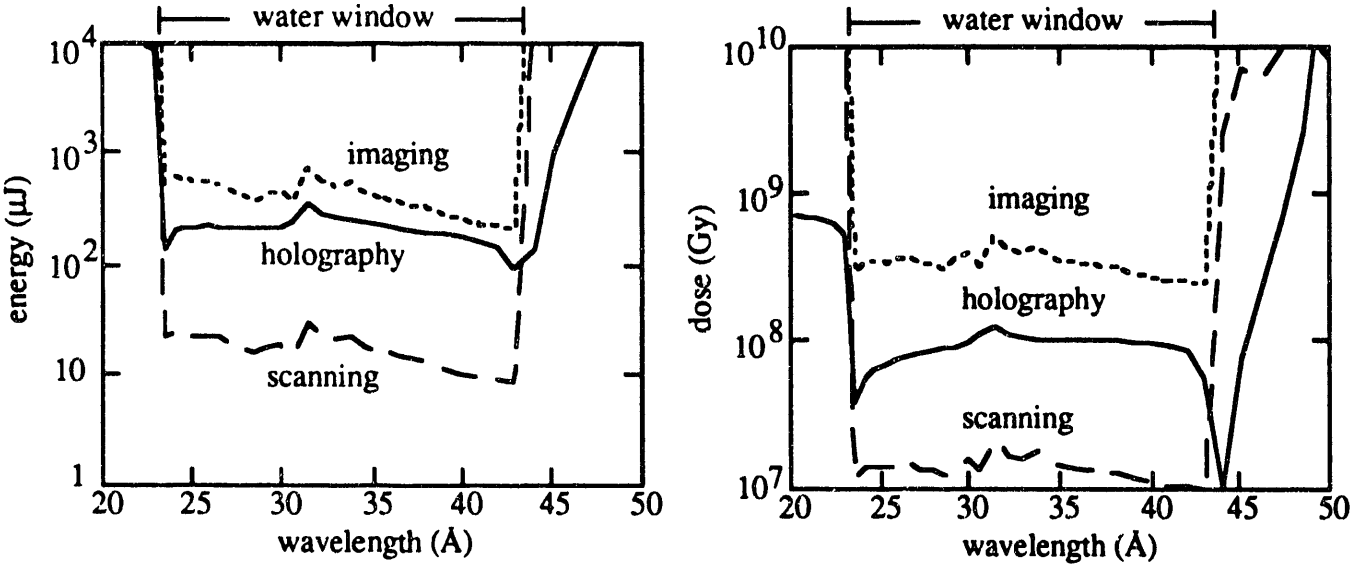


Figures 2a and 2b. The source energy and sample dose are shown for imaging microscopy, scanning microscopy and holography for wavelengths near the water window. Coherent radiation is required for holography and scanning microscopy but not for imaging. The dose is measured in Grays (Gy), where 1 Gy ≡ 1J/kg = $10^4$ erg/g = $10^2$ rad.

In Figure 2b we show the dose absorbed by the protein in making the image. The two microscopy methods have a relatively flat minimum throughout the water window, while holography has a sharp minimum just outside the water window at about 44 Å. This minimum for holography is due to the scattering by the real part of the refractive index (the "anomalous dispersion") due to carbon while absorption is low. Imaging microscopy has a high dose because the inefficiencies of the imaging optic and space resolving detector occur after the sample, thus requiring a higher fluence to irradiate the sample.

In order to reduce the source energy requirements and more importantly to reduce the sample dose, we consider the use of colloidal gold labeling. Such labeling has been developed for electron microscopy during the last 15 years[4]. In this method, spherical aggregates of gold atoms (called "particles") are formed in a colloidal suspension. The particles are then attached to antibodies, which are specific to various sites within a sample. The labeled antibodies are then introduced to the sample where they attach, marking specific sites. Colloidal gold particles between 10Å and 400Å in diameter have been used, although it is somewhat difficult to place the larger particles into wet samples. Gold is a very efficient scatterer and a good absorber. It can therefore be viewed at high contrast relative to moderate thicknesses of naturally occurring materials. In Figures 3a and 3b, we illustrate the source energy and dose for imaging such gold particles which are 300 Å in diameter. The energy and dose are reduce by at least a factor of 50 compared to optimal imaging of protein in water. For all cases, the optimal wavelength is outside the water window at wavelengths of 44Å - ~ 50Å. The results from the relative flatness of the gold absorption and scattering in this wavelength region combined with the large reduction in the protein absorption to the long wavelength side of the carbon K-edge. Such a technique would deliver a high resolution image of the positions of the gold particles superimposed upon a more modest resolution (as determined by shot noise due to the lower contrast) image of the natural structure, a combination that may prove useful in answering certain well-posed structural questions. The relative locations of various labeled sites could also be determined with high resolution. The lower dose accompanying such imaging is particularly attractive.

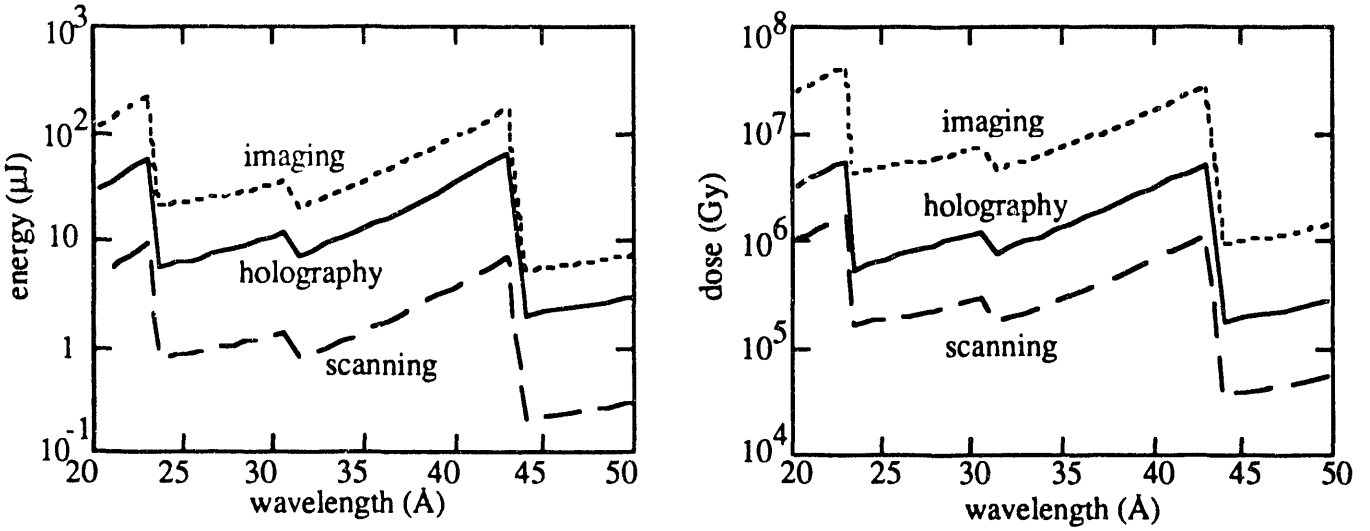


Figure 3a and 3b. The energy and dose are shown for imaging 300 Å gold spheres in a 50-50 protein-water background. The dose is to the protein in the background matter.

From the results shown in Figures 2 and 3, we suggest the following optimal wavelengths for imaging: For microscopy of natural, unlabeled samples (either imaging or scanning) wavelengths within the water window (23.2–43.6Å) are optimal as was realized long ago by Sayre and colleagues [5] For holography we suggest a wavelength just outside the water window at about 44Å, or near the short wavelength edge (24 Å) if thicker water layers or support foils are present. For imaging with gold labeled samples, wavelengths outside the water window in the range 44Å to about 50Å, appear to be optimal in that they minimize the dose to carbon containing biological materials, while maintaining large interaction cross sections and therefore low incident source energy.

## 3. DOSE AND TIMESCALE CONSIDERATIONS

In Tables 3a and 3b we compare several characteristic doses for biological sample damage of various sorts to the minimal (as function of wavelength) doses for imaging. Clearly the doses involved in high resolution x-ray imaging are very damaging to the sample. They will kill any live cell, cause chemical damage by ionization and subsequent bond breaking, possibly heat the sample and possibly vaporize the sample. If vaporization occurs, hydrodynamic motions will destroy the sample. In order to consider the effects of such doses on the quality of an image, we must compare timescales for damage to those need to make an image. The goal is then to capture an image before features of the sample of the desired resolution scale are destroyed.

Table 3a Characteristic damaging doses

| process | dose (Gy) |
|---|---|
| kill a hardy bacterium | $10^4$ |
| chemical damage | $10^5 - 10^7$ (??) |
| $\Delta T = 100K$ | $4x10^5$ |
| vaporize water | $2x10^6$ |
| 1 eV/ atom | $10^7$ |
| vaporize everything | $10^7$ |

Table 3b Characteristic imaging doses

| mode | dose (Gy) protein | gold-label |
|---|---|---|
| holography | $10^7$ | $10^5$ |
| imaging | $3x10^8$ | $10^6$ |
| scanning | $10^7$ | $4x10^4$ |

*Dose ~ $(res.)^4$

Several timescales associated both with natural motions of the sample and with the exposure to the x rays are listed in Table 4. One concern is movement of sample features by a distance comparable to the resolution element size. Such motion, if it occurs during the process of making the image, will blur the image, thus compromising the resolution. Several natural processes can cause motions. Normal dynamics of a living cell involves may well involve motions of 300Å in milliseconds. Brownian motion is a well know phenomenon in live cells, certainly at larger (visible light) scales. Certainly such motion may be inhibited by the structural components within the cell. However, it is reasonable to assume that objects of some size scale above the resolution scale will have freedom to move around in a Brownian manner. Using the classical formula for Brownian motion in water we estimate that objects of 1 μm in size will

move 300 Å in about 2 ms (see Table 4). If smaller structures (than 1 μm) are free to move, the timescale will be even shorter. The natural timescales set a minimum exposure time for an image to achieve a given resolution. If the exposure is made over a longer time, the motions will degrade resolution. Fixing and/or drying the sample can slow down, or even stop such motions. However, such sample preparation may alter the structure, thus defeating one of the main promises of x-ray micro-imaging– that of getting of structures in their live configuration.

Table 4. Timescales for natural motion and x-ray exposure related processes

| process | timescale (s) |
|---|---|
| | natural |
| biological dynamics | $(10^{-3}\text{s}\ ?)$ |
| Brownian motion | $2\times10^{-3}\ \text{s}\left(\frac{d}{300\text{Å}}\right)^2\left(\frac{R_b}{1\mu\text{m}}\right)$ |
| | Exposure |
| conductive cooling | $6\times10^{-2}\ \text{s}\left(\frac{D}{10^7\text{Gy}}\right)\left(\frac{R_c}{10\mu\text{m}}\right)^2\left(\frac{\Delta T}{10\ ^\circ\text{K}}\right)$ |
| x-ray-chem diffusion | $10^{-5}\ \text{s}\left(\frac{d}{300\text{Å}}\right)^2\left(\frac{R_f}{50\text{Å}}\right)$ |
| hydro expansion | $3\times10^{-11}\ \text{s}\left(\frac{D}{10^7\text{Gy}}\right)^{-1/2}\left(\frac{d}{300\text{Å}}\right)$ |

| | |
|---|---|
| d | resolution |
| $R_b$ | size of Brownian mover |
| $R_f$ | size of x-ray-chem fragment |
| D | dose |
| $R_c$ | size of cooled sample holder |

In addition to the natural processes, several time-dependent processes are associated with the x-ray dose to the sample. These processes include thermal expansion (both in the limit of heating and in the limit of vaporization) and radiochemical processes. Soft x-ray irradiation usually involves the creation of energetic photo-ejected and Auger electrons which then transfer energy to a number of secondary electrons; these secondary electrons deposit there energy within a limited range of order 200Å in organic materials. The radiochemical reactions which follow disrupt the functioning of the cell, causing reproductive death at doses of order 10 Gy, or physiological death at higher dosses. However, the important question for x-ray (and also electron) microscopy is not whether the cell is killed in the imaging process, but whether the image is a faithful representation of the structure of the cell. Therefore, secondary consequences such as mass loss and possible morphological changes are of primary concern. Soft x-ray microscopy studies of v. faba chromosomes[6] suggest that for doses of order $10^6$ Gy, mass loss and morphological changes occur over a timescale longer than 1 msec, so that structurally faithful images of radiation sensitive specimens can be obtained on msec or shorter timescales. Cryoprotection and the use of sulfhydryl reagents offer further strategies for reducing the consequences of radiation damage in non-flash imaging.

If the dose is high enough so that the retained energy would result in an unacceptable temperature rise (say to the boiling point of water) it may be possible to keep the sample cool by using a long exposure time (i.e. decreasing the flux onto the sample keeping the fluence constant ). The minimum such exposure time is called the conductive cooling time, estimated to be of order 60 ms for typical parameters in Table 4. This estimate is ideal in that it assumes that once the heat is conducted out of the water in the sample holder, it can be easily removed. Two other timescales set maximum exposure durations. We define an x-ray induced chemical diffusion timescale as the time for molecular fragments, resulting from x-ray ionization and subsequent chemical bond breaking, to diffuse away from their origin by a distance equal to the resolution element size. If the dose is high enough so that a significant number of such fragments are created, then it is important to keep the exposure shorter than the x-ray chemical diffusion timescale in order to get a clear image. The other timescale is the hydrodynamic timescale. This is important when the material becomes vaporized by the deposited x-ray energy. If vaporization occurs, small features (for example protein within water) will expand into surrounding material very rapidly. It is then necessary to get an image before these features have approximately doubled in size[7]. The hydro expansion timescale is of the order of 30 psec for typical doses associated with 300 Å resolution of unlabeled samples. Since the dose scales as the inverse fourth power of the resolution size, the hydro timescale goes like the third power of resolution size. For 100 Å resolution the time is approximately 1 psec.

Considering the characteristic doses and timescales, it is natural to define three possible imaging regimes. The first is the *low dose regime*. For doses less than about $10^6$ Gy we expect the temperature rise to be small enough so that the water is not to be vaporized. Therefore hydrodynamic motion is not expected to be a problem and ultrashort exposures (<1 nsec) are not necessary. Moderately short exposure (< 1 msec to 1 μsec) may still be needed to avoid image degradation due to natural motions and x-ray induced chemical diffusion. To keep the dose so low and still get high resolution (~300Å) 3D images will likely require labeling as we discussed for gold microspheres. Alternatively, lower resolution (~600Å) images may be possible in the *low dose regime*. The second imaging regime is the *high dose, long exposure regime*. This applies to doses > $2 \times 10^6$ Gy, and exposures longer than about 10 ms. Here it is possible to avoid heat build-up by conductive cooling. This mode is likely appropriate for synchrotron based imaging, but not for x-ray lasers which are typically much shorter in duration. There may still be a problem with natural motions and chemical diffusion for such long exposures. The third imaging mode is the *high dose, short exposure regime*. This corresponds to doses > $2 \times 10^6$ Gy and exposures < 30 psec. It is appropriate for the imaging of live natural samples. In this mode one captures the image before hydrodynamic motion ultimately destroys the sample. Such short exposures can easily stop natural motions and chemical diffusion. It is the natural mode for x-ray lasers or other high brightness short pulse sources.

## 4. CONCLUSIONS

Based on considerations of the x-ray interactions with the sample, and on schematic descriptions of imaging set-ups we make the following conclusion: The optimal energy for imaging is in the water window for microscopy and just outside for holography. With high particle labeling, for example colloidal gold, the optimal wavelengths are some what longer that the carbon K-edge. For 300 Å resolution images, 10 – 1000μJ of energy is required. Doses to protein are likely to be above $10^7$ Gy. Colloidal gold labeling can reduce the energy and dose by a factor of about 50. Finally, three regimes for high resolution imaging have been identified. They are the *low dose regime*, suitable for gold-labeled sample, the *high dose-long exposure regime* in which conductive cooling may keep the temperature down, but

natural motion and x-ray chemical induced diffusion may degrade resolution for wet unfixed samples, and the *high dose-ultra short exposure regime*, in which an image is captured before dose-induced hydrodynamic expansion degrades resolution.

## ACKNOWLEDGEMENTS

This work was performed under the auspices of the U. S. Department of Energy by the Lawrence Livermore National Laboratory under contract number W-7405-ENG-48.

## REFERENCES

1. R. A. London, M. D. Rosen, and J. E. Trebes, *"Wavelength Choice for Soft X-ray Laser Holography of Biological Samples,"* App. Optics **28**, 3397-3404 (1989).
2. B. L. Henke, P. Lee, T. J. Tanaka, R. L. Shimabukuro, and R. K. Fujikawa, *"Low-Energy X-Ray Interaction Coefficients: Photoabsorption, Scattering, and Reflection,"* Atom. Data and Nuc. Data Tables **27**, 1 (1982).
3. H. C. van de Hulst, *Light Scattering by Small Particles*, (Dover, New York, 1981).
4. G. M. Hodges, J. Southgate and E. C. Toulson, *"Colloidal Gold – A Powerful Tool in Scanning Electron Microscope Immunocytochemistry: An Overview of Bioapplications,"* Scanning Microscopy **1**, 301-318 (1987).
5. D. Sayre, J. Kirz, R. Feder, D. M. Kim, and E. Spiller, Ultramicroscopy **2**, 337-341 (1977).
6. S. Williams, X. Zhang, C. Jacobsen, J. Kirz, S. S. Lamm, S. Lindaas, and J. Van't Hof, *"Measurements of Wet Metaphase Chromosomes in the Scanning Transmission X-ray Microscope,"* to appear in J. Micros (1992).
7. J. C. Solem, *"Imaging Biological Specimens with High-Intensity Soft X Rays,"* JOSA-B **3**, 1551 (1986).

# Prospects for X-ray Microscopy in Biology

Joe W. Gray
415-476-3461
gray@dmc.ucsf.edu

Division of Molecular Cytometry
Department of Laboratory Medicine
University of California
San Francisco, CA
&
Lawrence Berkeley Laboratory
Berkeley, CA

Light microscopy, scanning and transmission electron microscopy, x-ray and electron diffraction and atomic force microscopy are all being applied to investigation of the organization of macromolecules in cells. The information generated by these combined techniques has led to our current understanding of the remarkable complexity and diversity of the cellular molecular environment. Light microscopy has proved particularly useful for non-destructive analysis of the dynamic behavior of living cells. Structures as small as a few hundred Angstroms in diameter can be detected in intact cells when distinctly stained and well separated from similar structures. However, true shape analysis of molecular structures in the light microscope is limited by the wavelength of light to ~0.25 μm. Electron microscopy, diffraction and scanning microscopes allow near atomic resolution of isolated structures and electron tomography is being applied in investigation of macromolecular organization in the cellular environment. However, these studies require some form of sample preservation (e.g. embedding, fixation, mounting in vitreous ice, critical point drying, etc.) and cellular disassembly (e.g. physical sectioning, cellular disruption and organelle isolation, etc.). These preparative techniques complicate analyses; especially those aimed at micromolecular assemblies intermediate in size (100-1000 Å). X-ray microscopy will be an appealing addition to these analysis techniques if it can be developed for analysis of intermediate sized structures in living cells.

The challenges facing X-ray microscopists can be appreciated by considering the role of X-ray microscopy in analysis of the organization of DNA in mammalian chromatin. An important goal of such studies is to understand how approximately 1 meter of DNA plus associated chromatin proteins are packed into a cell nucleus roughly 5 μm in diameter. This must be accomplished in a manner compatible with condensation of the DNA to form chromosomes at mitosis and almost complete, regional decondensation to permit DNA replication and translation. The packing density changes almost four orders of magnitude during these processes. In addition, the organization must permit the transport of macromolecules (enzymes, DNA binding regulatory proteins and RNA) into and out of the nucleus.

Much is known about the chromatin organization. The DNA is organized at several levels. First, the DNA is coiled around proteins called nucleosomes to form "beads on a string" which are visible in the electron microscope when spread on a flat surface. The "beads" are further packaged to form 30 nm fibers, also visible in the electron microscope. The 30 nm fibers are organized into high order structures. Details of these higher order structures are largely unknown. Eventually, however, the DNA and associated proteins are packaged into interphase nuclei or chromosomes. The higher order chromatin structure (e.g. shape, size, nuclear location, dynamic behavior and protein composition) are biologically interesting because they may play a controlling role in gene expression and transcription. However, these structures are difficult to study. They are too small to be resolved in the light microscope and the concern remains that they may be distorted by the preparative procedures required for electron microscopy and atomic force microscopy. Thus, alternate analysis procedures are needed.

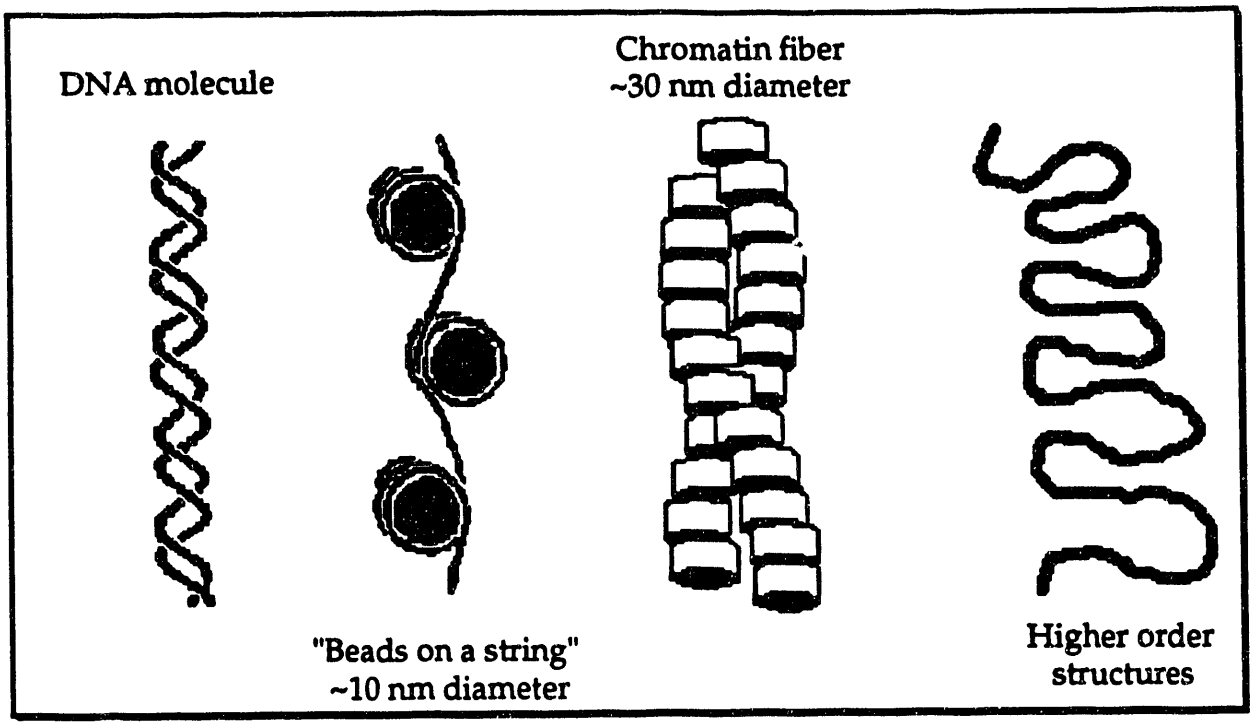


X-ray microscopy is an interesting adjunct to more well developed imaging techniques because it may, in theory, be used to image higher order structures of chromatin and other macromolecules in a physiologically normal environment or even in a living cell. In addition, it may provide limited dynamic information about the motion of macromolecules. However, several challenges must be met before X-ray microscopy can contribute to structural investigations. 1) Macromolecular structures are "embedded" in a dense protein environment of high complexity in a living cell. Procedures must be developed to stain selected macromolecules with X-ray dense materials so that they can be distinguished from the chemically similar protein milieu in which they are embedded. This must be accomplished without altering the organization of the structures under study. Protein structure specific staining is often accomplished using labeled monoclonal antibodies. Unfortunately, this approach may have limited utility in X-ray microscopy because antibody molecules, ~100Å in size, are almost as large as the structures to be studied. Thus, other approaches must be developed. One promising approach is to attach electron dense molecules to protein components that will subsequently be assembled into macromolecules by the living cell. 2) X-ray microscopy and associated image display and analysis techniques must be developed so that they can be used routinely by structural biologists. This will be especially important to assist biologists during the trial and error development of useful staining procedures. Systems capable of generating only the occasional image are not likely to be useful. 3) Most problems of interest in intermediate resolution structural biology are three dimensional. Thus, multi-view microscopy will be required to allow three dimensional reconstruction. The challenge will be to generate sufficient information for reconstruction without damaging the structures under study. 4) Investigation of time dependent changes in chromatin organization will be especially important to studies of the role of chromatin high order organization on gene

replication and transcription. Information about changes in structure during cellular response to external stimuli (e.g. mitogenic stimulation of DNA synthesis or induction of specific gene expression) will be especially important. The X-ray doses required to visualize specific structures directly are likely to be too destructive to allow sequential analyses. However, one idea worth considering is that X-ray microscopy may allow high resolution analysis of molecular movement using the concept of fluorescence recovery after photobleaching (FRAP) developed for visible light microscopy. In this application, cells are stained with a fluorescent dye that can be excited (and bleached) by a tightly focused X-ray beam. Fluorescence measured after a second X-ray pulse at the same site will provide information about the rate at which fluorescently stained but unbleached molecules can move into the measurement volume. Of course, localized X-ray damage such as cross-linking may frustrate these studies as well.

Perhaps the most significant challenge for x-ray microscopists interested in biological applications is to develop the technology to the point where its biological utility can be effectively tested. This is important since the feasibility of x-ray imaging is not yet proven, even theoretically. Structural biologists are likely to remain skeptical of the utility of x-ray microscopy until it is demonstrated esperimentally. Unfortunately, this will be an expensive undertaking at a time when resources are scarce.

# FEMTOSECOND OPTICAL PULSES?

by
Charles V. Shank
Lawrence Berkeley Laboratory

The prospect of femtosecond optical pulses is very exciting for the field of time resolved spectroscopy. Currently the only sources available to study ultrafast events are in the infrared to blue regions of the spectrum. In experiments to study such processes as fast chemical reactions and rapid phase changes, all the current tools only permit study through interactions with the electronic absorption. A far more desirable approach would be to directly determine the positions of nuclei. Techniques of X-ray measurements such as diffraction and EXFAS open up the possibility of making direct measurements of nuclear positions on a femtosecond time scale, a time scale less than a vibration.

The free electron source proposed at SLAC would be most desirable if the X-ray energy could be maximized at an energy of approximately 1 KeV. Secondly, if a means could be found for creating a synchronous optical pulse it would be possible to initiate events optically. Finally, if a trade-off between peak power X-ray power and repetition rate could be achieved, the source would be even more useful.

The proposed source is so novel and new it is my view that uses would be found to take advantage of its unique properties. Time resolved spectroscopy could be one of the more important applications.

To appear in the Proceedings of the
Workshop on Scientific Applications of
Short-Wavelength Coherent Light Sources
S.S.R.L., Stanford, 21 October, 1992

# Research in Chemical Physics, Surface Science,and Materials Science, with a Linear Accelerator Coherent Light Source

Charles S. Fadley

Department of Physics, University of California-Davis
Materials Science Division, Lawrence Berkeley Laboratory

A number of exciting possibilities would be opened up for research in chemical physics, surface science, and materials science by a short-wavelength linear-accelerator coherent light source (LCLS). However, radiation damage by such powerful pulses in studies of condensed matter samples presents potential problems that should be assessed further.

The proposed energy range for these sources overlaps that of prime interest at the soon-to-be-commissioned Advanced Light Source (i.e., approx. 100 to 1000 eV) and so a comparison of the brightnesses and time structures of these two sources is of interest. As illustrated in Fig. 1, at 300 eV and with an energy spread of 0.3 eV, the LCLS is estimated to deliver $10^{14}$ photons in a pulse of 0.2-0.5 psec in width and with a gap of 8 msec between pulses, for an overall flux of $10^{16}$ photons per second [1]. An ALS undulator by contrast should produce $10^{6}$ photons in a much broader pulse of 30 psec, but with a much shorter gap of 8 nsec, for an overall flux of $10^{14}$ photons per sec [1]. Thus, the LCLS is about $10^{8}$ times brighter during the pulse, and $10^{2}$ times brighter on average than the ALS, and the LCLS is much

better suited to time-resolved studies on the psec level, with the long gap between pulses suggesting the use of time-of-flight methods for detection.

Pump-probe experiments are an obviously advantageous type of measurement to do with such a source. These could be done in several modes:

-Pumping with a visible/uv laser to heat the sample, and then watching for structural changes or phase transitions via x-ray scattering, EXAFS, or photoelectron spectroscopy or diffraction. This type of experiment has also been discussed by C.V. Shank in this workshop.

-Pumping with x-rays to occupy low-lying excited states, and then probing these with a visible/uv laser, or reversing the assignment of the pump and probe radiation.

-Splitting the x-ray beam in some way and pumping and probing with the same wavelength.

-Using harmonics of the LCLS (odd on-axis and even off-axis) to yield different well-synchronized wavelengths for pumping and probing.

A crucial question in such experiments is the degree to which the pump and probe sources could be synchronized: splitting the beam or using harmonics as mentioned above represent two possible solutions to this problem, but more work also is needed to determine how well a visible/uv laser could be synchronized to an LCLS.

Time-resolved structural studies of either molecular beams or mass-selected clusters represent one particularly promising direction for study. Such dilute targets require high photon fluxes to be studied, and they also have the advantage of being continuously replenished, thereby reducing the

radiation damage problems that are inherent with fixed condensed-matter targets. As one example of such experiments, an extension of the recent pioneering work of Zewail and co-workers using lasers and an electron beam deserves mention [2]. As shown in Fig. 2, a molecular beam was in this case pumped at one wavelength ($\lambda_1$) by a single colliding-pulse mode-locked dye laser that also produced a synchronous amplified pulse at another wavelength ($\lambda_2$). The second pulse was used to excite electrons from a gold photocathode, and these were accelerated up to about 15 keV ($\lambda_e \simeq 0.1$ Å) to produce a pulse of about 1 psec in duration. The diffraction of these electrons from the molecular beam was then monitored by a two-dimensional CCD camera as a function of the delay between the two pulses. Thus, the time evolution of the structure of an excited molecule that is undergoing some sort of transformation or dissociation can in principle be studied. Replacing the electron beam with a suitably synchronized x-ray laser beam in the 0.1-1.0 Å range could permit doing even more precise time-dependent structural studies due the more ideal nature of x-ray scattering. Again, synchronization issues are crucial here, as is the need to detect extremely high scattered photon fluxes. Going to grazing angles of incidence on a single-crystal solid sample could also permit doing analogous time-resolved diffraction studies of processes on surfaces.

The high brightness of an LCLS could yield diffraction or spectroscopic data sets of sufficient statistics with only a few shots of the laser, provided that detection systems are developed which can handle the much higher rates of photons, electrons, ions, or neutral species that will emerge. For example, in photoelectron emission from a solid sample, a

single pulse of $10^{14}$ photons interacting with a single atomic subshell will produce a total of $10^{8}$-$10^{10}$ photoelectrons over the $\pi$ steradians above the surface. Thus, a spectrum or energy distribution curve in a well-defined direction of emission ($\pm$ a few degrees resolution) could be accumulated to 1% statistics in a single pulse or at most a few pulses. The left panel of Fig. 3 shows a calculation of the photon stimulated desorption from elemental Si due to L-shell excitation, and here again, the number of particles emitted is in the range of $10^{10}$, suggesting single-shot or few-shot measurement of photon-stimulated desorption, provided that the detection system can respond fast enough. Time-of-flight techniques with electrons, ions, or post-ionized neutrals could assist with this considerable detection problem. Ultimately, such a facility could permit carrying out what are often called "complete" experiments on atoms, molecules, clusters, or surfaces, in which not only the energies of the outgoing particles are measured, but also their angular distributions and their spins. Measuring electron spin is particularly demanding, since it entails a net increase in counting times of about $10^{4}$x.

The holographic imaging of various structures could also benefit from such a high-brightness x-ray source. Such imaging can be separated into two categories: that in which the reference wave is external to the object and is provided by the incident beam [3], and that in which the reference wave is localized in origin due to some sort of core-level atomic process [4]. The brightness of an LCLS would probably prevent focusing the external beam before its scattering from the sample, thus leading to what has been termed Gabor holography [3]. Experiments of this type with soft x-rays have

yielded resolutions in the 100-Å range to date [3]. By contrast, localized-source diffraction and holography from single-crystal surfaces can make use of x-ray excited photoelectrons, Auger electrons, or fluorescence x-rays [4], and in principle can image at the sub-Angström level. Electron emission holography is thus an extension of photoelectron diffraction, which is by now a well developed surface structural probe [5]. The holographic analysis of such data sets so as to directly yield three-dimensional atomic images was suggested some time ago [4], and this method has more recently been shown to be promising from an experimental point of view [5(b),6]. The basic principle of localized-source holography, together with the most simple mathematical imaging algorithm [4(b)], is shown in Fig. 4.

The localized-source holographic data sets are in general even larger than those required for a simpler diffraction study, and thus a brighter excitation source is a significant advantage. Measuring such electron diffraction patterns with an LCLS could in principle reduce data acquisition times to the microsecond level or smaller, permitting unique time-dependent studies of surface structural transformations. Doing the same holographic imaging experiment with fluorescence x-rays [4(a)] has the advantage that x-ray scattering is much more ideal, so that the final atomic images should be more accurate and aberration-free, but no experimental data of this type are as yet available. The potential advantage of XFH is illustrated for simulated images from a small cluster of atoms in Fig. 5 [7], However, the percent effect in the x-ray diffraction fringes is reduced by about $10^4$ relative to electrons, thus requiring much better counting statistics in the final data. An LCLS could be very useful for this type of atomic imaging as

well. Some other types of atomic structure studies that could benefit from an LCLS are time-dependent photoelectron diffraction, Fourier transform analyses of x-ray diffraction patterns, and the measurement and interpretation of x-ray speckle patterns.

Beyond the above experiments that would be of principle benefit in carrying existing techniques into much faster time domains, two additional effects could be studied fruitfully: Non-linear optical effects in the x-ray regime would be of interest, and studying them has hitherto been impossible due to a lack of brightness. Also, atom-specific photochemical or photodesorption processes could be studied by pumping certain core levels.

In studies on condensed matter specimens, the high number of photons per pulse and the higher overall average fluxes raise questions as to spectral broadening and specimen stability. Space charges of electrons and ions near the surface could influence outgoing particles. And the high amounts of power being absorbed by the sample could lead to rapid transformations (perhaps interesting to study, but perhaps a nuisance) and/or degradation. The approximate time scales of the various relaxation processes going on are shown in Fig. 6. The right panel of Fig. 3 indicates that, if we assume about 1 in 10 core-excited atoms at the surface are desorbed [8], the direct photon-stimulated desorption from Si would not ablate the surface faster than about 0.001 monolayer per sec. However, additional desorption and vaporization due to secondary absorption and relaxation processes could significantly increase this rate. An estimation

of the amount of local heating occurring for Si during a single pulse is shown in Fig. 7. During the pulse, the absorption depth ($d_{abs}$) is much shorter than the thermal diffusion length ($d_{diff}$), leading to a standard limiting approximation for estimating the time to heat to the melting point [9]. In this limit, one finds that the melting point would be reached in only about 1/5 of the pulse duration! A mitigating aspect is that, during the period between pulses, there will be diffusion away from the hot spot over distances of the order of about 5000 $d_{abs}$, permitting some sample recovery. However, this crude estimate suggests that there will be some rapid, irreversible alteration of a typical sample surface, and that more quantitative calculations of such effects are called for. Using grazing incidence to increase x-ray reflectivity R is one way to reduce such local heating effects. Scanning the sample surface under the beam so as to continually provide new material is another, although the mm-scale diameter of the beam would limit the degree to which this could be done with samples of normal size.

Thus, although there are obvious experimental challenges both in detecting the very high fluxes of particles that would be emitted by samples exposed to such ultrahigh-brightness x-ray sources and in assessing and dealing with various types of radiation damage to condensed matter specimens, there are nonetheless several very intriguing new areas of research that would become possible with such high-brightness x-ray sources.

## References:


[1] R. Tatchyn, private communication.

[2] J.C. Williamson, M. Dantus, S.B. Kim, and A.H. Zewail, Chem. Phys. Letters 196, 529 (1992).

[3] C. Jacobsen, M. Howells, J. Kirz, and S. Rothman, J. Opt. Soc. Am. A7, 1847 (1990); M. Howells and C. Jacobsen, Synch. Rad. News 3, 23 (1990).

[4] (a) A. Szöeke, in Short-Wavelength Coherent Radiation: Generation and Applications, edited by D.T. Attwood and J. Bokor, AIP Conference Proceedings No. 147 (AIP, New York, 1986); (b) J.J. Barton, Phys. Rev. Letters 61, 1356 (1988).

[5] (a) C.S. Fadley, in Synchrotron Radiation Research: Advances in Surface Science, edited by R.Z. Bachrach (Plenum Press, New York, 1992); (b) C.S. Fadley, Surf. Sci. Reports, in press.

[6 ] G.R. Harp, D.K. Saldin, and B.P. Tonner, Phys. Rev. Letters 65, 1012 (1990); G.S. Herman, S. Thevuthasan, Y.J. Kim, T.T. Tran, and C.S. Fadley, Phys. Rev. Letters 68, 650 (1992); L.J. Terminello, J.J. Barton, and D.A. Lapiano-Smith, J. Vac. Sci. Technol. B10, 2088 (1992); and S. Thevuthasan, R.X. Ynzunza, E. Tober, C.S. Fadley, M.A. van Hove, and C.S. Fadley, Phys. Rev. Letters, in press.

[7] P. Len, S. Thevuthasan, and C.S. Fadley, to be published.

[8] J. Yarmoff, R.S. Williams, and V. Rehn, private communication.

[9] N. Bloembergen, in Beam-Solid Interactions and Phase Transformations, Materials Research Society, Symposium Proceedings, Vol. 51 (MRS, Pittsburgh, 1986).

## Figures:

Fig. 1--Comparison of pulses from the proposed LCLS and the ALS.

Fig. 2--Synchronized laser pumping and electron diffraction from a molecular beam. From ref. 2.

Fig. 3--Estimation of photon stimulated desorption rates from elemental Si.

Fig. 4--Illustration of the formation of a localized-source hologram and the simple Fourier transform algorithm used to image atoms from it. Based on ref. 4.

Fig. 5--Calculated holographic images for both x-ray fluorescence and photoelectron emission from the central atom of the Mo cluster shown at the top of the figure. In the middle panel, the electron scattering strength is artificially reduced so as to be more ideal. From ref. 6.

Fig. 6--Approximate time scales of various processes occurring after the absorption of radiation are compared to the duration of the LCLS pulse.

Fig. 7--Estimation of the rate of heating of elemental Si during exposure to the LCLS pulse.

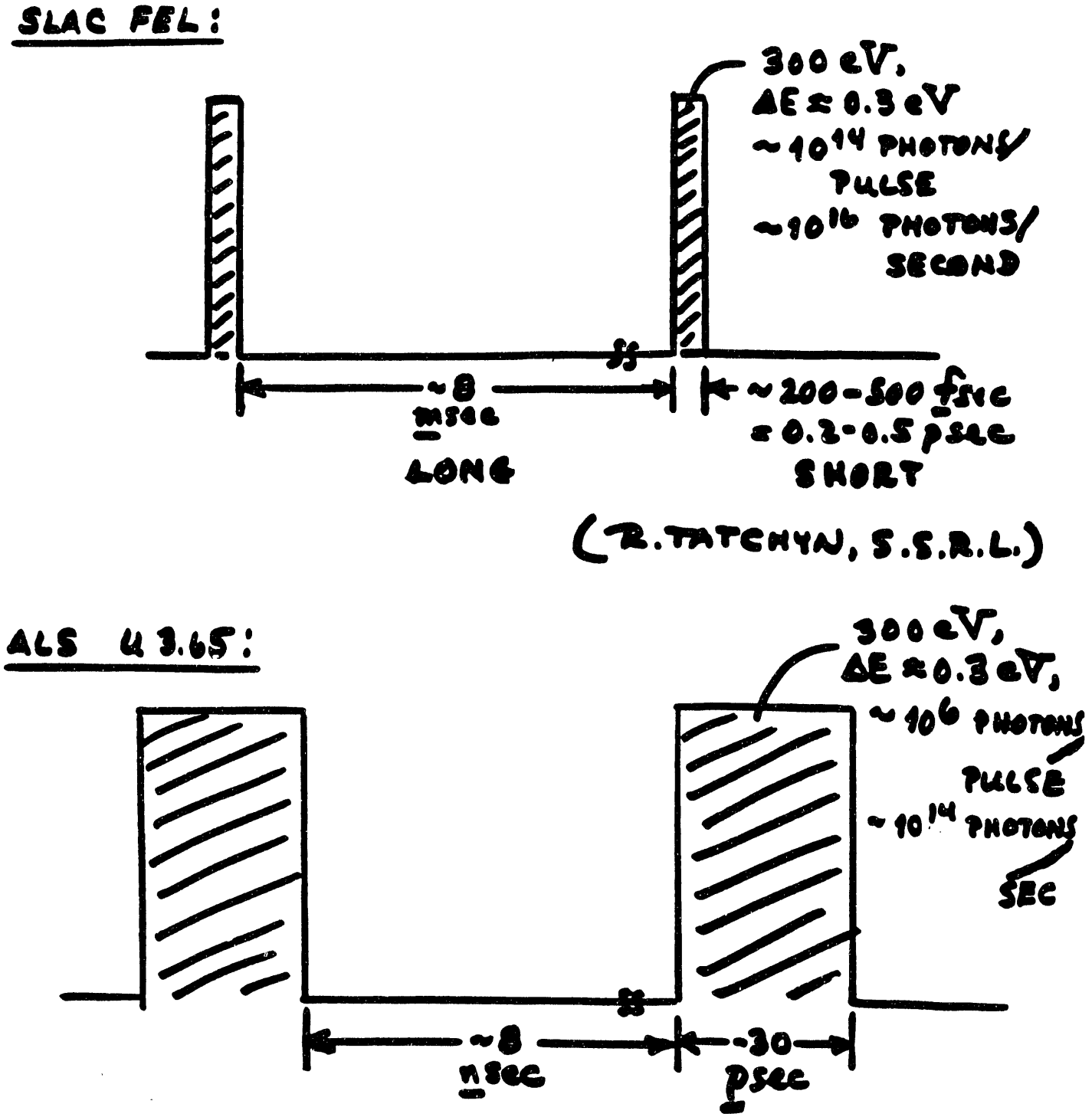
SLAC FEL:
300 eV,
ΔE ≈ 0.3 eV
~10^14 PHOTONS/
PULSE
~10^16 PHOTONS/
SECOND
~8
msec
LONG
~200-500 fsec
≈ 0.2-0.5 psec
SHORT
(R. TATCHYN, S.S.R.L.)
ALS U3.65:
300 eV,
ΔE ≈ 0.3 eV,
~10^6 PHOTONS
PULSE
~10^14 PHOTONS
SEC
~8
nsec
~30
psec

FIGURE 1

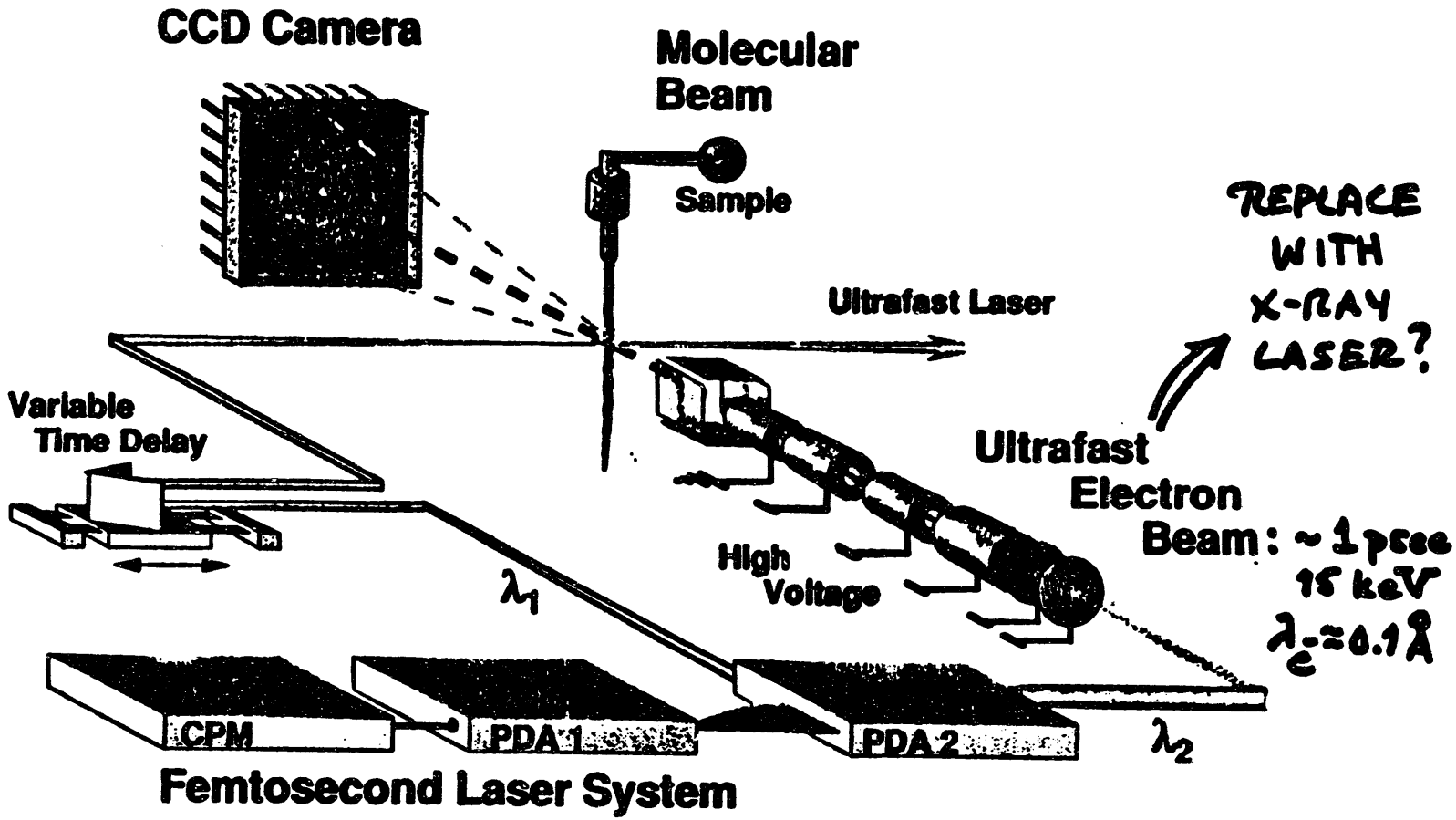


FIGURE 2

Fig. 1. The experimental arrangement for ultrafast diffraction. The colliding pulse mode-locked dye laser (CPM), when amplified (PDA), produces the two pulses: one at $\lambda_1$ to initiate the chemical changes and another at $\lambda_2$ to generate the ultrashort electron pulse. The electron beam, accelerated and focused by the high-voltage electrostatic lens arrangement, probes the molecular beam in the interaction region. The resulting gas phase electron diffraction pattern is recorded onto a two-dimensional CCD operated in direct electron bombardment mode. The delay time assembly is to control the relative timing between the two pulses.

WILLIAMSON . JANTUS . KIM . ZEWAIL

## PHOTON-STIMULATED ESTIMATED DESORPTION PER PULSE:

EXAMPLE : Si, $h\nu = 300$ eV, 1 mm$^2$
$\sim 10^{14}$ PHOTONS / PULSE

ASSUME : ~ 1/10 OF SURFACE-LAYER ATOMS CORE-EXCITED DESORB

$\sigma_{2s} + \sigma_{2p} \approx 1.4$ Mb

GET : $\frac{N(2s+2p \text{ EXCITED})}{N(@ \text{ SURFACE})} \approx 1 \times 10^{-4}$ / PULSE

$\frac{N(\text{DESORBED})}{N(@ \text{ SURFACE})} \approx 1 \times 10^{-5}$ / PULSE

$\sim 10^{10}$ ATOMS DESORBED PER PULSE
$\Rightarrow$ SINGLE-PULSE P.S.D.

1 ML AFTER ~1000 SEC. BUT WITH NO CONSIDERATION OF ADDITIONAL HEATING/VAPORIZATION

FIGURE 3

## Formation of a hologram

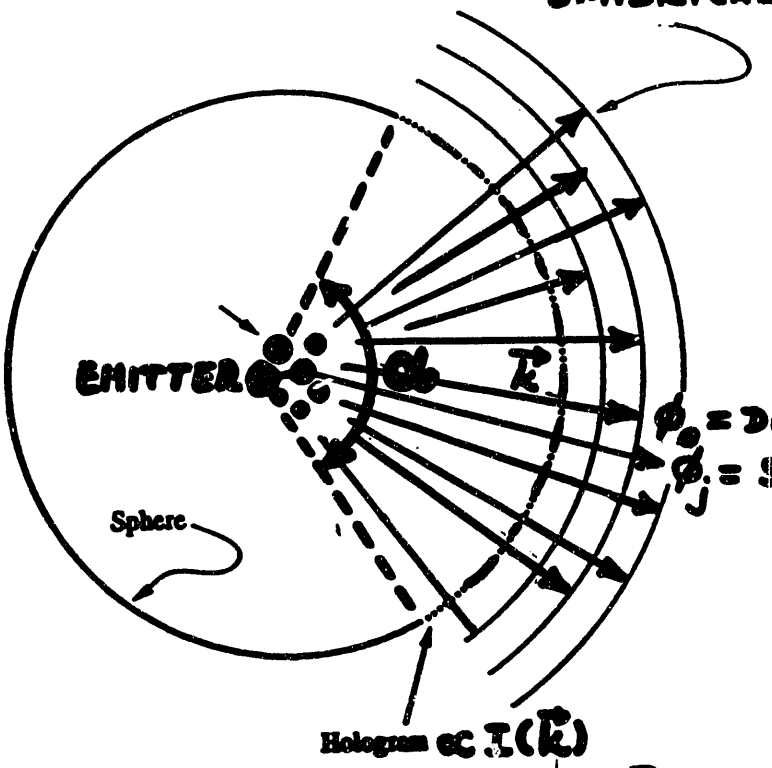


## Generation of a real image

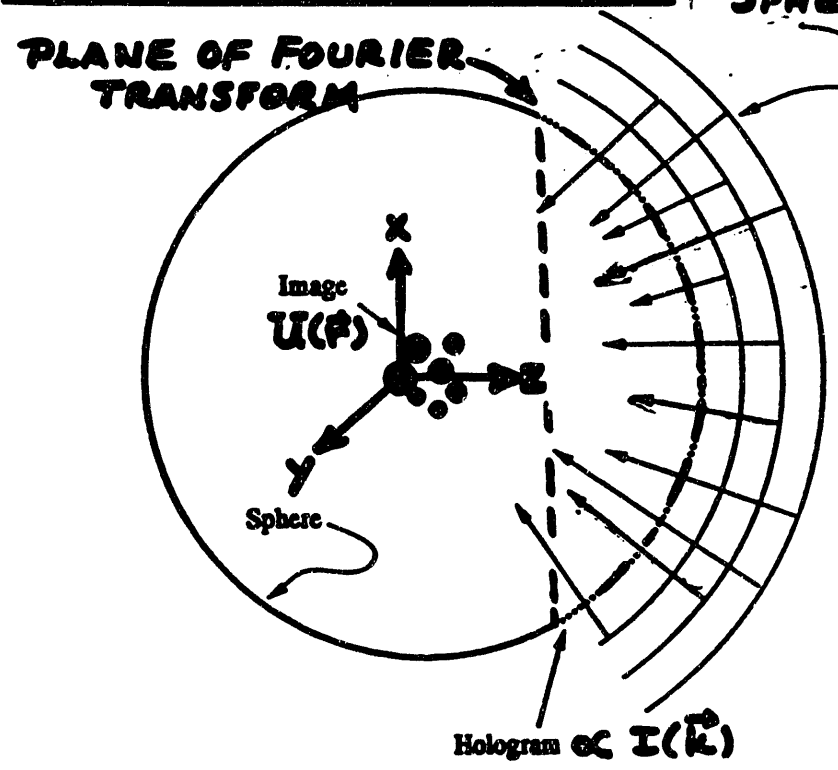


- NORMALIZE $I(\vec{k})$:

$$\chi(\vec{k}) = \frac{I(\vec{k}) - I_o}{I_o^{1/2}}$$

- GENERATE IMAGE:

$$U(\vec{r}) = U(x,y,z)$$

$$\propto \left| \iint_S \chi(\vec{k}) e^{-i\vec{k}\cdot\vec{r}} \, d\sigma \right|$$

$$\propto \left| \iint [\chi(\vec{k}) e^{-ik_z z}] \cdot e^{-ik_x x} e^{-ik_y y} \, dk_x \, dk_y \right|$$

$\propto$ 2-DIM. FOURIER TRANSFORM

[Szöke (1986), Barton (1988)]

FIGURE 4

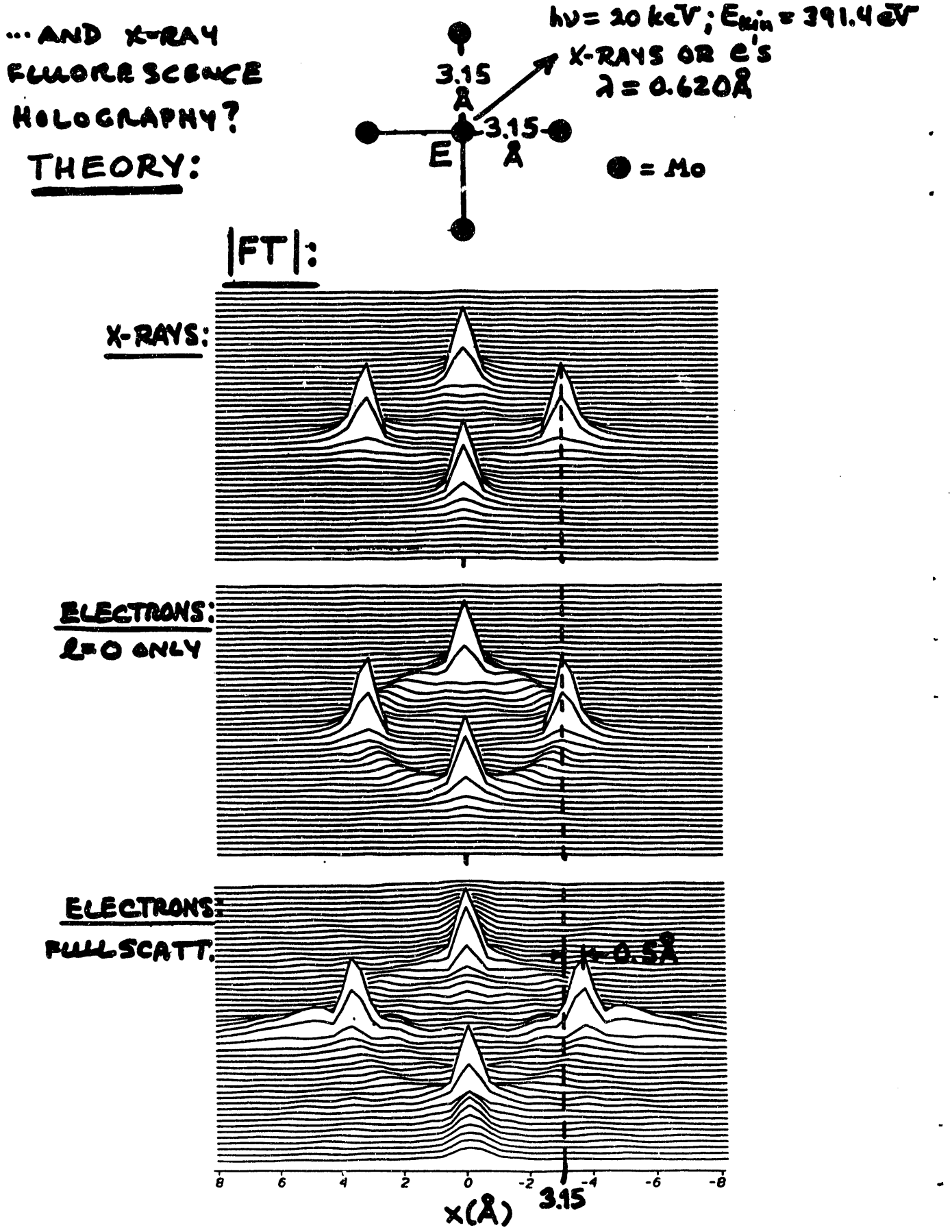
... AND X-RAY FLUORESCENCE HOLOGRAPHY?
THEORY:
hν = 20 keV; E_kin = 391.4 eV
X-RAYS OR e's
λ = 0.620 Å
3.15 Å
3.15 Å
E
= Mo
|FT|:
X-RAYS:
ELECTRONS: ℓ=0 ONLY
ELECTRONS: FULL SCATT.
d |r-0.5Å
8 6 4 2 0 -2 -4 -6 -8
3.15
x(Å)

FIGURE 5

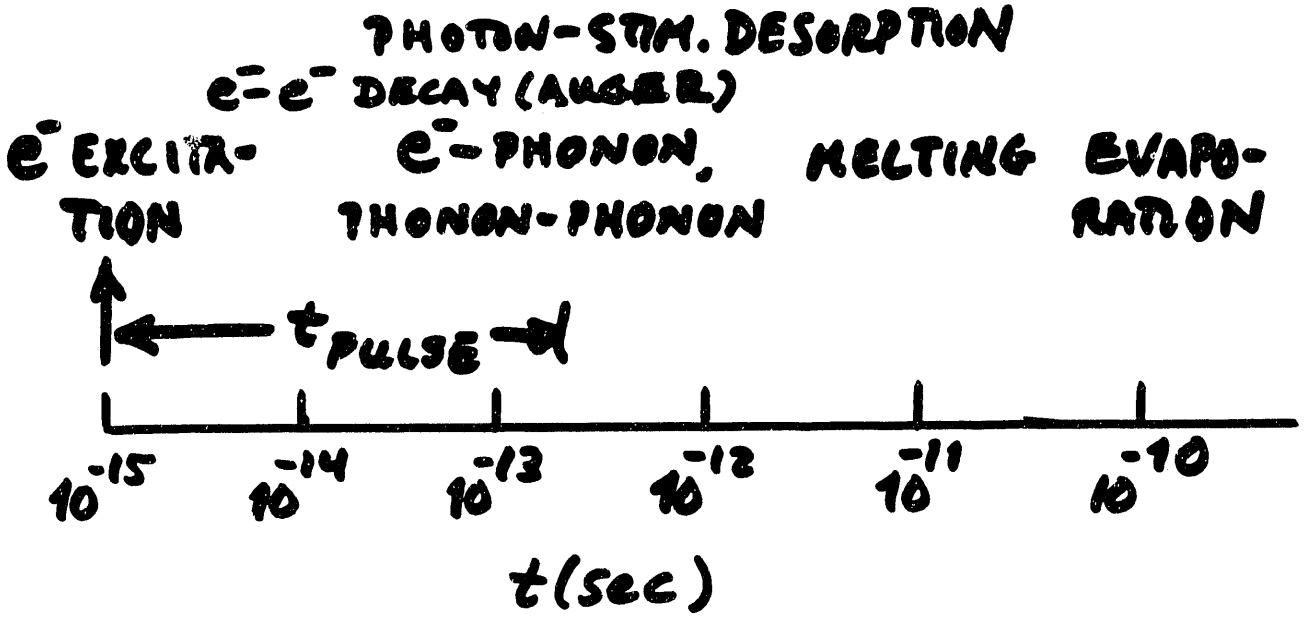
PHOTON-STIM. DESORPTION
e⁻-e⁻ DECAY (AUGER)
e⁻ EXCITA-TION
e⁻-PHONON, PHONON-PHONON
MELTING
EVAPO-RATION
t PULSE
10^-15
10^-14
10^-13
10^-12
10^-11
10^-10
t(sec)

FIGURE 6

## ESTIMATED HEATING DURING PULSE:

EXAMPLE: Si, $h\nu = 300$ eV ON ~ 1 mm²

PEAK POWER IN PULSE = $2.2 \times 10^{10}$ W

FOR RAPID HEATING WITH

ABSORPTION DEPTH << THERMAL DIFFUSION LENGTH

$$d_{abs} \ll d_{diff},$$

$$\rho C_v (T - T_0)\, d_{abs} \approx (1 - R) I_0 t$$

| | | | |
|---|---|---|---|
| $\rho$ | $C_v$ | $d_{abs}$ | $R$ |
| 2.33 g/cc | 0.168 cal/g-K | $1.4 \times 10^{-5}$ cm | 0 |

$\Rightarrow$ MELTING HEAT REACHED IN $\leq 1/5$ OF PULSE DURATION!

BUT $d_{diff} \approx (K/\rho C_v)^{1/2} t^{1/2} \approx 0.8 t^{1/2}$,

($K \sim 1.1$ W/cm-K)

SO PULSE HEATING DIFFUSES OUT OVER ~5000 $d_{abs}$ BETWEEN PULSES.

DAMAGE LIKELY. SUGGESTS GRAZING INCIDENCE TO ELEVATE R, INCREASE AREA

FIGURE 7

# III. SUMMARY OF OPEN DISCUSSION SESSION

## Open Discussion Session Summary

John Arthur, SSRL

The final session of the workshop consisted of an open discussion moderated by David Attwood of LBL and John Arthur of SSRL. Participants were asked to give opinions regarding the optimal wavelength, pulse duration, and polarization state for initial development in the 2 - 4 nm region. A request was also made for suggestions about potential applications for a SLAC FEL not mentioned in previous sessions, and for more speculative ideas. Participants were urged to elaborate on their comments in written form for inclusion in this proceedings.

The discussion period lasted nearly two and a half hours, with contributions from approximately 25 speakers. During the first half of this period the discussion centered on biological imaging and the problem of radiation damage to the sample. There was general agreement that images of natural (unstained) biological samples with resolution smaller than 500 Å would require radiation doses which would destroy the samples. However, there was no consensus regarding the significance of this fact. Many comparisons were made to techniques used in electron microscopy, such as cryofixation, in which the samples are also destroyed. These destructive techniques of structure analysis have become indispensable. But the microscopist's dream of a non-invasive imaging technique for live samples with hundred-angstrom resolution remains elusive.

Some other points were also raised about biological imaging. As pointed out in previous workshops, in addition to the water window itself, the slightly longer wavelength region just outside the water window, near the carbon k-edge, would give good imaging contrast due to the anomalous dispersion of the carbon scattering amplitude. It was also pointed out that the proposed SLAC FEL would suit some kinds of imaging better than others. This source, with its high coherence, would be particularly good for flash holography. On the other hand, a high-coherence source is not the best for conventional imaging, and the 120 Hz repetition rate of the SLAC source would make scanning imagery a very slow process.

During the second half of the session, condensed matter science applications were discussed. Here the radiation damage to the sample was not viewed as a limiting factor. For diffraction experiments, the shorter wavelengths (down to 1 Å or less) were thought to be more desirable. The ultra short pulse structure and high polarization of the FEL beam were seen as immediately useful to condensed matter research. Time resolution on the femtosecond scale, faster than typical phonon vibrational frequencies, seemed very intriguing. The high coherence of the beam was also viewed as an advantage, though the ideas for its use were more speculative. Suggestions included the use of speckle interferometry to measure coherence lengths in disordered systems, and the use of an x-ray laser to produce nuclear excitations, possibly creating a population inversion and a gamma-ray laser.

# IV. CONTRIBUTED PAPERS

LAUR-92-3695

# APPLICATION OF 10GeV ELECTRON DRIVEN X-RAY LASER IN GAMMA-RAY LASER RESEARCH

Johndale C. Solem
Theoretical Division
Los Alamos National Laboratory
Los Alamos, New Mexico 87545

Proceedings of Conference on Scientific Uses of X-Ray Laser

# Application of 10 GeV Electron Driven X-Ray Laser In Gamma-Ray Laser Research

Johndale C. Solem
Theoretical Division
Los Alamos National Laboratory
Los Alamos, NM 87544

**Abstract**

The proposed short wavelength coherent light source driven by the SLAC 3 km linac might be used to induce transitions between nuclear isomeric states. If an isotope were found with energetically adjacent isomeric states, one short-lived and one long-lived, and it were possible to separate and concentrate the long-lived species, and other nuclear and solid-state parameters were favorable, it might be possible to convert sufficient population to the short-lived state to realize $\gamma$-ray lasing. Even if the x-ray intensity were insufficient, study of such driven transitions would be quite valuable.

---

## Introduction

Researchers are presently exploring the possibility of using the 3-km electron accelerator at Stanford Linear Accelerator Center to drive an intense short-pulse x-ray laser. Preliminary studies indicate that it will be possible to tune the laser in the band from 0.1 to 10 nm . This is well within the range of many nuclear transitions between isomeric states. Thus such a light source might be a useful probe of certain aspects of nuclear structure, particularly the mechanisms of radiative transition. But a more speculative and perhaps more exciting application may be found in $\gamma$-ray laser research.

One approach to the development of a $\gamma$-ray laser[1] is to transform a long-lived isomer to a shorter-lived excited state capable of lasing by driving transitions between the states with an intense narrow-band photon source.[2] The process has been likened to a Raman laser[3], although the excited levels must both be real because the non-linear response of a nucleus would require exceedingly high field strengths.

---

[1] G. Baldwin, J. Solem, and V. Gol'danski, *Rev. Mod. Phys.* **53**, 687 (1981).

[2] J. Eerkens, U. S. Patent 3,430,046 (1969).

[3] E. Baklanov and V. Chebotaev, *Zh. Eksp. Teor. Fiz. Pis'ma Red* **21**, 286 (1975) [*JETP Lett.* **21**, 131 (1975)]; B. Arad, S. Eliezer, and Y. Paiss, *Phys. Lett. A* **74**, 395 (1979).

Several steps are necessary to practical realization of this $\gamma$-ray laser concept. The long-lived isomer would have to be separated from other activated material by radio- or photo-chemical processes[4], and formed into a rod of appropriate aspect ratio for lasing. The rod might be constructed of a host lattice in which the isomer nuclei are implanted. The host would have a higher Debye temperature in order to achieve a larger fraction of recoilless transitions of the isomer, and thereby minimize the lasing transition linewidth. The $\gamma$-ray laser is then triggered by the x-ray pulse pumping isomer population form the long-lived state to the short-lived state.

## Nuclear Interlevel Transfer

Figure 1 is an energy-level diagram of a fictitious nuclide with two isomeric states in energetic propinquity, $E_1 - E_2 = \Delta E \ll E_2$, but with a great disparity in lifetime, $\lambda_3 \ll \lambda_2$, where $\lambda_i$ is the probability per unit time for decay of the $i$th state. If the rate coefficient induced by the x-ray laser is sufficient, $W_{23} \gg \lambda_2$, this transition will saturate before population will have accumulated in the ground state, and nearly half the population of long-lived states will be converted to an inversion of the short-lived transition. If the conditions were satisfied for the short-lived transition to be recoilless,[5] and thereby very narrow,[6] and other nuclear parameters were favorable,[1,7,8] the transition might enjoy amplified stimulated emission — it might become a laser. The principal advantage of this scheme over the myriad of other $\gamma$-ray laser concepts is most of the energy is supplied by the nuclei rather than the pump. The cross section for pumping the transition is

$$\sigma = \frac{\Lambda^2}{2\pi}\frac{\Gamma_r}{\Gamma}, \tag{1}$$

where $\Lambda$ is the resonant wavelength of the $2 \leftrightarrow 3$ transition, $\Gamma_r$ is the radiative linewidth and $\Gamma$ is the total linewidth. It is easy to show[1] that

$$\frac{\Gamma_r}{\Gamma} = \frac{\beta}{1+\alpha}\frac{\lambda_3}{\lambda_2+\lambda_3}, \tag{2}$$

where $\alpha$ is the ratio of probabilities of internal conversion and gamma emission and $\beta$ is the fraction of all decays from level 3 that terminate at level 2. The induced rate coefficient is

$$W_{23} = \frac{I\sigma}{e\Delta E}, \tag{3}$$

---

[4] L. Szilard and T. Chalmers, *Nature* **134**, 462 (1934); V. Letokov, *Science* **180**, 451 (1973); G. Baldwin, J. Neissel, and L. Tonks, U. S. Patent 3,324,099 (1966).

[5] R. Mössbauer, *Z. Phys.* **151**, 124 (1958).

[6] B. Josephson, *Phys. Rev. Lett.* **4**, 341 (1960); R. Pound and G. Rebka, *Phys. Rev. Lett.*, **4**, 274 (1960).

[7] W. Visscher, *Ann. Phys.* **9**, 194 (1960); H. Lipkin, *Ann. Phys.* **9**, 332 (1960).

[8] G. Baldwin and J. Solem, *J. Appl. Phys.* **51**, 2372 (1980).

where $I$ is the x-ray laser intensity set at the resonant wavelength. To saturate the 3-2 transition, we must have $W_{23} \gg \lambda_2$. The required intensity is therefore

$$I \gg 6.5 \times 10^{-5} \frac{(\Delta E)^3 \Gamma \lambda_2}{\Gamma_r}, \tag{4}$$

where $I$ is in $\mathrm{W \cdot cm^{-2}}$, $\Delta E$ is in eV, and $\lambda_2$ is in $\mathrm{sec^{-1}}$.

### Some Candidate Isotopes

Figure 2 shows energy level diagrams that resulted from a search[9] of the computerized nuclear structure library, CDRL82[10], based on the compilation given in the *1978 Table of Isotopes.*[11] The search was based on two criteria: (1) the isomeric states must have a half-life greater than 5 sec, and (2) the spacing of a nearby level must have an excitation energy of less than 1 keV.

The value of $\Gamma_r/\Gamma$ is more difficult to obtain, but of the five isotopes shown, the most likely to have a large ratio is $^{183}$W. The storage state lifetime is only 5.3 sec, so some sort of on-line separation, concentration, and host-implantation would be necessary. The transition from the $11/2^+$-state to the $9/2^-$-state is an electric dipole, however, suggesting a relatively large $\Gamma_r$. This assertion is complicated by K-selection-rule constraints, and detailed theoretical evaluation of $\Gamma_r/\Gamma$ is a laborious process. The excitation energy for $^{183}$W is $\Delta E = 544$ eV. Recent calculations[12] suggest that a 2-to-5nm free electron laser driven by the SLAC linac could produce about $10^{14}$ coherent photons per pulse in a bandwidth of about 2%. This amounts to a peak power of about $10^{10}$ W, although driving the nuclear transitions may require a narrower bandwidth. From Eq. (4), driving a $^{183}$W $\gamma$-ray laser would require a linewidth ratio

$$\left(\frac{\Gamma_r}{\Gamma}\right)_{\mathrm{W}} \gg \frac{6.5 \times 10^{-5} \lambda_2 (\Delta E)^3}{I} = 5.5 \times 10^{-6}. \tag{5}$$

---

[9] D. Strottman, E. Arthur, and D. Madland, *Proceedings of the IST/IDA Gamma-Ray Laser Workshop*, B. Balko, L. Cohen, and F. Hartmann, Eds. (Institute for Defense Analyses, Alexandria, VA, 1986).

[10] R. Howerton, ENSL82 and CDRL82: The 1982 Version of Evaluated Nuclear Structure Libraries ENSL and CDRL, Lawrence Livermore Laboratory Report UCRL-50400 Vol. 23 Addendum (1983).

[11] C. Lederer and V. Shirley, Eds., *Table of Isotopes*, 7th Edition (Wiley & Sons, New York, 1978).

[12] C. Pellegrini, *et al.*, "A 2 to 5nm High Power FEL on the SLAC Linac," to be published in the proceedings of the 13th International FEL Conference, Kobe, Japan, August 1992.

To approach this linewidth ratio for an electric dipole transition does not seem unreasonable.

The smallest energy difference identified in the search was $^{179}$Hf at $\sim$ 200 eV. The isotope also has a 25.1-day half-life, which would make it quite manageable with off-line preparation. For this isotope, we must have a linewidth ratio,

$$\left(\frac{\Gamma_r}{\Gamma}\right)_{\rm Hf} \gg 1.1 \times 10^{-1}. \qquad (6)$$

It is exceedingly unlikely that an E9 transition could have such a favorable linewidth ratio, but at sufficiently high intensity, there is a remote possibility that the nonlinear collective response of the atomic electrons could introduce spatial harmonics, enhancing the driven-transition rate.[13]

## Discussion

The quantum energies offered by the proposed linac-driven FEL are clearly capable of driving several known transitions in energy-level arrangements appropriate for "storage-state" $\gamma$-ray lasers. The search described above was far from exhaustive — there are on the order of $10^5$ isomeric state, including all nuclei and all isotopes. But even this cursory search offered one transition that was within striking distance of being a $\gamma$-ray laser candidate. If the proposed SLAC x-ray laser becomes a reality, this would be a very interesting application. In the meantime, more research is necessary to locate other candidate isomers and appraise their nuclear properties, particularly their linewidth ratios as discussed above.

A curious variant using the transition pumping schemes described here, would be the so-called "inversionless" laser. Recent work has shown light amplification in sodium,[14] based on theoretical predictions[15] concerning "$\Lambda$-quantum-beat" schemes. An x-ray laser may allow extension of these concepts to $\gamma$-ray laser.

---

[13] J. Solem and L. Biedenharn, *JQSRT* **40**, 707 (1988); J. Solem, *JQSRT* **40**, 713 (1988); J. Solem and L. Biedenharn, "Primer on Coupling Collective Electronic Oscillations to Nuclei," Los Alamos National Laboratory Report LA-10878 (1987); J. Solem, L. Biedenharn, and K. Boyer, *Advances in Laser Science*, W. Stwalley and M. Lapp, Eds. (AIP, New York, 1986), p. 50 ; J. Solem, L. Biedenharn, G. Baldwin, and K. Boyer, *Advances in Laser Science*, W. Stwalley and M. Lapp, Eds. (AIP, New York, 1986), p. 52.

[14] J. Gao, *et al.*, *Optics Comm.* **93**, 323 (1992).

[15] O. Kocharovskaya and Ya. Khanin, *Zh. Eksp. Teor. Fiz.* **90**, 1610 (1986); M. Scully, S. Zhu, and A. Gavrielides, *Phys. Rev. Lett.* **62**, 2813 (1989); E. Fill, M. Scully, and S. Zhu *Optics Comm.* **77**, 36 (1990); S. Zhu *Phys. Rev. A.* **42**, 5537 (1990); S. Harris *Phys. Rev. Lett.* **62**, 1033 (1989); S. Harris and J. Macklin *Phys. Rev. A.* **40**, 4135 (1990).

## Figure Captions

Figure 1. Conversion from long to short lifetime. If the long-lived isomer, level 3, were prepared at high concentration and embedded in a host with high Debye temperature, $\gamma$-ray laser operation might be initiated on the 2-1 transition by intense x-radiation saturating the 3-2 transition. (From Ref. 1)

Figure 2. Results of a search for isomeric states with lifetime greater than 5 sec and energetic spacing less than 1 keV to a nearby short-lived state. (From Ref. 9)

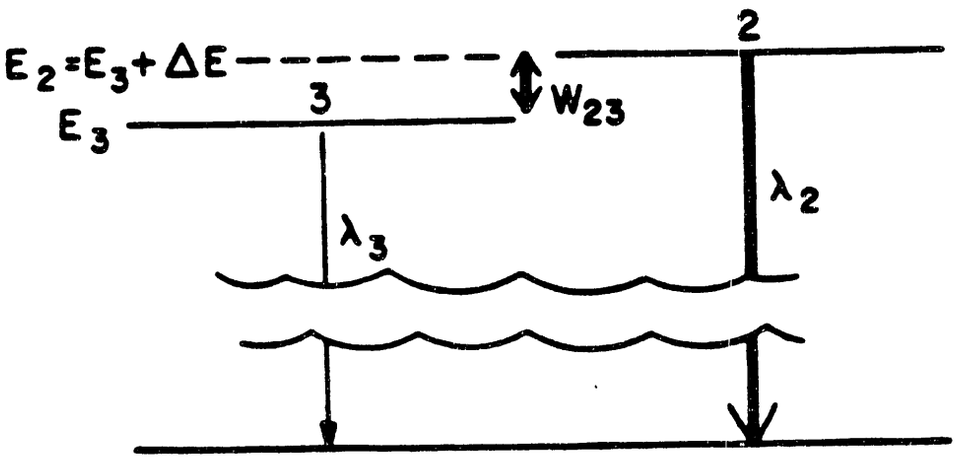


Figure 1

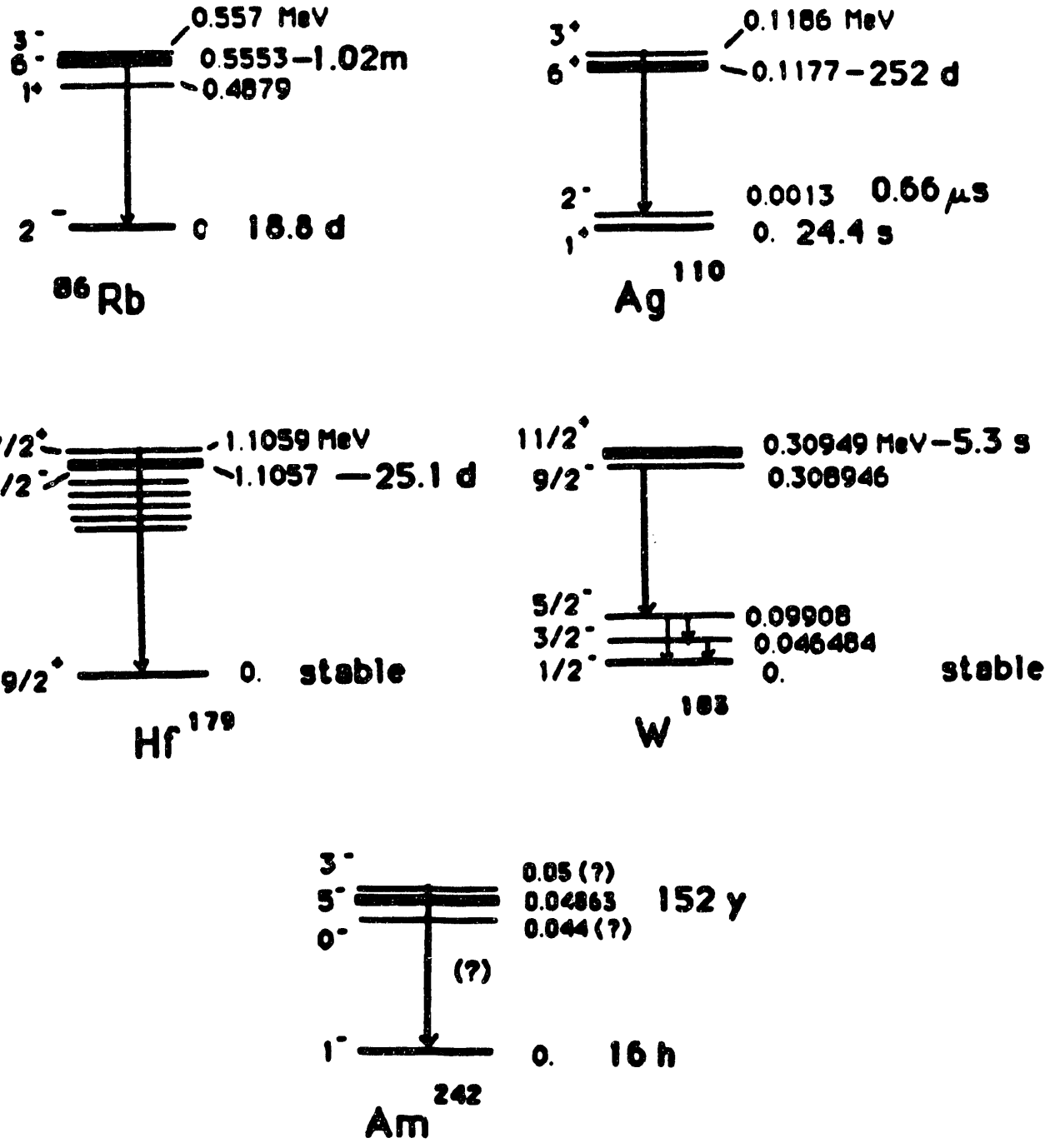
3⁻
6⁻
1⁺
0.557 MeV
0.5553–1.02m
0.4879
2⁻
0
18.8 d
86Rb
3⁺
6⁺
0.1186 MeV
0.1177–252 d
2⁻
1⁺
0.0013
0.66 μs
0.
24.4 s
Ag110
7/2⁺
25/2⁻
1.1059 MeV
1.1057 —25.1 d
9/2⁺
0.
stable
Hf179
11/2⁻
9/2⁻
0.30949 MeV–5.3 s
0.308946
5/2⁻
3/2⁻
1/2⁻
0.09908
0.046484
0.
stable
W183
3⁻
5⁻
0⁻
0.05 (?)
0.04863
0.044 (?)
152 y
(?)
1⁻
0.
16 h
Am242

Figure 2

ECOLE POLYTECHNIQUE FEDERALE DE LAUSANNE

# Non-Linear Optics, Fluorescence, Spectromicroscopy, Stimulated Desorption: We Need LCLS' Brightness and Time Scale!


**Giorgio Margaritondo**

Ecole Polytechnique Fédérale, CH-1015 Lausanne, Switzerland

**F. Cerrina**

Department of Electrical Engineering and Center for X-Ray Lithography

University of Wisconsin-Madison, USA

**N. H. Tolk**

Vanderbilt University

Center for Molecular and Atomic Studies at Surfaces

Department of Physics and Astronomy

Nashville, Tennessee 37235, USA

and

**Gelsomina De Stasio**

Istituto di Struttura della Materia, Consiglio Nazionale delle Ricerche

Frascati, Italy



ABSTRACT

We present and discuss several areas of interest for the international use of Stanford's Linac Coherent Light Source, with participation of institutions from Switzerland, Italy and the USA, and based on practical experience in the use of free-electron lasers for research. In each case, the unprecedented

characteristics of the new x-ray source allows previously impossible experiments in materials science and in the life sciences.

## I. Introductory Remarks

The proposed Linac Coherent Light Source (LCLS), because of its exceptional performances and unique characteristics, is not merely a national facility; it is a world resource, that challenges all scientists to develop new ways of thinking in x-ray research. Several groups from institutions in Switzerland, Italy and the USA took this challenge, developing a series of research ideas that make full use of some of LCLS' unmatched characteristics. The necessary technical background is provided by many years of experience in the use of synchrotron radiation, including ultrabright undulator sources,[1-3] and more recently, experience with some of the very few real experiments on a free-electron laser at the Vanderbilt University.[4]

The core proposals deal with four areas: non-linear optics,[5,6] frequency-domain and time-domain fluorescence,[7,8] spectromicroscopy,[1-3] stimulated desorption spectroscopy.[9,10] In each case, the envisioned experiments are quantum jumps into the future with respect to present and foreseeable applications of the same techniques. In the case of non-linear optics, the superlinear intensity dependence [5,6] will compensate the large energy of the x-rays, creating the feasibility of two-photon and multiphoton experiments in the x-ray domain. This technique will be the ultimate tool in solving symmetry problems in the electronic structure of condensed systems.

In the case of time-resolved fluorescence, we envision a push to new time domains of conventional experiments and of a novel technique based on

frequency-domain analysis.[7,8] This last technique has been used with some synchrotron sources to study fluorescence phenomena down to the picosecond range. The exceptional time structure and ultrahigh brightness of LCLS will take the approach into previously unreachable time scales.

Spectromicroscopy [1-3] combines into one experiment the full power of x-ray microscopy and conventional spectroscopy, making it possible to perform chemical and physical analysis on a microscopic scale. Techniques of this kind have been implemented with existing synchrotron sources, and applied to both materials-science [2] and life-science problems.[3] They are, however, affected by severe limitations mostly related to the low signal levels. The relief from the increase in brightness after commissioning of the third-generation sources will be only partial. With LCLS, techniques of this kind will reach their absolute limits, that are also the natural limits of many types of spectroscopies that have been used for years and sometimes decades in science and technology. In particular, it will be possible to perform one-shot microchemical analysis on the scale of tens of angstroms.

Finally, stimulated-desorption spectroscopy has been for many years a marginally exploited gold mine, the gate to the understanding of the dynamic properties of solid surfaces.[9,10] The use of this gold mine has been sharply limited by signal problems; consider for example that only a handful of experiments have dealt with emitted neutrals,[9] that are by far the most important component of the desorption yield, but difficult to detect. Time-resolved and angle-resolved experiments have remained either marginal or

impossible, and space-resolved experiments essentially a dream.[10] The brute force of the LCLS emission will change all this, and extract all of the information that these techniques can potentially provide. The very phenomena that create damage problems in other experiments will be the key in this case to the ultimate understanding of solid surfaces, well beyond the artificial stationary-state point of view.

## II. Non-Linear Optics: a Rebirth

The possibility to perform non-linear optics was one of the motivations for the development of pulsed lasers in the 1960's.[5] The theoretical background for non-linear optical phenomena had been developed by Maria Goeppert Mayer [6] in the 1930's, but the practical implementation of her theoretical results in the visible was delayed for decades because of the lack of suitable sources. And this research was never extended to the x-rays, essentially for the same reasons.

Consider the absorption transition probability [5,6] from a state $|i\rangle$ of energy $E_i$ to a state $|f\rangle$ of energy $E_f$ by absorption of two photons of energy $h\nu_2$ and $\nu_1$:

$$P(h\nu_1,h\nu_2) \propto |\Sigma_v(\langle i|\eta_1\cdot p|v\rangle\langle v|\eta_2\cdot p|f\rangle)/(E_v-E_i-h\nu_1)|^2 I_1 I_2 \delta(E_f-E_i-h\nu_1-h\nu_2), \quad (1)$$

where the $|v\rangle$'s are virtual intermediate states of energy $E_v$, $\eta_1$ and $\eta_2$ are the polarization vectors and $I_1$ and $I_2$ are the photon beam intensities. For two

photons hν of polarization vector η from the same source of intensity I, Eq. 1 becomes:

$$P(2h\nu) \propto |\Sigma_v((i|\eta\cdot p|v)\langle v|\eta\cdot p|f))/(E_v-E_i-h\nu)|^2 I^2 \delta(E_f-E_i-2h\nu). \quad (2)$$

The observation of two-photons optical transitions is made very difficult for high photon energies by the energy denominator of Eqs. 1 and 2. The optimal solution would be, in principle, to take two different photon energies, one of which as small as possible. But this is not often done in practice, because it is convenient to take both photons from the same laser. The only way to compensate for the denominator's effect in the case of large photon energies, is to increase the intensity, which is present in Eq. 2 as a square -- hence, the need for high peak power in the photon source.

This makes a straightforward case for the LCLS when considering two-photon optical studies in the x-ray range. In fact, only one experiment has been so far attempted in this domain,[11] combining lasers and synchrotron radiation, but with only preliminary results.

Why is nonlinear x-ray optics important? For a variety of reasons, the most relevant being in our opinion the possibility to settle once and forever all issues about the symmetry of electronic states.[12] The transition probability of Eqs. 1 and 2 depends on matrix elements involving the initial and final states and also intermediate virtual states. As a result, the symmetry selection rules for two-photon processes are complementary to those of one-photon

phenomena. This means that state symmetries can be checked or cross-checked (with respect to the results of one-photon studies), provided that the initial-state symmetry is well defined and known.

This last point may not be true for valence states, but is certainly very true for core levels. Therefore, it would be better in principle to use core levels as initial states. But in practice this means moving from the visible to the ultraviolet or to the x-rays, with the disadvantages already discussed, that can be offset by the large intensity of the LCLS.

Note that the arguments presented here are quite general, and can be easily extended to multiphoton processes. Furthermore, they can be generalized to a variety of nonlinear optical processes besides pure two-photon absorption, such as those involving real rather than virtual intermediate states.[6]

## III. Ultrafast Time-Resolved Fluorescence in the Frequency Domain

Synchrotron radiation has been used in many experiments to excite fluorescence and study its time decay, thereby deriving precious information both on materials science and life science specimens.[13] The decay analysis exploits the time structure of synchrotron radiation sources, consisting of short pulses separated by long intervals.

Note [7,8] that the minimum possible decay time scale that can be analyzed is determined by the pulse width of the source, and the maximum is affected by the repetition rate. Hence, the interest of LCLS, with its predicted ultrashort pulses (0.2 ps, possibly decreased to a few tens femtoseconds), and relatively large intervals between pulses.

This approach greatly profited from a technical breakthrough due to E. Gratton: the frequency-domain analysis.[7] The Fourier transform of the time structure of a synchrotron source is a series of harmonics of the sources fundamental frequency, whose envelope is a Gaussian, with half width at half maximum given by the reciprocal of the source pulse width.

In a time-resolved fluorescence experiment, one can analyze the amplitude and phase of a given Fourier component of the excitation and fluorescence signals. From a comparison of the results for excitation and fluorescence signals, it is easy to extract the desired information and in particular the fluorescence decay time.[7,8]

For example, the decay time is determined [7,8] by the tangent of the phase difference between excitation and fluorescence for a given Fourier component, divided by the frequency. Similarly, the decay time can be extracted from the amplitude data. Multiple exponential decay times - and even continuously distributed decay times - can be easily extracted by analyzing several harmonics. The phase analysis is actually made possible [7,8] by modulating the detectors' gain of the excitation and fluorescence

signals, creating low-frequency beatings, and measuring the excitation-fluorescence phase shift at those low frequencies.

The limitations of this approach in studying short decay times arise from three factors: first, the decreasing intensity of the high-frequency Fourier harmonics, that becomes small for frequencies much above the reciprocal of the source pulse time width. Second, the capability to modulate the detectors at high frequency and create low-frequency beatings for high-frequency components. Third, the source intensity, since the accuracy of any phase analysis is limited when too much noise is present.

The LCLS will greatly help us to overcome the first and third limiting factors. The actual limits of the experiments will be determined by our capability to modulate at high frequency, and it will go beyond the present limitations by at least one order of magnitude. Further progress may be possible either by achieving higher-frequency modulation or by resorting to a more traditional time-domain scheme allowed by the excellent source characteristics -- at least in the case of simple exponential decays.

The applications of this approach will be quite extensive in materials science, since it will enable us to study core-initiated fluorescence in a new time domain typical of vibrational frequencies. A space-resolved version of the technique is not out of the question. As far as life-science is concerned, some aspects of the new time domain are quite interesting.

Typical phenomena of the new time domain are photostimulated chlorophyll chemistry and the eye vision's photochemistry of rhodopsin. One can envision a time-resolved analysis of these phenomena based on core-level excitations, that will nicely complement the present studies of the main mechanisms in the visible and near-UV photon-energy domains.

## IV. Spectromicroscopy to its Limits

Spectromicroscopy [1-3] is the combination of established spectroscopies with lateral resolution. The best known example is photoemission spectroscopy: for decades, after the original work of Kai Siegbahn and Bill Spicer,[14] this spectroscopy has become the leading tool in the study of electronic structures. It has been, however, severely affected by one limitation: the lack of lateral resolution and the consequent space-averaged character of the information that it provides.[1]

In the past two-three years, very rapid progress has been made in overcoming this obstacle,[3,4] and in fact photoemission experiments can now be performed on the most advanced instruments, such as the scanning spectromicroscope MAXIMUM at Wisconsin, with a lateral resolution better than 0.1 micron. This rapid progress is the result of two factors.

First, the advances in the optical instrumentation. The art of focusing x-rays and that of electron optics have been optimized, in the first case beginning

from almost non-existence. New and old tools such as the Fresnel zone plate and the Schwarzschild objective have been improved by technical breakthroughs, for example, multilayer coating for enhancing reflectivity.[1]

But this progress would have been largely useless without a parallel progress in the brightness of the photon sources.[13] The advances in that area have initiated with the commissioning of second-generation bending magnet sources of synchrotron radiation such as Aladdin or the Brookhaven rings. Then it has accelerated with the commissioning of the first undulators on these new sources, for example the redeployment on Aladdin of the Stanford-Berkeley undulator.[2] And it will further accelerate with the forthcoming commissioning of third-generation, ultrabright sources such as ELETTRA at Trieste and the Advanced Light Source at Berkeley.

One can observe a close correlation between the progress in photoemission spectromicroscopy and the increase in the source brightness. The reason is quite fundamental: the Liouville theorem requires the conservation (except for absorption, reflection and scattering losses) of the brightness along an optical system such as a synchrotron beamline, therefore the concentration of the beam in a small area requires an initial high brightness.[1]

This fundamental reason applies not only to photoemission spectromicroscopy, but to a long series of other techniques, such as absorption and transmission microscopy and spectromicroscopy, desorption spectromicroscopy, etc., all in the x-ray an ultraviolet domains.[1,13]

Why are these techniques important? In essence,[1] they bring to the microscopic scale the full power of the most advanced tools in experimental materials science -- the full power of their chemical, electronic and structural analytical capabilities. They are, therefore, the techniques of the future in materials science. Consider again photoemission spectromicroscopy: this technique can identify the structural morphology of a specimen, then zoom into the most promising areas and explore their chemical composition, the chemical status of each element, the valence electronic structure, many-body phenomena, potentially band structures, etc., etc., etc.[1]

And since these investigations take place on a submicron scale, they are no longer limited to materials science, but can be extended to the life sciences as well. In the past two years, rapid progress has been made, for example, in the photoemission spectromicroscopy imaging and chemical microanalysis of neuron networks, in preparation for systematic studies of the possible relations between the chemical properties and physiologic functions such as the nerve pulse broadcasting.[3] Figure 1 shows an example of photoemission micrograph in this domain.[3]

The rapid recent progress notwithstanding, synchrotron-light spectromicroscopies are not yet reaching their natural performance limits.[1] They are not reaching the limits of the lateral resolution, and they cannot operate at very high energy resolution (the top performance for photoemission spectromicroscopy has been achieved [2] again with

MAXIMUM, and it is of 350-400 meV). One step ahead will be the commissioning of the third-generation source, that will bring most spectromicroscopies to their natural resolution limits, for example, those determined by diffraction. And further progress is envisaged with the arrival of fourth-generation sources such as the proposed SLS (Swiss Light Source).

But the ultimate limits of all of these techniques will only be reached with the LCLS, that will truly allow in each case the maximum efficiency in extracting information from the underlying physical phenomena. Take again photoemission spectromicroscopy as an example. The progress of photoemission over a century has been the progress in finding methods to extract more information from the photoelectric effect. In principle, this effect is a wonderful source of information, ranging from chemistry to electronic properties, to correlation phenomena, to atomic structure, etc. -- but for many decades its exploitation has been limited by insufficient instrumentation.

The researchers active in this field have experienced the frustration of the gold miner that knowingly walks on a mountain full of gold, but does not have the tools to mine it. Some of the tools have been made available, as we have seen, by the rapid progress of synchrotron radiation in the past years. But most of the gold is still beyond reach. Specifically, the most advanced photoemission techniques, present and foreseeable, push to the limits one of the performances or at most two, optimizing the extraction of some types of information -- for example, spin polarisation and magnetic properties.[13,14]

But they cannot *simultaneously* optimize more than two performance aspects, therefore we are still far from the ultimate photoemission probe that would have at the same time ultrahigh energy, lateral and angular resolution, spin resolution and time resolution. This would also be one of the foundations of microscopy, since because of the short photoelectron escape depth photoemission spectroscopy is already a "vertical" microscopy, capable of reaching atomic resolution in a fully tunable way.[13,14]

This dream instrument is precisely what the LCLS will give us in the case of photoemission spectromicroscopy: the ultimate spectroscope and the ultimate vertical-lateral microscope. From a practical point of view, the instrumentation progress recently achieved in this area has solved many of the technical problems for the exploitation of a source like LCLS. Specifically, we do not foresee difficulties in the extension to the LCLS of today's techniques for electron-optics photoemission spectromicroscopy,[1] except for the need of new data processing hardware and software as required by the very large data production rate.

Technical difficulties must be solved instead for scanning-focusing techniques, since the present focusing devices may not survive the high power emitted by the LCLS. Grazing-incidence focusing is likely to be required. Even without focusing, however, one could limit the source size with a pinhole and still have more intensity than before LCLS. Or one could reach very low noise level in an extremely short time, recovering the space information *a posteriori*.

We note that photoemission spectromicroscopy, although very exciting, is only one example of the "dream" instruments made possible in this domain by the LCLS. Each spectromicroscopy can produce a similar dream instrument.[1] For example, desorption spectroscopy with lateral resolution - discussed in the next section - can extend on a microscopic domain surface science from static properties to dynamics.[9,10]

As to the applications of these "dream machines", there are really no limits, in materials science and in the life sciences. In materials science, the corresponding spectroscopies, with all of their limitations, are used by tens of thousands of scientists and technologists worldwide and producing important advances every day.[13,14] Not only fundamental advances, but practical as well: the optimization of industrial processing - notably at Xerox - has produced savings of millions of dollars.[14] Every problem currently explored with photoemission and other spectroscopies can profit from the technical superiority of the new "dream" spectromicroscopes -- hence, a very wide and varied array of applications.

## V. Exploiting Stimulated Desorption to the Maximum Possible Extent

Photon-stimulated desorption has been for years perhaps the most promising technique of surface science.[9,10,13] The stimulated desorption process carries a tremendous amount of high-quality information, specifically information

on surface dynamics that goes well beyond what can be extracted from photoemission and optical properties, and potentially can have a dramatic impact on the industrial exploitation of surface chemistry.

On the other hand, the practical use of photon-stimulated desorption in experiments has been severely limited by the low signal level, that, in turn is due to low source brightness.[13] The limitations are particularly dramatic for the emission of neutral species,[9] that are quite difficult to detect but form the overwhelming majority of the emission in most cases.

The superior intensity of the LCLS will bring new life into this domain. Furthermore, the fast time structure will make it possible to perform real-time desorption studies of the evolution of surfaces, and even in some cases, real-time studies of the desorption process.

The unique capabilities of the LCLS provide unparalleled research opportunities to probe the subtle features of photon-matter interactions using variable wavelength and pulse structure, as well as two-color pump-probe techniques, to investigate *selective, resonant bond-breaking* on inanimate and living-state materials. The underlying and unifying scientific scheme of this work is to identify and characterize selective electronic, vibrational and other non-thermal processes which occur when short-pulse, intense, widely tunable light is incident on matter. Our recent research using the University of Wisconsin synchrotron has shown that it is possible to selectively break specific chemical bonds within a molecule by choosing the correct photon

energy. This has obvious applications in chemical engineering for the production of novel molecules and in electrical engineering for nano-structure fabrication associated with electronic chip production. The technique could also result in a gigantic step forward in the medical use of lasers. When conventional fixed-energy lasers are used to cut, burn or ablate tissue, the laser is simply being used as a convenient tool for delivering power in the form of thermal energy. Selective resonant excitations and bond-breaking would allow selective modifications on the molecular level resulting in specific dysfunction without undesirable side effects on the cellular and the tissue levels. In other words, cancer cells could be selectively destroyed without harming normal cells.

The fundamental scientific rationale for these studies is the crucial question of how incident photon energy can be spatially and temporally localized at a single atomic or molecular site to produce bond-breaking, point defects, desorption, and, ultimately, for biological materials, changes in structure, function and dynamics on the molecular, cellular and tissue levels. Materials to be studied include simple wide-gap insulators, semiconductors and ultimately living state material.

This last possibility is extremely exciting, in particular when coupled to the potential extension of LCLS' spectral domain to photon energies suitable for real-time crystallography. The applications of this advanced structural technique could be extended not only to vibrations, but also to desorption

dynamics, eliminating the need for theoretical modeling and removing the difficulties that are unavoidable with indirect, time-averaged studies.

In essence, the extreme case of LCLS-based stimulated desorption is the ultimate experimental system for the study of surface dynamics, the complementary tool to the spectromicroscopes discussed in the previous section. In fact, the high intensity of the LCLS will make it possible to perform photon-stimulated desorption experiments in a lateral-resolved mode, implementing the previously mentioned technique of desorption spectromicroscopy.[1]

Note that much of the detection hardware is common to both spectromicroscopy and stimulated desorption. With a bit of optimism, one could even envision an integrated supersystem, for the simultaneous implementation of photoemission and photon-stimulated desorption spectromicroscopy, with high lateral, time, energy and angular resolution. Most of the technology of this supersystem is already available, except for the photon source. Such a system would be unsurpassed in studying at once the static and dynamic properties of surfaces, and in establishing the relations between them that are, in our opinion, the ultimate objective of surface science and technology.

## VI. Free-Electron Lasers as Research Tools: Our Practical Experience

The programs described in the previous sections are based on realistic extrapolations of the present experiments, and also on already established experimental technologies except in a few cases that have been clearly identified. It is, therefore, a realistic program.

The realism concerning the experimental tools must, however, be complemented with realism concerning the photon source. It is precisely in this area that we can bring an unique practical experience. We have, in fact, implemented one of the few real experimental programs with a free electron laser, producing the first materials-science data with the Vanderbilt source.[4]

This result is relevant to the present proposals because it brings practical experience. It shows that experiments with a free-electron laser are possible not only in principle but also in practice. We see in this domain a repeat of the situation that was present [13] in synchrotron radiation 15-20 years ago, with wonderful machines that are perhaps not yet fully optimized for routine use -- but that can and do produce top-quality results.

We believe, in fact, that our practical experience [4] with one of the first free-electron-laser experimental programs will be of invaluable help in establishing an aggressive and effective program at the LCLS. The superior and unmatched qualities of this wonder source, and the impact of the experimental programs that we have briefly outlined, fully justify this special effort, at the forefront of modern condensed-matter and surface science, of surface technology and of important branches of the life sciences like

neurophysiology. The message is quite clear: we need the brightness and time structure of LCLS.

## Acknowledgments

Work supported by the Fonds National Suisse de la Recherche Scientifique and by the Ecole Polytechnique Fédérale de Lausanne, by the Office of Naval Research under contract N00014-87-C-0146 and grant N -00014-91-J-4040, and by the National Science Foundation. We are grateful to Fabia Gozzo, Hermann Winick and Claudio Pellegrini for interesting discussions on this subject.

## References

1. G. Margaritondo and F. Cerrina, Nucl. Instr. Meth. A291, 26 (1990).
2. F. Cerrina, B. Lai, C. Gong, A. Ray-Chaudhuri, G. Margaritondo, M. A. Green, H. Höchst, R. Cole, D. Crossley, S. Collier, J. Underwood, L. J. Brillson and A. Franciosi, Rev. Sci. Instrum. 60, 2249 (1989); F. Cerrina, S. Crossley, D. Crossley, C. Gong, J. Guo, R. Hansen, W. Ng, A. Ray-Chaudhuri, G. Margaritondo, J. H. Underwood, R. Perera and J. Kortright, J. Vac. Sci. Technol. A8, 2563 (1990); W. Ng, A. K. Ray-Chadhuri, R. K. Cole, S. Crossley, D. Crossley, C. Gong, M. Green, J. Guo, R. W. C. Hansen, F. Cerrina, G. Margaritondo, J. H. Underwood, J. Korthright and R. C. C. Perera, Phys. Scripta 41, 758 (1990); C. Capasso, A. K. Ray-Chaudhuri, W. Ng, S. Liang, R. K. Cole, J. Wallace, F. Cerrina, G. Margaritondo, J. H. Underwood, J. B. Kortright and R. C. C. Perera, J. Vac. Sci. Technol. A9, 1248 (1991).3. Gelsomina De Stasio, W. Ng, A. K. Ray-Chaudhuri, R. K. Cole, Z. Y. Guo, J. Wallace, G. Margaritondo, F. Cerrina, J. Underwood, R. Perera, J. Kortright, Delio Mercanti and M. Teresa Ciotti, Nucl. Instrum. Methods A294, 351 (1990); Delio Mercanti, Gelsomina De Stasio, M. Teresa Ciotti, C. Capasso, W. Ng, A. K. Ray-Chaudhuri, S. H. Liang, R. K. Cole, Z. Y. Guo, J. Wallace, G. Margaritondo, F. Cerrina, J. Underwood, R. Perera and J. Kortright, J. Vac. Sci. Technol. A9, 1320 (1991); Gelsomina De Stasio, C. Capasso, W. Ng, A. K. Ray-Chaudhuri, S. H. Liang, R. K. Cole, Z. Y. Guo, J. Wallace, F. Cerrina, G. Margaritondo, Underwood, R. Perera, J. Kortright, Delio

Mercanti, M. Teresa Ciotti and Alessandro Stecchi, Europhysics Lett. **16**, 411 (1991).

3. Gelsomina De Stasio, P. Perfetti, S. F. Koranda, B. Tonner, J. Harp. D. Mercanti, M. Teresa Ciotti and G. Margaritondo, Europhys. Letters (in press).
4. C. Coluzza, E. Tuncel, J.-L. Staehli, P. A. Baudat, G. Margaritondo, J. T. McKinley, A. Ueda, A. V. Barnes, R. G. Albridge, N. H. Tolk, D. Martin, F. Morier-Genoud, C. Dupuy, A. Rudra and M. Ilegems, Phys. Rev. (in press).
5. D. A. Kleinman, Phys. Rev. **125**, 87 (1962).
6. M. Göppert-Mayer, Ann. Physik **9**, 273 (1931).
7. E. Gratton and R. Lopez-Delgado, Nuovo Cim. B56, 110 (1980); E. Gratton, D. N. Jameson, N. Rosato and G. Weber, Rev. Sci. Instrum. **55**, 486 (1984).
8. G. De Stasio, A. M. Giusti, T. Parasassi, G. Ravagnan and O. Sapora, Rev. Sci. Instrum. 63, 1393 (1992); G. De Stasio, N. Zema, F. Antonangeli, A. Savoia, T. Parasassi and N. Rosato, Rev. Sci. Instrum. **62**, 1670 (1991).
9. N. H. Tolk, M. M. Traum, J. S. Kraus, T. R. Pian, W. E. Collins, N. G. Stoffel and G. Margaritondo, Phys. Rev. Letters **49**, 812 (1982).

10 N. H. Tolk, M. M. Traum, J. C. Tully and T. E. Madey, eds., *Desorption Induced by Electronic Transition* (Springer-Verlag, Heidelberg, 1983)

11. F, Antonangeli, N. Zema, M. Piacentini, R. Pizzoferrato, M. Casalboni, R. Francini, U. M. Grassano and F. Bassani, in *Abstracts of the 1986 SRC Users Meeting* (Synchrotron Radiation Center, Madison, Wisconsin 1986).

12 F. Bassani and M. Altarelli, in *Handbook of Synchrotron Radiation*, E.-E. Koch ed. (North-Holland, Amsterdam 1983), Vol. 1.

13. G. Margaritondo, "*Introduction to Synchrotron Radiation*" (Oxford, New York 1988).

14. G. Margaritondo, C. Coluzza and R. Sanjinés, Eds.: *Photoemission, from the Past to the Future* (EPFL, Lausanne, 1992).

## Figure Captions

Fig. 1 - Three-dimensional Spyglass© computer reconstruction of a total-yield photoelectron micrograph of a portion of a neuron network, taken with today's most advanced scanning photoemission spectromicroscope, the MAXIMUM system at Wisconsin (Refs. 2 and 3).

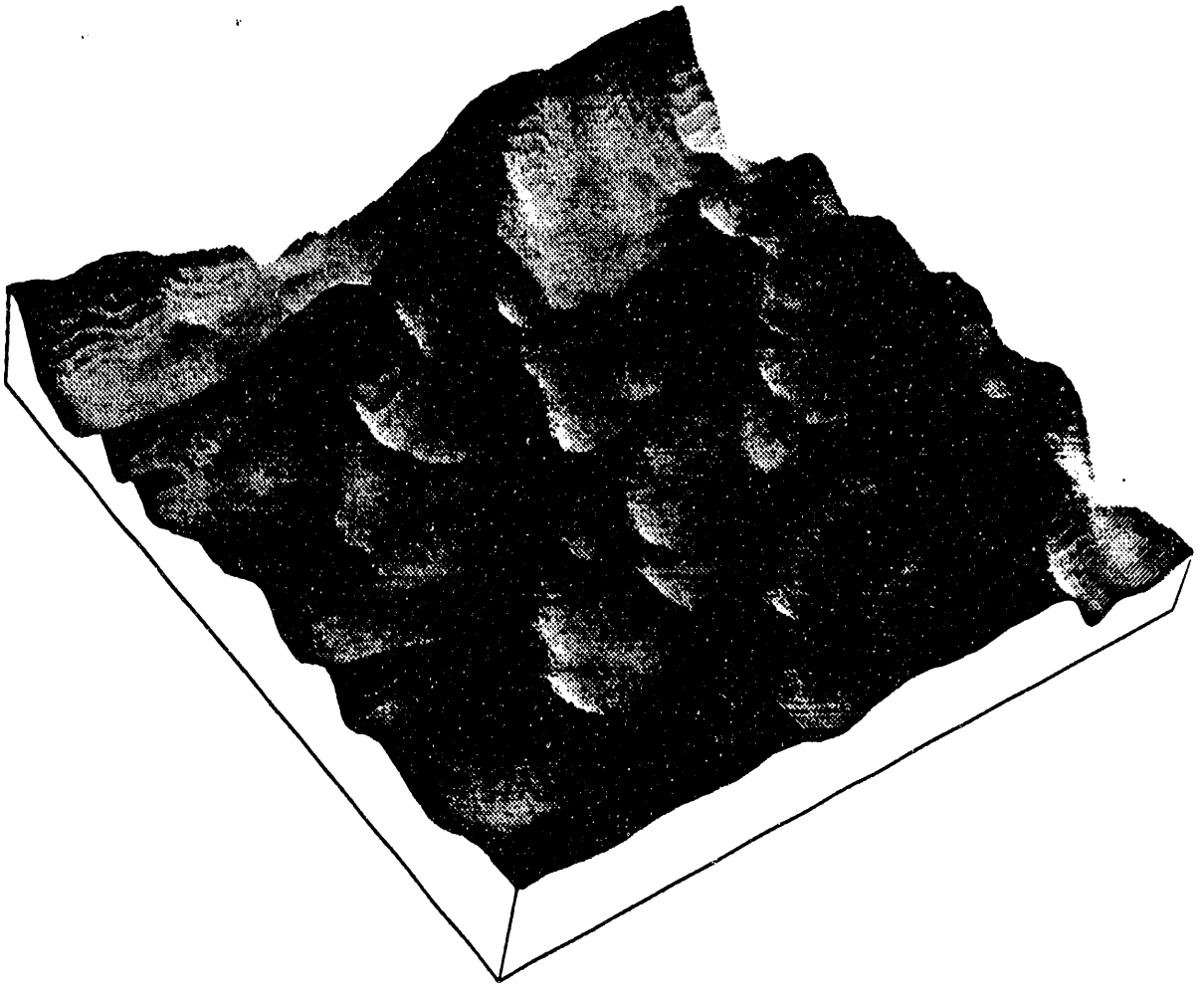

may14a1inv_norm vs. ( row, col )

# Applications of High Intensity X-rays to Materials Synthesis and Processing

**W. Walukiewicz**

**Lawrence Berkeley Laboratory**

Development of a high intensity x-ray FEL could open a new , uncharted and potentially very promising research area. In recent years several groups have attempted to use x-rays to either modify properties or to induce epitaxial growth of materials [1-8]. These initial studies have shown very clearly that in order to fully utilize the this new processing technique, very high intensity photon sources will be required. So far, sufficient x-ray beam intensities have been achieved only by using white synchrotron radiation. In this approach however one is loosing a main advantage of the technique , the possibility of illumination with a monochromatic radiation for selective excitation of specific chemical species. The advent of new x-ray sources (ALS and APS) would improve the situation but still the beam intensities expected at these facilities may not be high enough for most of materials. A real breakthrough can be achieved only with x-ray intensities offered by the proposed FEL source.

There are two research areas that would benefit from an intense x-ray source:

**1. X-ray induced (enhanced) deposition or etching of thin films.**

**2. Selective post-growth processing of materials.**

**1)** In the first area the research has been focused on using x-rays to induce a decomposition of the chemicals used in the epitaxial growth and to enhance the surface mobility of the host crystal lattice atoms. A variety of materials were grown with this technique. Growth of silicon nitrite films [1], [2], [6] and Si epitaxial layers [7] was studied using high intensity x-rays. Synchrotron radiation induced etching of silicon oxide, silicon nitrite and carbon films has been demonstrated in a number of works [3-5]. It has been also shown that high energy photon illumination can be used to affect interactions of adsorbed atoms with semiconductor substrates.

In all these experiments, in order to increase the photon flux, a white, wide-band radiation has been utilized. So far there is only one known instance where a psuedo-monochromatic light from an undulator has been used to enhance etching of silicon oxide [5]. An extremely high intensity of the FEL source would greatly expand the range of possible experiments on radiation enhanced epitaxial growth and etching. Selective excitation of chemical reactions in the precursors used for epitaxial growth or etching could lead to new, exotic modes of the crystal growth or decomposition.

**2)** Low temperature, selective processing of materials could be even more exciting area of application of high photon flux x-ray sources. Although both

optical lasers and high energy electron beams are quite extensively used for processing of materials there is only a very limited number of cases where the effects of illumination with high intensity x-ray beams on materials properties were studied [9-12]. In most instances these studies were concerned with deterioration of the properties of semiconductor devices exposed to high fluxes of hard x-rays or $\gamma$-rays.

It has been shown recently that a prolonged exposure of Mg doped GaN to 5 keV electrons results in activation of Mg dopants as electrically active acceptors [13]. This was the first demonstration of the p-type conductivity in this wide gap semiconductor. This annealing technique relies on a local excitation of material with a high energy electron. There are obvious disadvantages of the method. All the electrons are absorbed in a very thin layer of the material. Also, this process does not provide any element specific selectivity.

Use of x-rays could significantly expand the range of applications of this type of annealing. One could selectively excite specific impurities incorporated in a semiconductor matrix or to selectively deposit x-ray energy in a buried layer in a multilayer structures or in inhomogenous material systems (e.g. metallic precipitates in semiconductors). It should be emphasized that these type of experiments would require very long exposure times in the existing synchrotron radiation facilities. However they could be readily performed with the beam intensities expected in the FEL.

**References**


[1] F. Cerrina, et. al., Appl. Phys. Lett. **50**, 533, (1987)
[2] H. Kyuragi, et.al., J. Appl. Phys., **61**, 2035, (1987)
[3] T. Urisu, et. al., J. Vac. Sci. Technol. **B 5**, 1436, (1987)
[4] H. Kyuragi, et. al., Appl. Phys. Lett., **50**, 1254, (1987)
[5] K. Shobatake, et. al., Appl. Phys. Lett., **56**, 2189, (1990)
[6] H. Kyuaragi, et. al., J Electrochem. Soc., **138**, 3412, (1991)
[7] Jun-chi Takahashi, et. al., Appl. Phys. Lett. **58**, 2776, (1991)
[8] R. Zanoni, et. al., **VUV-10** (1992)
[9] N. Abdullaev, Sov. Phys. Semic., **20**, 1092, (1987)
[10] N. I. Maslov, Sov. Phys. Semic., **18**, 365, (1984)
[11] E. M. Pashaev, et.al., Sov. Phys. Semic., **25**, 651, (1991)
[12] D. Boyne, et. al., **58**, 2687, (1991)
[13] H. Amano et.al., Jpn J. Appl. Phys. **28**, L2112, (1989)

# LCLS OPTICS: SELECTED TECHNOLOGICAL ISSUES AND SCIENTIFIC OPPORTUNITIES*

**Roman Tatchyn**

Stanford Synchrotron Radiation Laboratory, Stanford Linear Accelerator Center, Stanford, CA 94305, USA

## Abstract

The Stanford Linac Coherent Light Source (LCLS) promises to generate photon pulses of unprecedented brevity and peak brightness in the soft x-ray range. In this presentation selected limitations and novel opportunities for technology and science associated with the availability of such pulses will be briefly assessed. Special emphasis will be placed on possible techniques for extending the peak power density and the temporal and spectral regimes of the LCLS output radiation by orders of magnitude beyond their nominal (calculated) values, and to the associated instrumentation for processing this radiation.

*Supported by DOE Offices of Basic Energy Sciences and High Energy and Nuclear Physics

## I. LCLS output characteristics

In recent work, systematic studies of various linac-driven Free-Electron Laser (FEL) configurations, primarily in the vicinity of the water window (≈40 Å), based on excitation with a laser-excited photocathode electron gun, were conducted [1]. A comprehensive list of the associated system parameters for selected configurations at this and substantially differing wavelengths may be found in the columns under the "RF Gun Based" heading in Figure 1. Brief definitions of the descriptive parameters are shown in Fig. 2. From the rows labelled "$\sigma_s$," "$E_{\lambda\,(coh)}$," "DIAM. @ 50m," and "DIAM. @ 250m," the peak output power density at normal incidence can be estimated to lie in a range of $10^{11}$-$10^{12}$ W/cm$^2$, at associated (full) pulse lengths of ≈ 0.5 ps. In addition to the major coherence parameters listed in Fig. 1, these may be taken as the nominal output parameters of the (water-window) LCLS running at 6 GeV.

An important property of the electron bunch accelerated through the linac is the development of an energy gradient (or "correlated energy spread") in the forward direction due to electrons in the front of the bunch loading the accelerating fields addressed by the trailing particles [2]. This energy spread is superimposed on the "uncorrelated" energy spread of the bunch characterized by its (stochastic) emittance parameters. For our purposes, we note that these energy spreads show up as, respectively, "inhomogeneous" and "homogeneous" line broadenings in the FEL photon pulse. Due to the $\gamma^2$ (or $E^2$) dependence of the

FEL's output photon energy, these broadenings can be shown to appear with roughly twice the relative size in the photon spectrum as in the electron bunch.

In the following parts of our presentation we will address: 1) selected peak intensity and materials damage issues; 2) peak intensity damage mitigation using a) solid-state materials in grazing incidence configurations, b) gas optics, or c) disposable optics; 3) pulse-length limitations on monochromator performance; 4) enhanced monochromatization via pulse lengthening; 5) LCLS pulse compression techniques based on the linac-induced correlated energy spread and selected applications; and 6) power density enhancement via microfocussing and selected applications.

## 2. Peak intensity and materials damage

At normal incidence, it is easy to estimate from typical attenuation coefficients in the soft x-ray range [3] and the tabulation in Figure 1 that 1 eV or more of energy can be deposited per atom in 0.5 ps. Apart from photoemission, which typically accounts for only a few-to-several percent of the absorbed energy, the primary energy-removal channels (radiation, conduction, etc.) all have time constants that are considerably longer. Keeping in mind that typical atomic or molecular lattice binding energies are of the order of 1 eV, we can appeal to the "pigeonhole principle" to infer that the probability of atomic and

molecular bonds beginning to break and the absorbed energy being transported away by fragmentation must start becoming appreciable under the cited conditions. We can consequently expect enhanced probability of damage in solid state materials by the LCLS photons from two primary effects: 1) lattice disruption/ablation, and 2) photoemissively-generated field stresses.

It should be noted that the enhanced probability of structural damage and ablation is likely to be particularly important with regard to the LCLS beam line optics, or, more generally, for samples in which the same area gets repeatedly irradiated, effectively integrating the probability of damage over long periods of time. For example, even if the probability of any irradiated atom ablating is as low as 1 part in $10^7$ per pulse, substantial damage to an optical surface could be expected after only 10 hours of operation at a 120 Hz rep rate. We may note here that both lattice disruption and ablation can in principle be highly deleterious to the performance of multilayer optics, especially those with small periods. Photoemissively-induced field stresses, which clearly merit a more systematic and detailed study, will also affect the design and operating strategy of optical elements and experimental samples. For example, to enhance the rate of charge neutralization, one would probably want to avoid using mirrors (even at grazing incidence) consisting of thin metallic films deposited on dielectric or semiconducting substrates with large areas.

## 3. Special techniques for peak intensity damage mitigation

The most intuitively evident way to mitigate peak intensity damage is to dilute the energy deposited per unit area (and thereby per atom) by the artifice of grazing incidence. General parameters associated with this approach for specular reflectors are shown in Figs. 3-5. We note the quantitative definition of $\eta$ [eV/atom] in terms of the LCLS parameters, the grazing-incidence parameters, and the physical constants (including the reflectivity R) of the mirror material. Since the grazing-incidence geometry is necessary to attain high values of R in the soft x-ray range, we also see that good optical performance and intensity-related damage inhibition are mutually consistent in this energy range. This result may be only partially generalized to multilayer reflectors, where smaller grazing incidence angles imply thicker periods, resulting not only in lesser damage, but in lesser sensitivity of performance to damage. Unfortunately, the typically large absorption of many multilayer materials in the soft x-ray range will also tend to restrict the reduction of the grazing incidence angle to overly small values, where the diminishing reflectivity may start countering the effects of the grazing-incidence dilution of $\eta$.

The methods outlined in Figs. 3-5 have currently been applied to generate a practical design for a mirror station for the LCLS, which has been described during the course of the workshop.

Notwithstanding the apparent effectiveness of grazing-incidence optics for the given LCLS parameters and the

assumed spectral range, future x-ray FEL configurations can be posited (e.g., the tapered wiggler [4]) whose peak outputs might be too high to be adequately handled by solid-state specular reflection even at extreme grazing incidence. To this end, we can consider two additional options: 1) gas optics, and 2) disposable normal-incidence optics.

Two possible schemes utilizing gas optics are shown in Fig. 6. The first, a "gas prism" deflects the LCLS output beam by inducing a phase gradient in its wavefront, similarly to an ordinary optical prism. The major difference lies in the rather large differential attenuation accompanying the phase gradient, which is seen to incur an appreciable intensity-loss penalty per degree of deflection. Numerical studies indicate that this penalty is virtually prohibitive for all gases but hydrogen and helium, and is rather severe even for the former. An alternative possibility would be to configure a "gas grating" with period a, enabling a minimum deflection angle of $\lambda/a$ to be attained. Here, however, the relative efficiency of the diffracted orders will be determined by the density contrast attained in the gas and their absolute efficiency by the average gas thickness, and it will probably prove to be difficult to generate thin gas sheets with significant density or particle-number contrasts for grating periods extending down to 10μ and beyond. We can also note here that although fully or partially ionized plasmas could in principle offer more advantageous optical constants for effective beam steering, the preparation of sufficiently small and dense jets would in general be expected to be significantly more difficult than with unionized

gases.

Given these observations, we note that the relatively sparse pulse structure (120 Hz) of the LCLS can easily allow mechanical motion of optical surfaces and shutters over distances significantly greater than the beam waist to occur between pulses. This makes feasible the notion of using "disposable" optics at normal or near-normal incidence to deflect or otherwise process the LCLS beam. For example, with a beam spot size of 1 mm, we can estimate that if the 1 mm area of impact is totally obliterated by one pulse, we would require a renewal rate of the optical surface of about 1 $m^2$/hour. For ultra-thin optics (e.g., zone plates or transmission gratings), suitably-placed rotating shutters could be used to effectively trap and collect the debris, and recovery and re-fabrication schemes could perhaps be developed to sustain economic feasibility. With regard to the numerous comments made at this workshop concerning experimental limitations caused by damage to solid state or liquid samples, we note that a similar "inter-pulse" scanning stratagem could be used to significantly ease the apparent restrictions. To wit, rather than probing one sample only (as is conventionally done), one could prepare, say, N identical samples (viz., an experimental ensemble) and "step" them through successive LCLS pulses. This would amount to introducing an additional (statistical) degree of freedom into the LCLS experimental algorithm, and would - especially for large N - tend to be more costly and involved than using just one sample. However, the increase in the dynamic range of otherwise conventional parameter space gained by this approach should allow

the systematic probing of high-intensity physical phenomena inaccessible by other techniques at alternative SR facilities.

## 4. Pulse-length limitations on attainable coherence

Under the condition that the correlated and uncorrelated energy spreads in the electron bunch are equal, the FEL radiation spectrum will be broadened to more than twice its natural relative width ($\rho_{eff}$). For larger correlated energy spreads the inhomogeneous broadening will be correspondingly greater. The present lack of detailed knowledge of the actual spread in the width of the LCLS pulses underscores the desirability of being able to monochromatize the emitted FEL photon pulses, and a number of important scientific applications such as, e.g., high-precision absorption or photoemission spectroscopy, will demand it.

As indicated in Figs. 7 and 8, conventional soft x-ray monochromators usually process temporal pulses that are considerably longer than the coherence length of the wave trains corresponding to their resolving power. For the LCLS, however, the pulse length could approach or even become smaller than this coherence length. For example, if the FEL pulse length is 0.1 ps long, this corresponds to 7500 wavelengths of 40 Å light, and the resolution attainable by a conventional monochromator designed to attain a resolution of, say, $10^{-4}$ at this wavelength could not exceed 1/7500. A geometrical outline of the propagation of this effect is sketched at the bottom of Fig. 7 and a tabulation of

typical pulse length loading on attainable resolving power is given in Fig. 8.

The natural way to try to improve the situation is, evidently, to devise schemes for lengthening the LCLS pulse. As can be seen in the bottom schematic of Fig. 7, the diffraction process itself can be used to lengthen the pulse diffracted into any order, along with a corresponding increase in angular spread. By selecting a small fraction of the dilated pulse with suitable angular filtering, one can obtain an attenuated and dilated pulse suitable for further monochromatization. It is evident that methods like these, based on dispersive and angular filtering, will discard significant fractions of the emitted in-band photons; however, the initially high values of this parameter in the LCLS pulse should make their implementation potentially useful and interesting. An alternative approach, which would also result in significantly fewer in-band photons, would be to underutilize the compression stages in the accelerator to produce longer electron bunch lengths with smaller peak currents.

## 5. Pulse compression techniques for the LCLS

As stressed elsewhere in this workshop (e.g., Refs. [5-6]), the sub-picosecond temporal structure of the LCLS as contrasted with those of conventional synchrotron radiation (SR) facilities promises to open up important new avenues for scientific research in photon-based spectroscopies and other areas. At the same time,

specialized applications such as, e.g., the study of molecular and chemical dynamics were identified that could benefit from x-ray pulse lengths as short as 10-15 fs [7]. To this end, it is important to point out that different methods of shortening the LCLS pulses to values beyond those listed in Fig. 1 might be applicable. Perhaps the most direct approach would be to compress the electron bunch even further. Preliminary assessments indicate that another factor of 10 (viz., down to 50 fs) could perhaps be feasible [8]. This method, while non-trivial to implement, would evidently be the most attractive, since it would deliver the maximum number of in-band photons to the experimenter. Apart from developments associated with the electron bunch, it is useful to note that the inhomogeneous energy gradient of the photon beam in the forward direction could also be used to extract x-ray pulses from the LCLS with durations down to 100 fs range and beyond. The method for accomplishing this, based on dispersion by a transmission grating with a chirped period at normal incidence, is schematized at the top of Fig. 9. Table 2 in Fig. 9 shows some of the attainable pulse lengths ($\tau_c'$), required inhomogeneous energy spreads, grating line densities, and expected loss factors associated with the proposed technique.

## 6. Microfocussing and selected applications

A research program aimed at developing and exploiting high-intensity SR and its coherence properties has been in

progress at SSRL since 1983. One initial goal of the program has been the development of optics and physical systems for pumping soft x-ray transitions in atomic Lithium with SR with the ultimate aim of producing a soft x-ray laser at 66 eV [9]. To this end, an ellipsoidal "superfocussing" specular reflector was designed and fabricated and in a series of experiments power densities of $10^9$ Watts/cm$^2$ were attained (see Fig. 10) at Beam Line 5 on SPEAR. In the literature reporting on this work [10], a number of potential experimental applications of SR beams microfocussed down to densities of $10^{10}$-$10^{12}$ Watts/cm$^2$ were noted, including: 1) pumping of soft x-ray transitions in solids, liquids, and gases, 2) study of non-linear phenomena associated with outer and inner-shell processes, 3) "flash" holography and microscopy of living organisms, 4) microprobing, and 5) the study of saturation effects in surface and bulk photoemission. Due to unfavorable emittance parameters on SPEAR, which limited the attained power density, plans were developed for a soft x-ray insertion device facility on PEP [11,12] which was expected to attain the microfocussed power densities required for the cited research. It is noteworthy that we now expect that the power densities that were once anticipated to be generated on PEP with the optic shown in Fig. 10 can in principle be generated without any special focussing by the LCLS. Although all of the above named research areas, together with an interferometry/imaging program aimed at exploiting the coherence properties of SR [13], are consequently still of extreme scientific interest, it is equally appropriate at this point to consider some of the implications of

extrapolating our developed microfocussing technology to the unfocussed LCLS beam.

As opposed to the cited exercise on Beam Line 5, which was limited by a relatively large source size, it is noteworthy to observe that the LCLS laser output will, by definition, be diffraction-limited. Consequently, a similar demagnification could be attempted to attain a diffraction-limited focus with a waist approaching the FEL wavelength. In order to assess the parameters associated with this feat, a log-log chart showing the equivalent energy density, power density, and field strength that could be attained at the focus is presented in Fig. 11. To emphasize the numbers involved, the Beam Line 5 experimental point is plotted along with equivalent numbers for an electron. With regard to the excitation of non-linear processes, we can recall that a standard criterion for assessing the strength of induced higher-order photon processes is the ratio of external field strength to the average field strength in an atom ($\approx 10^{10}$ V/m) [14]. Bearing in mind that high-power visible lasers can attain ratios of the order of 1, it is interesting to observe that the LCLS could, in principle attain ratios as high as $10^4$. The implications are that a perturbation approach may no longer be applicable, and that new theoretical frameworks may have to be sought to predict experimental results. It seems noteworthy that we may well be within reach of investigating this speculation.

## 7. Acknowledgements

Useful discussions with members of the LCLS research group are acknowledged. This research was performed at SSRL which is operated by the Department of Energy, Office of Basic Energy Sciences, Division of Chemical Sciences. That Office's Division of Materials Sciences has provided support for this research.

## 8. References


[1] C. Pellegrini, J. Rosenzweig, H.-D. Nuhn, P. Pianetta, R. Tatchyn, H. Winick, K. Bane, P. Morton, T. Raubenheimer, J. Seeman, K. Halbach, K.-J. Kim, and J. Kirz, "A 2 to 4 nm High Power FEL on the SLAC Linac," presented at the 1992 FEL Conference, August 1992, Kobe, Japan; to appear in Nucl. Instr. and Meth. 1993.

[2] R. B. Palmer, "Prospects for High Energy $e^+e^-$ Linear Colliders," Annu. Rev. Nucl. Part. Sci. 1990.40:529-92.

[3] B. L. Henke, P. Lee, T. J. Tanaka, R. L. Shimabukuro, and B. K. Fujikawa, "The Atomic Scattering Factor, $f_1 + if_2$, for 94 Elements and for the 100 to 2000 eV Photon Energy Region," AIP Conference Proceedings No. 75, 340(1982).

[4] G. A. Deis, A. R. Harvey, C. D. Parkinson, D. Prosnitz, J. Rego, E. T. Scharlemann, and K. Halbach, "A Long Electromagnetic Wiggler for the Paladin Free-Electron Laser Experiment," IEEE Trans. Mag. 24, 1090(1988).

[5] R. Tatchyn and H.-D. Nuhn, "A Comparison between the Coherence Parameters of Short Wavelength FELs Based on the SLAC Linac and Selected 2nd and 3d Generation Storage Ring Sources," elsewhere these proceedings.

[6] C. S. Fadley, "Research in Chemical Physics, Surface Science, and Materials Science, with a Linear Accelerator Coherent Light Source," elsewhere these proceedings.

[7] C. Shank, "The Prospect of Femtosecond X-Ray Pulses," elsewhere these proceedings.

[8] T. Raubenheimer and K. Bane, private communication.

[9] P. L. Csonka, "Suggested Method for Coherent X-Ray Production by Combined X-Ray and Low Energy Pumping," Phys. Rev. 13A(1), 405(1976).

[10] R. Tatchyn, P. Csonka, H. Kilic, H. Watanabe, A. Fuller, M. Beck, A. Toor, J. Underwood, and R. Catura, "Focusing of undulator light at SPEAR with a lacquer-coated mirror to power densities of $10^9$ Watts/$cm^2$," SPIE Proceedings No. 733, 368(1987).

[11] R. Tatchyn, "The Potential of PEP as a High-Brightness Soft X-Ray Source for Coherence and Micro-Imaging Studies," Proceedings of the Workshop on X-Ray Microimaging for the Life Sciences, Berkeley, May 24-26, 1989, Report Nos. LBL-27660, UC-600, CONF-8905192, p. 185.

[12] R. Tatchyn, T. Cremer, and P. Csonka, "Design considerations for a new weak-field soft X-ray undulator/FEL driver for

PEP," Nucl. Instrum. Meth. A308, 152(1991).

[13] R. Tatchyn, E. Källne, A. Toor, T. Cremer, and P. Csonka, "Operation of a normal-incidence transmission grating monochromator at ALLADIN (invited)," Rev. Sci. Instrum. 60(7), 1579(1989).

[14] N. Bloembergen, Nonlinear Optics, W. A. Benjamin, Inc., London, 1965.

| | DR Based | | RF Gun Based | | | | | | | | |
|---|---|---|---|---|---|---|---|---|---|---|---|
| | HYBRID UNDULATOR | | | | | PALADIN | | FIELD SYNTHESIZER | | | |
| E | 6.0 † | 6.0 ‡ | 6.0 | 6.0 | 6.0 | 3.0 | 6.0 | 6.0 | 50.0 | 50.0 | GeV |
| $\sigma_z$ | 12.4 | 12.4 | 5.0 | 5.0 | 6.0 | 9.8 | 5.0 | 5.0 | 4.0 | 4.0 | $x10^{-4}$ |
| $\varepsilon_n$ | 3.6 | 3.6 | 1.5 | 2.5 | 4.0 | 2.5 | 1.5 | 2.5 | 1.0 | 1.0 | mm-mrad |
| $\varepsilon_{x,y}$ | 3.03 | 3.03 | 1.28 | 2.13 | 3.41 | 4.26 | 1.28 | 2.13 | 0.102 | 0.102 | Å-rad |
| $\beta_{x,y}$ | 30.5 | 20.9 | 15 | 15 | 15 | 7.8 | 10 | 45 | 90 | 90 | m |
| $\sigma_s$ | 1.8 | 1.8 | 0.2 | 0.2 | 0.2 | 0.2 | 0.2 | 0.2 | 0.1 | 0.1 | ps |
| I | 0.7 | 0.7 | 2.4 | 2.4 | 2.4 | 2.4 | 2.4 | 2.4 | 5.0 | 5.0 | kA |
| $f_{rep}$ | 12 | 12 | 120 | 120 | 120 | 120 | 120 | 120 | 120 | 120 | Hz |
| < I > | 0.038 | 0.038 | 0.14 | 0.14 | 0.14 | 0.14 | 0.14 | 0.14 | 0.3 | 0.3 | μA |
| λ | 140 | 40 | 40 | 40 | 40 | 40 | 10.6 | 40 | 1 | 1 | Å |
| $\lambda_u$ | 10 | 5.1 | 10 | 10 | 10 | 8 | 8 | 36.1 | 36.1 | 20 | cm |
| $B_u$ | 0.93 | 1.35 | 0.47 | 0.47 | 0.47 | 0.3 | 0.31 | 0.04 | 0.062 | 0.157 | T |
| $K_u$ | 8.7 | 6.4 | 4.4 | 4.4 | 4.4 | 2.2 | 2.3 | 1.41 | 2.07 | 2.93 | |
| $z_R$ | 8.3 | 20.2 | 6.1 | 10.2 | 16.4 | 15.1 | 10.3 | 29.5 | 115.36 | 115.36 | m |
| ρ | 11.4 | 7 | 19.5 | 16.5 | 14.1 | 18.8 | 13.2 | 19.9 | 8.45 | 7.18 | $x10^{-4}$ |
| $\rho_{eff}$ | 5.9 | 1.5 | 18.6 | 15.4 | 12.8 | 18.4 | 11.8 | 19.0 | 7.17 | 5.92 | $x10^{-4}$ |
| $L_G$ | 7.8 | 15.6 | 2.5 | 3.0 | 3.6 | 2.4 | 3.1 | 8.7 | 23.13 | 15.53 | m |
| $L_{sat}$ | 170 | 339 | 54 | 65 | 78 | 44 | 68 | 190 | 503 | 337 | m |
| $\sigma_r$ | 122 | 92.7 | 37 | 40.6 | 44.4 | 36.3 | 21.4 | 69.4 | 17.8 | 14.6 | μm |
| $\sigma_{r'}$ | 9 | 3.44 | 8.6 | 7.8 | 7.67 | 8.8 | 3.95 | 4.58 | 0.446 | .545 | μrad |
| $\sigma_{Ix,Iy}$ | 155.3 | 122.2 | 57.4 | 69.6 | 84.2 | 68.1 | 41.7 | 120 | 35.1 | 33.6 | μm |
| $\sigma_{Ix',Iy'}$ | 9.5 | 5.1 | 9.1 | 8.7 | 9.03 | 11.5 | 5.3 | 5.1 | 0.56 | 0.64 | μrad |
| DIAM. @ 50m | 3.6 | 3.1 | 1.9 | 1.96 | 2.2 | 2.24 | 1.22 | 2 | 0.51 | 0.43 | mm § |
| DIAM. @ 250m | 8.3 | 5.7 | 6.45 | 6.3 | 6.7 | 8 | 3.9 | 4.7 | 0.79 | 0.75 | mm § |
| $\Delta\lambda_{FEL}/\lambda$ | 5.9 | 1.5 | 18.6 | 15.4 | 12.8 | 18.4 | 11.8 | 19.0 | 7.17 | 5.92 | $x10^{-4}$ |
| $\Delta\lambda_{\perp}/\lambda$ | 2 | 2 | 2 | 2 | 2 | 2 | 2 | 2 | 2 | 2 | $x10^{-3}$ * |
| $[(\Delta\lambda_{FEL}^2+\Delta\lambda_{\perp}^2)]^{1/2}/\lambda$ | 2.09 | 2.006 | 2.73 | 2.52 | 2.37 | 2.72 | 2.322 | 2.76 | 2.13 | 2.09 | $x10^{-3}$ |
| $P_{coh}$ ◊ | 2.5 | 0.63 | 26.7 | 22.1 | 18.5 | 11.7 | 17.0 | 27.3 | 179.3 | 148 | GW |
| $<P_{coh}>$ ◊ | 0.135 | 0.34 | 1.6 | 1.33 | 1.11 | 0.7 | 1.02 | 1.64 | 5.38 | 4.45 | W |
| $N_{coh}$ ◊ | 8.0 | 0.57 | 2.7 | 2.2 | 1.9 | 1.16 | 0.45 | 2.75 | 0.23 | 0.186 | $x10^{14}$/pls |
| $<N_{coh}>$ ◊ | 0.95 | 0.685 | 3.2 | 2.68 | 2.24 | 1.41 | 0.54 | 3.3 | 0.27 | 0.224 | $x10^{16}$/s |
| $E_{N(coh)}$ ◊ | 11.3 | 2.84 | 13.4 | 10.9 | 9.4 | 5.85 | 8.42 | 13.6 | 45.7 | 37.8 | mJ |
| B | 0.44 | 0.18 | 0.91 | 0.6 | 0.35 | 0.18 | 1.0 | 0.68 | 71 | 48.7 | $x10^{31}$ ^ |
| < B > | 0.24 | 0.097 | 0.55 | 0.365 | 0.21 | 0.11 | 0.6 | 0.41 | 21.3 | 14.6 | $x10^{21}$ ^ |

† Damping Ring (DR) energy 600 MeV; ‡ DR energy 600 MeV; § beam diameter at specified distance from end of undulator; ◊ over the entire inhomogeneous bandwidth; * 0.001 correlated energy spread in electron beam assumed;
^ [photons/sec,mm$^2$,mr$^2$,0.1%BW]

Figure 1. LCLS machine, electron beam, insertion device, photon output, and coherence parameters for various electron beam sources, spectral ranges, and insertion device types.

PARAMETERS FOR ASSESSING APPLICATIONS OF LINAC-BASED FEL RADIATION
(R. Tatchyn 3/26/92)

| | |
|---|---|
| E [GeV] | (linac energy) |
| $\sigma_\varepsilon$ | (relative energy spread) |
| $\varepsilon_n$ | (normalized emittance) |
| $\varepsilon_{x,y}$ [nm-rad] | (vertical and horizontal emittances) |
| $\beta_{x,y}$ [m] | (vertical and horizontal beta functions) |
| $\sigma_s$ [ps] | (standard deviation of temporal bunch length) |
| I [Amp] | (peak current in bunch) |
| $f_{rep}$ [Hz] | (pulse repetition rate) |
| <I> [μA] | (average current) |
| λ [Å] | (first harmonic wavelength) |
| $\lambda_u$ [cm] | (undulator period) |
| $B_u$ [T] | (on-axis field amplitude) |
| $K_u$ | (undulator deflection parameter) |
| $z_R$ [m] | (Rayleigh length) |
| ρ | (ideal FEL gain parameter) |
| $\rho_{eff}$ | (effective FEL gain parameter) |
| $L_G$ [m] | (e-folding power gain length) |
| $L_{sat}$ [m] | (undulator length for saturation) |
| $\sigma_r$ [μm] | (diffraction-limited phot. beam size ($\lambda^{1/2}L_{sat}^{1/2}/4\pi$)) |
| $\sigma_{r'}$ [μrad] | (diffraction limited phot. beam angle ($\lambda/L_{sat}$)$^{1/2}$)) |
| $\sigma_{\Sigma x,\Sigma y}$ [μm] | (total phot. beam waist size) |
| $\sigma_{\Sigma x',\Sigma y'}$ [μrad] | (total phot. beam angle) |
| DIAM. @250m [mm] | (phot. beam diameter 250m from undulator center) |
| $(\Delta\lambda/\lambda)_h$ | (homogeneously broadened bandwidth ( = $\rho_{eff}^{-1}$))* |
| $(\Delta\lambda/\lambda)_i$ | (inhomogeneously broadened bandwidth)* |
| $P_{coh}$ [GW] | (peak coherent power over inh. BW) |
| <$P_{coh}$> [W] | (average coherent power over inh. BW) |
| $N_{coh}$ [ph/pulse] | (peak coherent photons per pulse, over inh. BW) |
| <$N_{coh}$> [ph/s] | (average coherent photons per second, over inh. BW) |
| $E_{coh}$ [J] | (peak coherent energy in 1 pulse, over inh. BW) |
| B [ph/sec,mm$^2$,mr$^2$,0.1%BW] | (peak brightness) |
| <B> [ph/sec,mm$^2$,mr$^2$,0.1%BW] | (average brightness) |

* if both profiles are assumed Gaussian, total BW = $(\Delta\lambda_h^2+\Delta\lambda_i^2)^{1/2}$).

**Figure 2. Glossary for Figure 1.**

# SPECULAR REFLECTORS

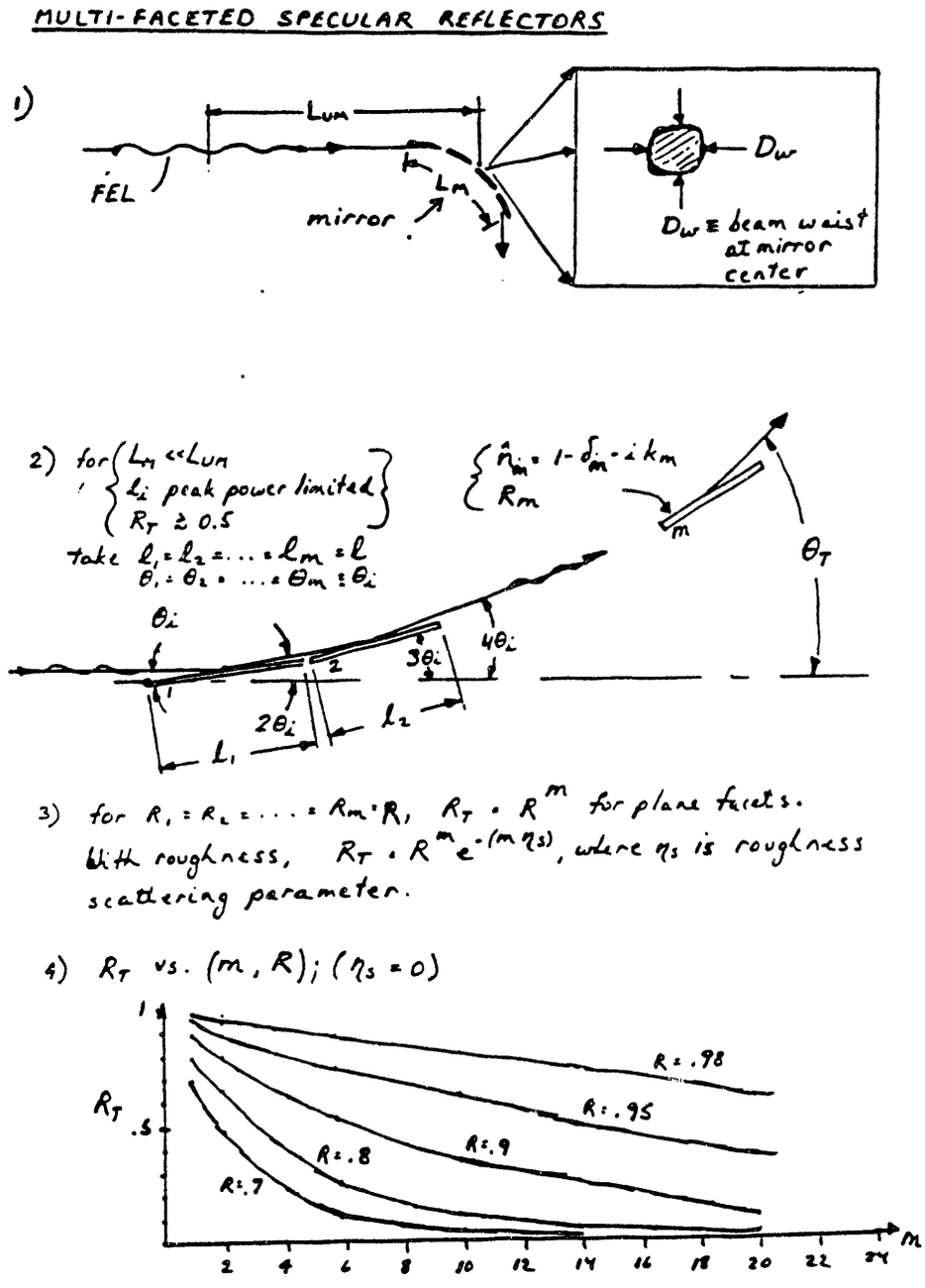


Figure 3. Beam and mirror facet parameters for multi-faceted reflectors.

# DAMAGE ISSUES IN SPECULAR REFLECTORS

5) Define:

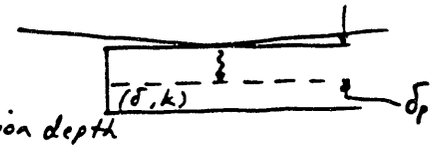


- $\delta_p$ ($\cong \frac{\lambda}{4\pi\beta k}$)
  ≡ 1/e penetration depth
- # [$cm^{-3}$] ≡ atomic density
- $\hat{P}_{coh}$ [W] ≡ peak FEL power
- $\sigma_\tau$ [s] ≡ st. dev. of photon pulse length

6) Introduce $\eta_A$, energy loading/atom
(when $\eta_A$ is of the order of 1, it is known that surfaces can ablate)
Thus, introduce criterion for each mirror facet:

$$\eta_A \cdot \left(\frac{\hat{P}_{coh}\sqrt{2\pi}\sigma_\tau}{g}\right)\left(\frac{\theta_i}{D_w^{\frac{1}{2}}}\right)\left(\frac{1-R}{\delta_p \#}\right) \ll 1 \qquad (1)$$

7) Example:
$\hat{P}_{coh} = 10^{10}/2$; $\sigma_\tau = .2\times10^{-12}$; $D_w = 0.2$; $\# \cong 2\times10^{23}$;
$\delta_p \approx \lambda$ (= 40Å); set criterion at $\eta_A \leq .01$

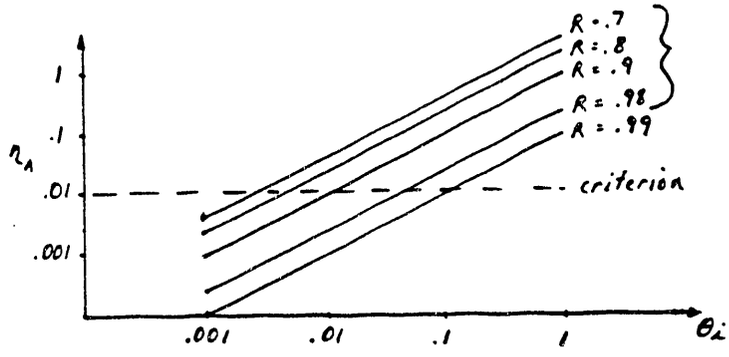


8) - BLS experiment attained ~$10^9$ W/$cm^2$
(no definite ablation damage on Ni foils was observed) *

* R. Tatchyn et al, SPIE Proc. 733, p.368 (1987)

Figure 4. Energy loading parameters and damage threshhold criteria for specular reflectors.

9) DESIGN:
- select $\theta_T$, $m$ for a given $D_w$
- $\ell = D_w/\theta_i$
- $\theta_i = \frac{1}{2}\theta_T/m$
- for $\theta_i$ small, mirror contour approximates a circle:

$$R_n \approx \frac{2m^2 D_w}{(\theta_T)^2} \quad (2)$$

$$\theta_m \approx \theta_T \quad (3)$$

$$L_m \approx m\ell \quad (4)$$

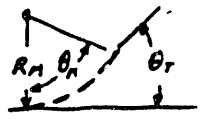


10) STUDY ($D_w = .2$ cm, use $Al_2O_3$ + Au constants *)

| $\theta_T$ \ m | | 2 | 4 | 8 | 16 |
|---|---|---|---|---|---|
| 0.2 (~10°) | $\theta_i$ → | .05 | .025 | .0125 | .00625 |
| | $L_m$ [m] → | .08 | .32 | 1.28 | 5.12 |
| | $R_T(Al_2O_3)$ → | 0.9 | 0.85 | 0.82 | 0.8 |
| | $R_T$(Au) → | 0.29 | 0.31 | 0.31 | 0.25 |
| 0.4 (~22°) | $\theta_i$ → | .1 | .05 | .025 | .0125 |
| | $L_m$ [m] → | .04 | .16 | .64 | 2.56 |
| | $R_T(Al_2O_3)$ → | 0.67 | 0.78 | 0.69 | 0.72 |
| | $R_T$(Au) → | 0.6625 | 0.079 | 0.08 | 0.075 |
| 0.8 (~45°) | $\theta_i$ → | .2 | .1 | .05 | .025 |
| | $L_m$ [m] → | .02 | 0.08 | .32 | 1.28 |
| | $R_T(Al_2O_3)$ → | ~0 | 0.45 | 0.61 | 0.44 |
| | $R_T$(Au) → | ~0 | 0.004 | 0.007 | 0.0065 |
| 1.6 (~90°) | $\theta_i$ → | .4 | .2 | .1 | .05 |
| | $L_m$ [m] → | .01 | .04 | .16 | .64 |
| | $R_T(Al_2O_3)$ → | ~0 | ~0 | 0.22 | 0.44 |
| | $R_T$(Au) → | ~0 | ~0 | ~0 | ~0 |

11) RESULTS WILL BE SENSITIVE TO SCATTERING PARAMETER $\eta_s$. FOR APPRECIABLE $\eta_s$, $m$ MUST BE KEPT MINIMAL.

* from Henke's compilation

Figure 5. Design study for a multifaceted reflector with facets of equal length, composed of either Au or $Al_2O_3$.

# GAS OPTICS

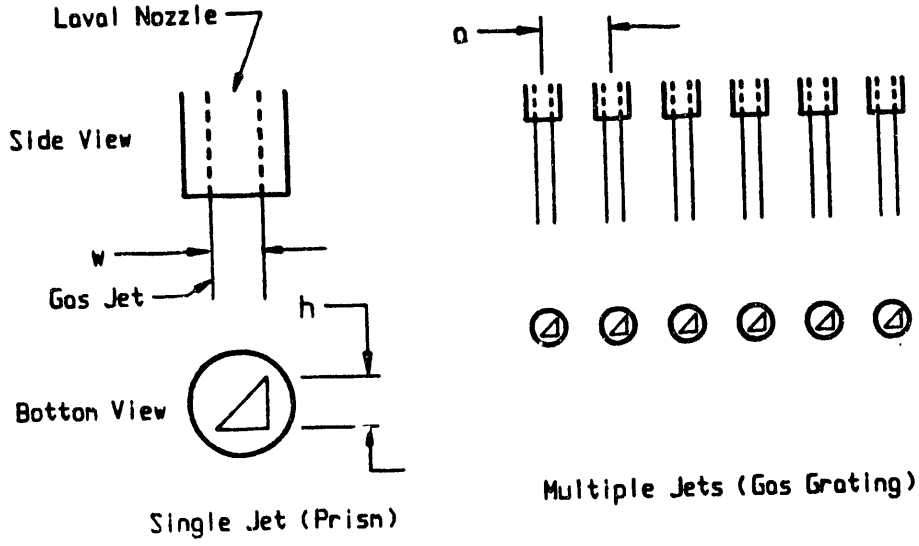


1) $\Delta\phi_{21} = 2\pi h\delta/\lambda$ ; $\eta = \exp\{-4\pi hk/\lambda\}$

2) for $H_2$, [$\delta = 4\times10^{-7}$ ; $k = 1.44\times10^{-8}$ @ STP]

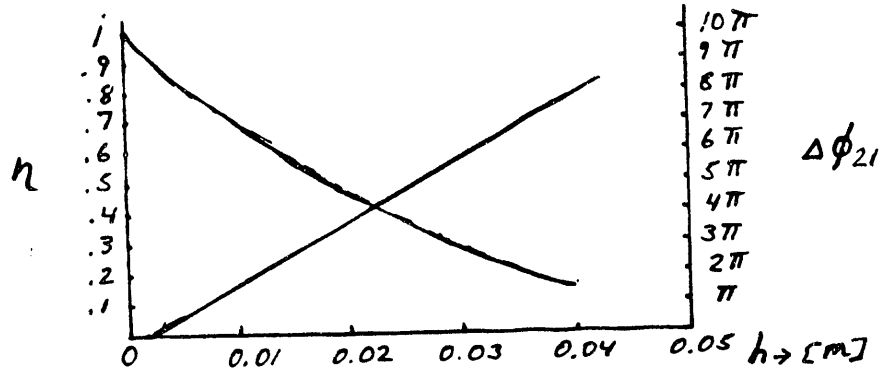


3) for 1 mm beam, can get ~ 0.1mr - 0.2mr with 0.99 - 0.999 loss.

4) with gas grating, deflection angle is determined by period a ($\theta_1 = \lambda/a$). @ a=40μ, $\theta_1$=0.1mr.

5) technical issues: how small can a be made while sustaining effective density variation? could liquid jets be used?

Figure 6. Gas-jet optical elements: gas prism (top left) and gas grating (top right). Attenuation and phase-gradient curves for an $H_2$ gas prism (bottom).

# MONOCHROMATIZATION (Short-pulse limitations)

**1) TEMPORAL EFFECTS:**

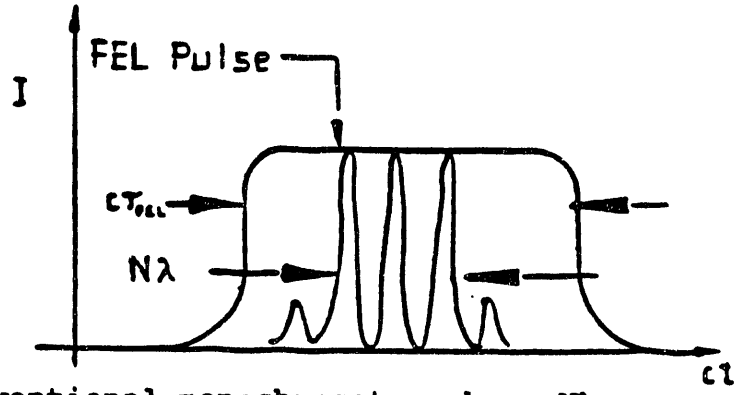


- conventional monochromators have $N\lambda \ll c\tau$
- for $N\lambda \gg c\tau$, resolving power of conventional monochromator will be reduced

**2) GEOMETRICAL PICTURE:**

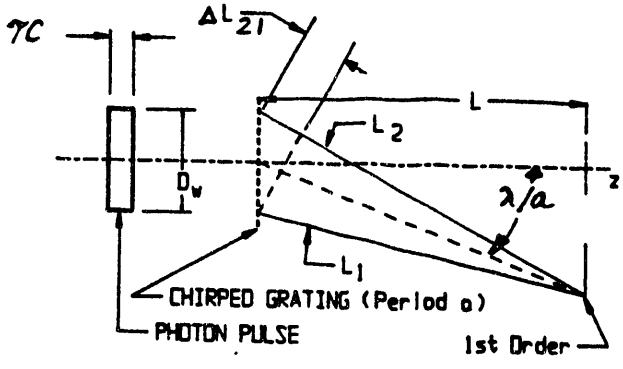


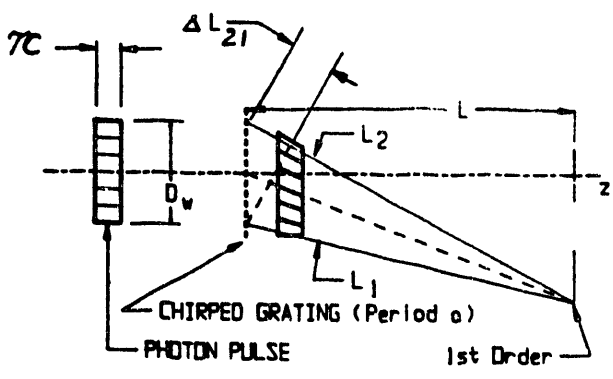


- $L_2 - L_1 \approx (D_w/a)\{\lambda + (D_w a/2L)\}$; $(D_w/a) \approx R_M$ (maximal resolving power)
- condition for attaining $R_M$: $R_M \ll \{\tau c/(\lambda + (D_w a/2L))\}$

Figure 7. Aspects of Fourier-Transform-limited monochromatization. Temporal-spectral picture (top). Angular-spatial picture (bottom).

3) FOR GENERAL MONOCHROMATOR CONFIGURATION:

$$R \cong \left[ \frac{1}{\left(\frac{1}{R_M}\right)^2 + \left(\frac{\lambda'}{\pi c}\right)^2} \right]^{\frac{1}{2}} \; ; \; \lambda' = \lambda + \frac{D_w a}{2L}$$

TABLE 1

$R$ vs. $\tau$[s] for $\lambda = 40$ Å ; $D_w = .002$ m ; $\lambda/a = .01$ ; $L = 2$ m

| $R_M$ \ $\tau$ | | $0.5 \times 10^{-12}$ | $0.3 \times 10^{-12}$ | $0.2 \times 10^{-12}$ | $0.1 \times 10^{-12}$ |
|---|---|---|---|---|---|
| $10^4$ | $R =$ | 9700 | 9100 | 8300 | 6000 |
| $5 \times 10^3$ | $R =$ | 4960 | 4880 | 4700 | 4200 |
| $2.5 \times 10^3$ | $R =$ | ~2500 | ~2500 | 2470 | 2371 |

4) CAN PHOTON PULSE BE LENGTHENED? SHORTENED?

METHODS: a) length dilation (contraction) of e⁻ beam in linac. Most effective

b) dilation (contraction) of "correlated" energy gradient of e⁻ beam in linac. Implies loss.

Figure 8. Pulse-length loading of optimum monochromator resolving power. Formula (top). Case study (Table 1).

# COMPRESSION

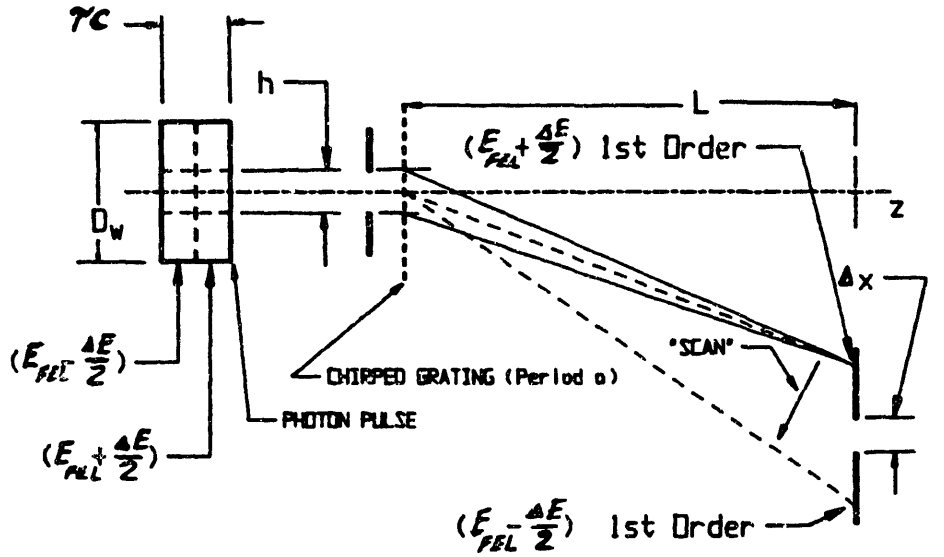


**conditions:** $1/\ N_{(h)} \propto \Delta E_{FEL}/\Delta E_{hv} = \Delta x a\{L(\lambda_{HIGH}^{-1}-\lambda_{LOW}^{-1})\}^{-1}$
**(N(h) = number of grating bars subtended by h)**

**TABLE 2**

$D_w = 0.001m$ ; $L = 2m$ ; $\Delta E_{FEL}/E_{FEL} = 0.001$

| τc[fs] | h[m] | N(h) | 1/mm | $\Delta E_{hv}/\Delta E_{FEL}$ | $\Delta E_{corr}/E_{LINAC}$ | τ'c[fs] | loss[%] |
|---|---|---|---|---|---|---|---|
| 0.5 | 2.5 | 10 | 40 | 2 | 0.001 | 0.25 | 12.5 |
| 0.5 | 1.0 | 25 | 250 | 5 | 0.0025 | 0.1 | 2.0 |
| 0.5 | 0.5 | 50 | 1000 | 10 | 0.005 | 0.05 | 0.5 |
| 0.5 | 0.25 | 100 | 4000 | 20 | 0.01 | 0.025 | 0.125 |
| 0.5 | 0.125 | 200 | 16000 | 40 | 0.02 | 0.0125 | 0.031 |

Figure 9. Pulse compression based on chirped photon bunch energy. The front of the bunch diffracts into a smaller angle than the rear. A small slit Δx placed between the two extremes will filter out a temporally abbreviated slice of the original pulse as it scans between the extremes.

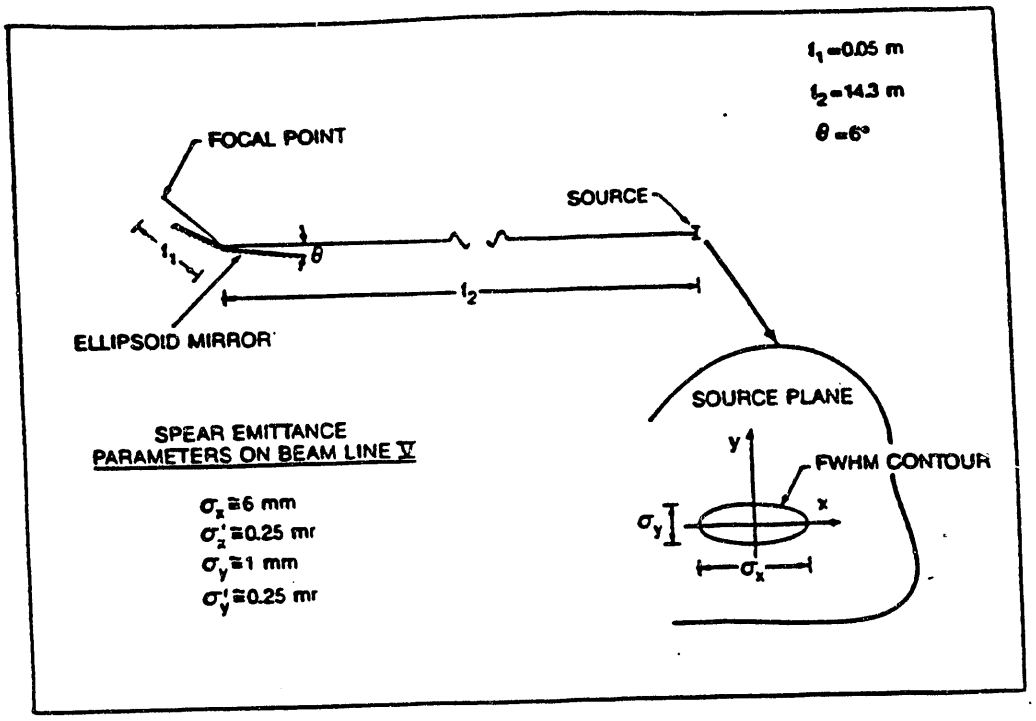


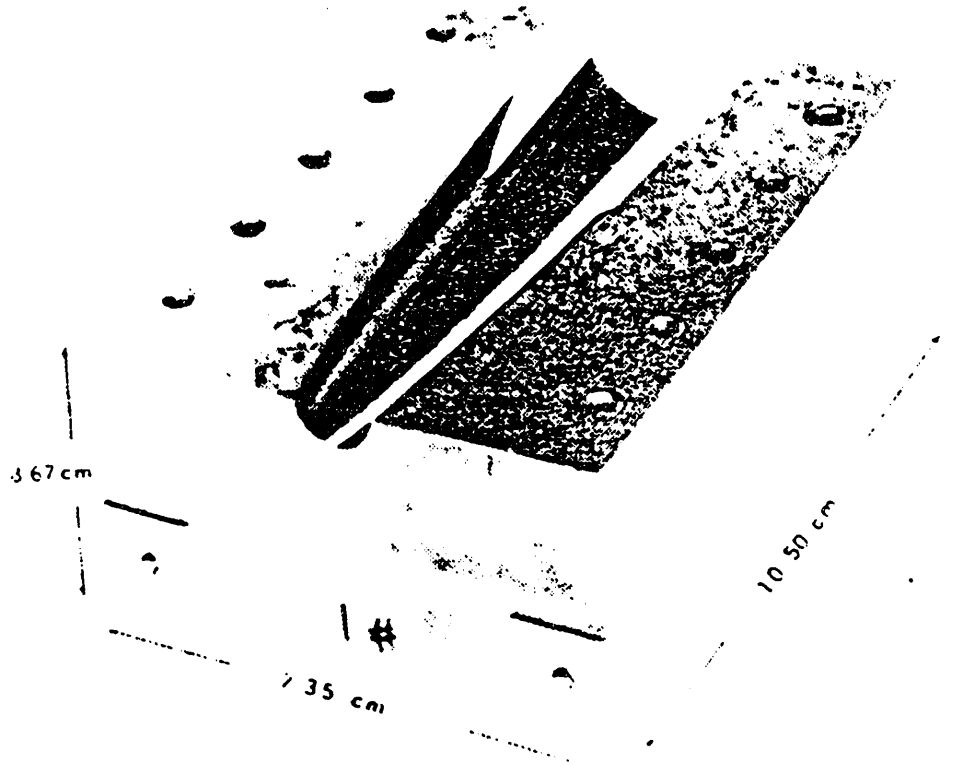


Figure 10. Microfocussing geometry on Beam Line 5 on SPEAR with a specular ellipsoidal reflector (top). Diamond-turned, lacquer-coated, and metallized ellipsoid (bottom). Defocussing ratio 300:1.

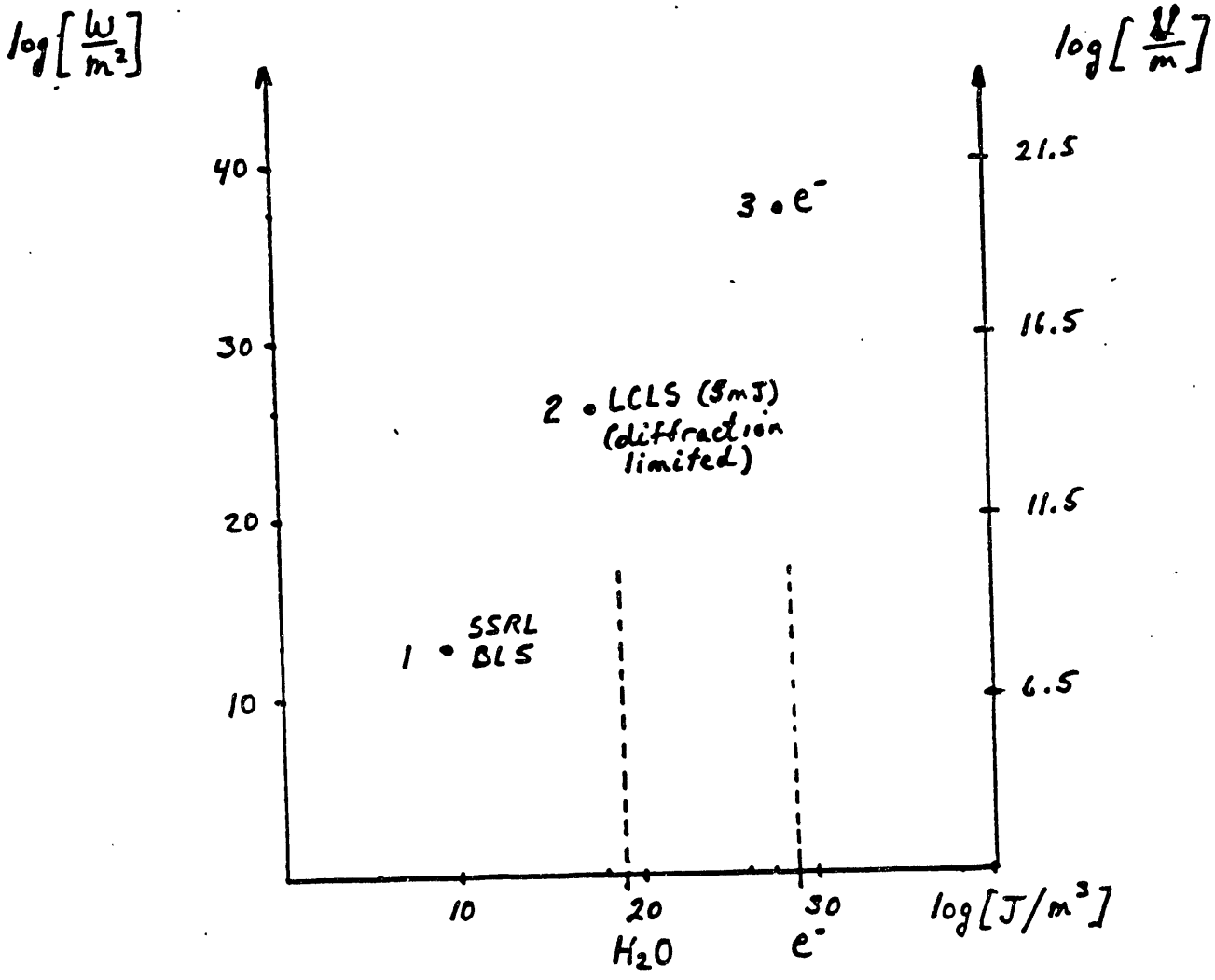


Figure 11. Equivalent field strengths and energy densities attained: 1) with ellipsoidal reflector on Beam Line 5 on SPEAR; 2) at the diffraction-limited focus of the LCLS FEL; and 3) at the classical radius of an electron. The equivalent energy densities of water and electronic matter are marked on the abscissa.

# POSSIBLE APPLICATIONS OF AN FEL FOR MATERIALS STUDIES IN THE 60 eV TO 200 eV SPECTRAL REGION

by

Z.X. Shen and W.E. Spicer
SSRL and Stanford University

After the workshop, we were asked to suggest possible applications of an FEL at lower photon energies, e.g. 60 - 200 eV. These are some immediate thoughts. At best, they should be thought of as ideas to stimulate discussion, rather than well thought out plans for action.

Although one can only learn very limited information about structural issues at photon energies near 100 eV, one can get information about the electronic structure and spin dynamics of novel materials. For materials containing rare earth and transition metal elements, (e.g. high-Tc superconductors, magnetic thin films and multilayers, dilute spin materials, heavy Fermion and mixed valence compounds) the 60 - 200 eV photon energy is very useful because it covers 3p to 3d and 4d to 4f transtions. These transitions allow us to perform resonance photoemission and x-ray absorption experiments. The high intensity and pulsed structure allows us to probe new physics that is not possible now.

All of the suggestions below are dependent on the ability to split the beam (so that we can do pump and probe experiments) and on the assumption that the samples under study are not destroyed by the beam. We also assume that we can get around the space charge problem. Obviously, these technical problems need to be worked out carefully.

## DILUTE SPIN SYSTEMS

Assume now that we have material containing dilute elements with a net spin moment (e.g. rare earth or transitionmetal elements). Doing a pump and probe study, we can investigate the electronic structure and possibly the spin fluctuations by monitoring the resonance photoemission intensity of the 4f or 3d states, or by monitoring the multiplets in the 4d to 4f absorption spectra (this is particularly suitable for rare earths).

The high intensity makes it possible to study very dilute materials. The giant resonance near the 4d to 4f absorption (at photon energies from 100 to 200 eV) can help us distinguish the signal from the elements containing the 4f electrons and those from the hosting matrix. The high intensity also makes it possible to do spin detection in these materials. (e.g. we can put the sample in an external field to align the spin and perform a spin resolved study).

## SPIN DYNAMICS OF MAGNETIC MATERIALS ABOVE THE CURIE TEMPERATURE

The Stonner model of magnetism captures many important aspects of magnetic materials. However, it fails to account for the properties of these materials above their Curie temperature. A microscopic understanding of magnetic materials above the Curie temperature is an outstanding problem in magnetism. The high intensity of the laser enables one to perform spin-resolved, time-resolved photoemission experiments to study the spin dynamics above the Curie temperature.

The above examples are magnetic materials. One can, of course, also study the electron-photon coupling using the laser if the time structure is right. At any rate, we believe 60 - 200 eV photons are very useful for materials research.

# V. APPENDICES

## APPENDIX A - WORKSHOP ANNOUNCEMENT

# WORKSHOP ON SCIENTIFIC APPLICATIONS OF SHORT WAVELENGTH COHERENT LIGHT SOURCES

**SSRL/SLAC October 21, 1992**

**Chairman: W. Spicer**
**Cochairmen: J. Arthur, H. Winick**

We are exploring the feasibility of using the SLAC 3 km linac to drive short wavelength coherent light sources - x-ray lasers. This raises new possibilities to produce high peak power (several gigawatts), short pulse (< 0.5 picoseconds), short wavelength (0.1-10 nm) photon beams. This workshop will explore the usefulness of such a source to the scientific community.

For example, preliminary calculations indicate that, using linac energies below about 10 GeV, it should be possible to build a tunable laser operating in the 2-5 nm range which could produce about $10^{14}$ coherent photons within a 0.5 ps pulse at a repetition rate of 120 Hz. This corresponds to a peak power of several gigawatts and average power of about 0.5 watts. Furthermore, using higher electron energies (up to the full 50 GeV available from the SLAC linac) x-ray lasers operating down to 0.1 nm are possible.

It now appears to us that applications of such a source to biological imaging are most exciting. However, we expect that the unique properties of this source may open other applications unforeseen by us. We welcome such innovative ideas at the workshop, which will explore the scientific applications of x-ray lasers spanning the wavelength range from about 10 nm to 0.1 nm. Recognizing the very high peak power levels of this source, we anticipate that it will be important to examine questions of sample damage.

We invite your participation. The preliminary program is on the back of this page.

## APPENDIX B - WORKSHOP AGENDA
## WORKSHOP ON SCIENTIFIC APPLICATIONS OF SHORT WAVELENGTH COHERENT LIGHT SOURCES

*SLAC Orange Room; October 21, 1992*

7:45 AM **Registration & Continental Breakfast** (Auditorium Breezeway)

Session I: Richard E. Taylor (SLAC) - Chair

8:30 Welcome; *Burt Richter (SLAC), Arthur Bienenstock (SSRL)*

8:45 Opening Remarks; *William Spicer (SSRL)*

8:55 "Some DOE Perspectives on Future Light Sources"; *Bob Marianelli (DOE, Chemistry Division, Office of Basic Energy Sciences)*

9:05 "Producing and Using Short Wavelength Coherent Sources"; *Claudio Pellegrini (UCLA)* and *Herman Winick (SSRL)*

9:45 "Atomic Physics Research with an X-ray Laser"; *Richard Pratt (Univ. of Pittsburgh)*

10:15 **Coffee Break** (Orange Room)

Session II: Johndale C. Solem (LANL) - Chair

10:45 "Imaging in 3 Dimensions with X-rays"; *James Trebes (LLNL)*

11:15 "X-ray Damage Issues and Wavelength Optimization in Biological Imaging"; *Richard London (LLNL)*

11:45 "Targets of Opportunity in Biological Imaging"; *Joe Gray (UCSF)*

12:15 PM **Lunch** (Auditorium Breezeway)

Session III: Louis J. Terminello (LLNL) - Chair

1:30 "The Prospect of Femtosecond X-Ray Pulses"; *Chuck Shank (LBL)*

2:00 "Research in Surface Science, Materials Science and Chemical Physics using an X-Ray Laser"; *Chuck Fadley (UC Davis/LBL)*

2:30 **Coffee Break** (Orange Room)

Session IV: John Arthur (SSRL) and David Attwood (LBL) - Chairs

3:00 Open session for short presentations, comments, questions from participants

5:30 Closing Remarks

6:00 **Reception together with SSRL and SLAC Users Organizations** (Auditorium Breezeway)

Written contributions relevant to the workshop are solicited for inclusion in the workshop report.

# APPENDIX C- LIST OF ATTENDEES

OCTOBER 21, 1992

Aharoni, Rami
Stanford University
EE Department
Stanford CA 94305
Phone: 415-723-0470
Bitnet: Rami@KAOS.Stanford.edu
Fax: 415-725-3377

Allen, Matthew
SLAC
PO Box 4349, MS 84
Stanford
Phone: (415)926-2820
Bitnet:
Fax: (415)926-3030

Ando, Ainosuke
RIKEN
2-28-8, Honkomagome, Bunkyo-Ku
Tokyo 113
Phone: 03-5395-2800
Bitnet:
Fax: 03-3941-3169

Arthur, John
SSRL
PO Box 4349, MS 69
Stanford, CA 94309-0210
Phone: (415)926-3169
Bitnet: ARTHUR@SSRL750
Fax: (415)926-4100

Attwood, David
LBL
Ctr. for X-ray Optics
Berkeley, CA 94720
Phone: (510)486-4463
Bitnet:
Fax: (510)486-4550

Baron, Alfred
SSRL
PO Box 4349
Stanford, CA 94309-0210
Phone: (415)926-3033
Bitnet: BARON@SSRL750
Fax: (415)926-4100

Barty, Christopher P.J.
Stanford Univeristy
Ginzton Lab #29
Stanford CA 94305
Phone: 415-725-4942
Bitnet: Barty@Sierra
Fax: 415-725-7509

Batterman, Boris
Cornell University
CHESS
Ithaca, NY 14853
Phone: 607-255-5161
Bitnet: Batterman@CHES
Fax: 607-255-9001

Beguiristain, H. Raul
LBL
MS 2-400
Berkeley, CA 94720
Phone: (510)486-4079
Bitnet: RAUL@ROSE.LBL.GOV
Fax: (510)486-4550

Belyaev, Spartak
Academy of Science
U1.Kosygina 2, Syn. Rad. Comm.
117334 Moscow
Phone:
Bitnet: BST@BST.KIAE.SU
Fax: (095)196-45-46

Benson, Stephen
CEBAF
12000 Jefferson Ave.
Newport News VA
Phone: 804-249-5026
Bitnet:
Fax:

Bienenstock, Arthur
SSRL
PO Box 4349, MS 69
Stanford, CA 94309-0210
Phone: (415)926-3153
Bitnet: A@SSRL750
Fax: (415)926-4100

Bowman, Michael
Argonne National Laboratory
Chem. Div., Bldg. 200/E117
Argonne, IL 60439
Phone: (708)252-3546
Bitnet:
Fax: (708)252-9289

Cerino, John
SSRL
PO Box 4349, Bin 69
Stanford, CA 94309-0210
Phone: (415)926-2154
Bitnet: CERINO@SSRL750
Fax: (415)926-4100

Corbett, Jeff
SSRL
PO Box 4349, MS 99
Stanford, CA 94309-0210
Phone: (415)926-3645
Bitnet: CORBETT@SSRL750
Fax:

David, Peter
Stanford University
Cell Biology, MS 5400
Stanford, CA 94305-5400
Phone: (415)725-0754
Bitnet: DAVID@LAMA.STANFORD.EDU
Fax: (415)723-8464

Dexheimer, Susan
LBL
MS 70-193A
Berkeley, CA 94720
Phone: (510)486-6555
Bitnet: SLDEXHEIMER@LBL
Fax: (510)486-6720

Dodd, James
University of California
421 - 16th St.
Santa Monica, CA 90402-2233
Phone: (310)393-7705
Bitnet:
Fax: (310)206-1091

Eder, David
LLNL
PO Box 808, L-477
Livermore, CA 94550
Phone: (510)423-3483
Bitnet:
Fax: (510)423-9208

Eliezer, David
Stanford University
Dept. of Physics
Stanford, CA 94305
Phone: (415)723-2479
Bitnet: ELIEZER@SSRL750
Fax:

Epp, Paul
Stanford University
704 Campus Dr., Rains Apt. 27J
Stanford CA 94305
Phone: 415-497-1221
Bitnet: EPP@Leland.Stanford.edu
Fax:

Fadley, Charles S.
LBL
One Cyclotron Rd., MS 2-100
Berkeley, CA 94720
Phone: (510)486-5774
Bitnet: FADLEY@LBL.GOV
Fax: (510)486-5530

Falcone, Roger
UC Berkeley
Physics Dept
Berkeley CA 94720
Phone: 510-642-8916
Bitnet: RWF@Physics.berkeley.edu
Fax: 510-642-8916

Frank, Patrick
Stanford University
Dept. of Chemistry
Stanford, CA 94305
Phone: (415)723-2479
Bitnet: FRANK@SSRL750
Fax: (415)725-0259

Fuoss, Paul
AT&T
7C-201, 600 Mountain Ave.
Murray Hill, NJ 07974
Phone: (908)582-4951
Bitnet: FUOSS@PHYSICS.ATT.COM
Fax: (908)582-7660

Garwin, Edward
SLAC
PO Box 4349, MS 72
Stanford, CA 94309-0210
Phone: (415)926-2415
Bitnet: GARWIN@SLACVM
Fax:

George, Graham
SSRL
PO Box 4349, MS 69
Stanford, CA 94309-0210
Phone: (415)926-3109
Bitnet: George@SSRL750.BITNET
Fax: (415)926-4100

Gex, Jean Pierre
SYLAREC
Route de Nozay
Marcoussis 91460
Phone: (331)64544957
Bitnet:
Fax: 69-80-6283

Glaeser, Robert
LBL
MCB - BMB Dept., 363 Donner Lab.
Berkeley, CA 94720
Phone: (510)642-2905
Bitnet: RMGLAESER@LBL
Fax: (510)486-5342

Gordon, Susanna
UC Berkeley
Physics Dept., Le Conte Hall
Berkeley CA 94720
Phone: 510-642-1181
Bitnet: Susannag@physics.berkeley.edu
Fax: 510-643-8497

Gordon, III, C.L.
Stanford University
Ginzton Laboratory
Stanford CA 94305
Phone: 415-725-2258
Bitnet:
Fax: 415-725-7509

Gray, Joe
UC San Francisco
1855 Folsum Street, MCB-230
San Francisco, CA 94103
Phone: (415)476-3461
Bitnet: GRAY@DNC.UCSF.EDU
Fax: (415)476-8218

Halbach, Klaus
LBL/SSRL
1492 Grizzly Peak Blvd.
Berkeley CA 94708
Phone: 510-845-1309
Bitnet:
Fax: 510-845-4215

Hedman, Britt
SSRL
PO Box 4349, MS 69
Stanford, CA 94309-0210
Phone: (415)926-3052
Bitnet: HEDMAN@SSRL750
Fax: (415)926-4100

Hirsch, Greg
Hirsch Scientific
365 Talbot Ave., Suite D8
Pacifica, CA 94044
Phone: (415)359-3920
Bitnet:
Fax: (415)359-2292

Hodgson, Keith
SSRL
PO Box 4349, MS 69
Stanford, CA 94309-0210
Phone: (415)926-3109
Bitnet: HODGSON@SSRL750.BITNET
Fax: (415)926-4100

Howells, Malcolm
LBL

Berkeley CA 94720
Phone: 510-482-4949
Bitnet: Howells@LBL.bitnet
Fax: 510-486-4949

Irtel von Breundorff, Alexander
LBL
MS 2-400
Berkeley, CA 94720
Phone: (510)486-4079
Bitnet: AIRTEL@ROSE.LBL.GOV
Fax: (510)486-4550

Jacobsen, Chris
SUNY Stony Brook
Dept. of Physics, 7-3800
Stony Brook, NY 11794
Phone: (516)632-8093
Bitnet: JACOBSEN@SBHEPNY
Fax: (516)632-8101

Johnson, Erik
BNL
NSLS - Bldg. 725D
Upton, NY 11973
Phone: (516)282-4603
Bitnet:
Fax: (516)282-3238

Kim, Kwang-Je
LBL
MS 71-259
Berkeley, CA 94720
Phone: (510)486-7224
Bitnet: KWANGJE@LBL
Fax: (510)486-7981

Kincaid, Brian
LBL
2-400
Berkeley, CA 94720
Phone: (510)486-4810
Bitnet: BMK@LBL.GOV
Fax: (510)486-7696

Lemoff, Brian
Stanford University
Ginzton Box 33
Stanford CA 94305
Phone: 415-725-2258
Bitnet: Lemoff@fizzle
Fax: 415-725-7509

London, Richard
LLNL
PO Box 808, L-477
Livermore, CA 94550
Phone: (510)423-2021
Bitnet:
Fax: (510)423-9208

Margaritondo, Giorgio
Institut de Physique Applique
Ecole Polytechnique Federale
CH-1015 Lausanne
Phone: (0041) (21) 6934475
Bitnet:
Fax: (0041) (21) 6934666

Marianelli, Robert
DOE
Div. of Chem. Sci., ER-14, MS G-236
Washington, DC 20585
Phone: (301)903-5804
Bitnet: MARIANEL@MAILGW.ER.DOE.GOV
Fax: (301)903-6594

Matthews, Dennis
LLNL
PO Box 808, L-473
Livermore, CA 94551
Phone: (510)422-5360
Bitnet:
Fax: (510)422-8395

McNulty, Ian
Argonne National Laboratory
9700 South Cass Ave.
Argonne, IL 60439
Phone: (708)252-2882
Bitnet:
Fax: (708)252-3222

McPhillips, Timothy
CALTECH
147-75CH, Caltech
Pasadena, CA 91125
Phone: (818)356-8392
Bitnet: TIM@CITRAY.CALTECH.EDU
Fax:

Meyer-Ilse, Werner
LBL
MS 2-400
Berkeley, CA 94720
Phone: (510)486-6892
Bitnet: W.MEYER-ILSE@LBL
Fax: (510)486-4550

Nakagawa, Kent
Stanford University
Mudd Chemistry, Box 78
Stanford, CA 94305-5080
Phone: (415)723-2479
Bitnet: NAKAGAWA@SSRL750
Fax:

Newnam, Brian
Los Alamos National Lab.
MS J564
Los Alamos, NM 87545
Phone: (505)667-7979
Bitnet:
Fax: (505)665-5823

Nuhn, Heinz-Dieter
SSRL
PO BOX 4349, MS 69
Stanford CA 94309-0210
Phone: (415)926-2275
Bitnet: NUHN@SSRL750.BITNET
Fax: (415)926-4100

Pape, Jeff
SSRL
PO Box 4349, Bin 69
Stanford, CA 94309-0210
Phone: (415)926-3042
Bitnet: PAPE@SSRL750
Fax: (415)926-4100

Pellegrini, C.
UCLA
405 Hilgrad Ave.
Los Angeles, CA 90024-1547
Phone: (310)206-1677
Bitnet: UCLA::PELLEGRINI
Fax: (310)206-1091

Perry, Michael
LLNL
PO Box 808, L-493
Livermore, CA 94550
Phone: (510)423-4915
Bitnet:
Fax: (510)422-1930

Phizackerley, Paul
SSRL
PO Box 4349, MS 69
Stanford, CA 94309-0210
Phone: (415)926-3431
Bitnet: PHIZ@SSRL750
Fax: (415)926-4100

Pickering, Ingrid
SSRL
PO Box 4349, MS 69
Stanford, CA 94309-0210
Phone: (415)926-3109
Bitnet: PICKERING@SSRL750.BITNET
Fax: (415)926-4100

Pratt, Richard H.
University of Pittsburgh
Department of Physics
Pittsburgh, PA 15260
Phone: (412)624-9052
Bitnet: RPRATT@VMS.CIS.PITT.EDU
Fax: (412)624-9163

Rothman, Stephen
UCSF
Box 0444, 3rd & Parnassus St.
San Francisco CA 94143
Phone: 415-476-2934
Bitnet: Ruthman@LBL
Fax: (510) 486-6348

Rowen, Michael
SSRL
PO Box 4349, MS 99
Stanford CA 94309-0210
Phone: (415)926-3487
Bitnet: ROWEN@SSRL750.BITNET
Fax: (415)926-3600

Ruby, Stan
SSRL
PO Box, 4349 MS 69
Stanford, CA 94309-0210
Phone: (415)926-3957
Bitnet: RUBY@SSRL750
Fax: (415)926-4100

Sato, Yukio
RIKEN
2-28-8, Honkomagome
Bunkyo-Ku, Tokyo 113
Phone: 03-5395-2801
Bitnet:
Fax: 03-3941-3169

Schabel, Matthias
Stanford University
3330 Alpine Rd.
Portola Valley, CA 94028
Phone: (415)851-9560
Bitnet: SCHABEL@LELAND
Fax:

Schoenlein, Robert
LBL
MS 70-193A
Berkeley, CA 94705
Phone: (510)486-6557
Bitnet: RWSCHOEN@UXS.LBL.GOV
Fax: (510)486-6720

Serimaa, Ritva
SSRL
PO Box 4349, MS 69
Stanford, CA 94309-0210
Phone: (415)926-3039
Bitnet: RSERIMAA@SSRL01
Fax:

Shank, Charles V.
LBL
1 Cycltron Road, Bldg. 50A, Rm. 4133
Berkeley, CA 94720
Phone: (510)486-5111
Bitnet:
Fax: (510)486-6720

Solem, Johndale
LANL
Theoretical Division
Los Alamos, NM 87545
Phone:
Bitnet:
Fax:

Spicer, William
Stanford University
SEL, McCullough 228
Stanford, CA 94305-4055
Phone: (415)723-4634
Bitnet: SPICER@SIERRA
Fax: (415)723-4659

Taylor, Richard
SLAC
MS 96
Stanford, CA 94309-0210
Phone: (415)926-2417
Bitnet: RETAYLOR@SLACVM
Fax: (415)926-2923

Templeton, Lieselotte
LBL
Dept. of Chemistry
Berkeley, CA 94720
Phone: (510)486-5615
Bitnet: LILO@LBL
Fax: (510)486-5596

Templeton, David
LBL
Dept. of Chemistry
Berkeley, CA 94720
Phone: (510)486-5615
Bitnet: LILO@LBL
Fax: (510)486-5596

Terminello, Louis
LLNL
MS L-357, PO Box 808
Livermore, CA 94550
Phone: (510)423-7956
Bitnet: TERMINELLO@CMS.LLNL.GOV
Fax: (510)423-7040

Tobin, James
LLNL
PO Box 808, L-357
Livermore, CA 94550
Phone: (510)422-7247
Bitnet: TOBIN1@LLNL.GOV
Fax: (510)423-7040

Travish, Gil
UCLA
Dept of Physics
Los Angeles, CA
Phone: (310) 206-5584
Bitnet: Travish@uclaph.physics.ucla.edu
Fax:

Trebes, James
LLNL
PO BOX 5508, L-473
Livermore CA 94550
Phone: (510)423-7413
Bitnet:
Fax: (510)422-8395

Tsuruta, Hiro
SSRL
PO Box 4349, MS 69
Stanford, CA 94309-0210
Phone: (415)926-3104
Bitnet: TSURUTA@SSRL750
Fax: (415)926-4100

Varfolomeev, Alexander
Academy of Science
U1.Kosygina 2, Syn. Rad. Comm.
117334, Moscow
Phone:
Bitnet:
Fax:

Vylet, Vaclan
SLAC
MS 48, PO Box 4349
Stanford CA 94305
Phone: 415-926-2048
Bitnet:
Fax:

Walukiewicz, Wladek
LBL
MS 2-200, 1 Cyclotron Rd.
Berkeley, CA 94720
Phone: (510)486-5329
Bitnet:
Fax: (510)486-5530

Westphal, Larsten
LBL
MS 2-300
Berkeley, CA 94720
Phone: (510)486-7633
Bitnet:
Fax: (510)486-4299

Westre, Tami
Stanford University
Chemistry Dept.
Stanford, CA 94305
Phone: (415)723-2479
Bitnet: WESTRE@SSRL750
Fax: (415)723-4817

Winick , Herman
SSRL
PO Box 4349, Bin 69
Stanford, CA 94309-0210
Phone: (415)926-3155
Bitnet: WINICK@SSRL750
Fax: (415)926-4100

Wu, Dandan
SSRL
PO Box 4349, Bin 69
Stanford, CA 94309-0210
Phone: 926-3035
Bitnet:
Fax: 926-4100

Xie, Ming
LBL
MS/B71H
Berkeley, CA 94720
Phone: (510)486-5616
Bitnet: MINGXIE@LBL.GOV
Fax: (510)486-7981

Yun, Wenking
Argonne National Lab
800 Kimberly Way
Lisle, Illinois
Phone: 708-252-5320
Bitnet:
Fax: 708-252-3222

Zege, Andrew
LBL
MS/B71H
Berkeley, CA 94720
Phone: (510)486-6714
Bitnet:
Fax: (510)486-7981

Ziemann, Volker
SLAC
PO Box 4349
Stanford CA 94309
Phone: 415-926-4775
Bitnet: Volker@SLACVM
Fax: 415-926-2407

# END

# DATE FILMED

5/4/93